AD-A097 296 IOWA STATE UNIV AMES ENGINEERING RESEARCH INST F/G 20/4
MEASUREMENT AND ANALYSIS OF THE PERIODIC VARIATION OF TOTAL PRE--ETC
NOV 80 W C ZIERKE, T H OKIISHI F49620-79-C-0002
UNCLASSIFIED ISU-ERI-AMES-81121 AFOSR-TR-81-0327 NL

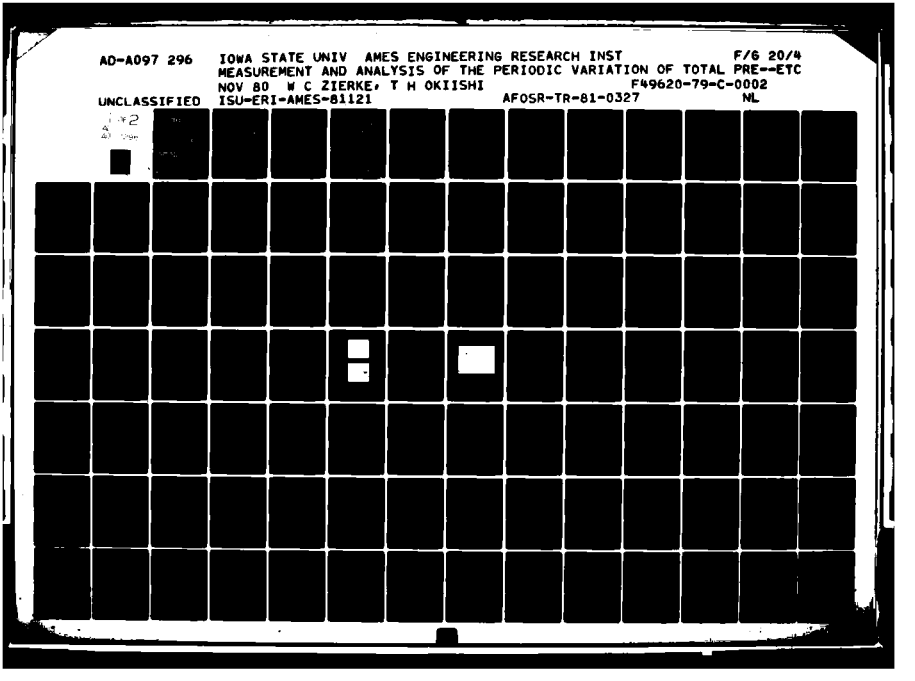

LEVEL II

W. C. ZIERKE
T. H. OKIISHI
NOVEMBER 1980

MEASUREMENT AND ANALYSIS OF THE PERIODIC VARIATION OF TOTAL PRESSURE IN AN AXIAL-FLOW COMPRESSOR STAGE

TURBOMACHINERY
COMPONENTS RESEARCH PROGRAM

ENGINEERING RESEARCH INSTITUTE
IOWA STATE UNIVERSITY
AMES, IOWA 50010 USA

ISU-ERI-Ames-81121
TCRL-18
ERI Project 1394

UNCLASSIFIED
SECURITY CLASSIFICATION OF THIS PAGE (When Data Entered)

(19) REPORT DOCUMENTATION PAGE

READ INSTRUCTIONS BEFORE COMPLETING FORM

1. REPORT NUMBER: AFOSR TR-81-0327	2. GOVT ACCESSION NO.: AD-A097296
3. RECIPIENT'S CATALOG NUMBER: 9	
4. TITLE (and Subtitle): MEASUREMENT AND ANALYSIS OF THE PERIODIC VARIATION OF TOTAL PRESSURE IN AN AXIAL-FLOW COMPRESSOR STAGE	5. TYPE OF REPORT & PERIOD COVERED: INTERIM, 1 Oct 78 - 30 Sep 80
	6. PERFORMING ORG. REPORT NUMBER
7. AUTHOR(s): WILLIAM C. ZIERKE, THEODORE H. OKIISHI	8. CONTRACT OR GRANT NUMBER(s): F49620-79-C-0002
9. PERFORMING ORGANIZATION NAME AND ADDRESS: ENGINEERING RESEARCH INSTITUTE, IOWA STATE UNIVERSITY, TURBOMACHINERY COMPONENTS RESEARCH, AMES, IOWA 50011	10. PROGRAM ELEMENT PROJECT, TASK AREA & WORK UNIT NUMBERS: 61102F, 2307/A4
11. CONTROLLING OFFICE NAME AND ADDRESS: AIR FORCE OFFICE OF SCIENTIFIC RESEARCH/NA, BLDG 410, BOLLING AFB, DC 20332	12. REPORT DATE: NOV 80
	13. NUMBER OF PAGES: 103
14. MONITORING AGENCY NAME & ADDRESS (if different from Controlling Office)	15. SECURITY CLASS. (of this report): UNCLASSIFIED
	15a. DECLASSIFICATION DOWNGRADING SCHEDULE

16. DISTRIBUTION STATEMENT (of this Report)

14 ISU-ERI-AMES-81121, TR-1

Approved for public release; distribution unlimited.

17. DISTRIBUTION STATEMENT (of the abstract entered in Block 20, if different from Report)

18. SUPPLEMENTARY NOTES

19. KEY WORDS (Continue on reverse side if necessary and identify by block number)

AXIAL-FLOW TURBOMACHINERY
AXIAL-FLOW COMPRESSOR
AXIAL-FLOW TURBINE
PERIODICALLY UNSTEADY FLOW
UNSTEADY FLOW
TOTAL PRESSURE
TURBOMACHINE FLOW MEASUREMENT

20. ABSTRACT (Continue on reverse side if necessary and identify by block number)

A fast-response, total-pressure probe was used with a periodically sampling and averaging data acquisition system to study the unsteady total-pressure field in an axial-flow turbomachine. Periodically unsteady total-pressure data were used to demonstrate some of the ways in which turbomachine blade wake transport and interaction influences the energy transfer involved. Observed trends of periodic variations in local total pressures could be explained in terms of the details of energy transfer associated with the different kinds of fluid particles (freestream, wake segment, blade surface

DD FORM 1 JAN 73 1473 EDITION OF 1 NOV 65 IS OBSOLETE

4-644

UNCLASSIFIED
SECURITY CLASSIFICATION OF THIS PAGE (When Data Entered)

boundary layer, mixed) moving through a blade row. Some frequency response requirements of measurement systems used for turbomachine unsteady total-pressure research are proposed. Examples of how the system and its components (probes, filters and amplifiers) respond to idealized wakes illustrate the necessity of a system that will faithfully respond to anticipated wake forms. The importance of the harmonic content of the unsteady data being measured is demonstrated.

ENGINEERING RESEARCH

ENGINEERING RESEARCH

ENGINEERING RESEARCH

ENGINEERING RESEARCH

ENGINEERING RESEARCH

TECHNICAL REPORT

MEASUREMENT AND ANALYSIS OF THE PERIODIC VARIATION OF TOTAL PRESSURE IN AN AXIAL-FLOW COMPRESSOR STAGE

W. C. Zierke
T. H. Okiishi
November 1980

ISU-ERI-Ames-81121
TCRL-18
ERI Project 1394

DEPARTMENT OF MECHANICAL ENGINEERING
ENGINEERING RESEARCH INSTITUTE
IOWA STATE UNIVERSITY, AMES

TABLE OF CONTENTS

	Page
LIST OF FIGURES	vii
LIST OF TABLES	xi
ACKNOWLEDGMENTS	xiii
SUMMARY	xv
SYMBOLS AND NOTATION	xvii
1. INTRODUCTION	1
2. RESEARCH COMPRESSOR FACILITY	3
2.1. Axial-Flow Research Compressor	3
2.2. Stationary Blade Row and Probe Actuators	10
2.3. Pressure and Temperature Measurement Instrumentation	10
2.4. Fast-Response Measurement System	13
2.5. Calibration Equipment	16
3. EXPERIMENTAL PROCEDURE	17
3.1. Periodic Sampling and Averaging Technique	17
3.2. Static Calibration	18
3.3. Dynamic Calibration	20
3.4. Data Acquisition	38
3.5. Data Reduction	40
4. PRESENTATION AND DISCUSSION OF DATA	43
4.1. Turbomachine Wake Transport and Interaction	43
4.2. Data Uncertainty	48
4.3. First Rotor Exit Flow Data	57
4.3.1. Local Total-Head Data	57
4.3.2. Blade-to-Blade-Average Data	68

4.4. First Stator Exit Flow Data 70

4.5. Second Rotor Exit Flow Data 77

5. CONCLUSIONS 81

6. RECOMMENDATIONS FOR FUTURE RESEARCH 83

7. REFERENCES 85

8. APPENDIX: TABULATION OF PERIODIC-AVERAGE TOTAL-HEAD DATA 89

LIST OF FIGURES

		Page
Figure 2.1.	Research compressor apparatus side view	4
Figure 2.2.	Research compressor with probe measurement stations	5
Figure 2.3.	Blade nomenclature	7
Figure 2.4.	Schematic diagram showing axial location of probe measurement stations (dimensions in mm)	8
Figure 2.5.	Blade cascade showing relative positions of blades for several rotor sampling positions. (S_R is rotor blade spacing; S_S is stator spacing; Y is measurement circumferential location; YO_R is reference rotor blade circumferential location; YO_{1S} is reference first stator blade circumferential location.)	9
Figure 2.6.	Fast-response total-pressure probe details	11
Figure 2.7.	Periodic-average total-pressure measurement system	14
Figure 3.1.	Variation of periodic-average values of total head for different sample sizes	19
Figure 3.2.	Typical sensitivity calibration curve	21
Figure 3.3.	Harmonic analysis of a wake given by an idealized function of the two parameters h and b/s	25
Figure 3.4.	Response of a second-order system to an idealized wake input with K = 2.21	26
Figure 3.5.	Response of a second-order system to an idealized wake input with K = 7.29	27
Figure 3.6.	Response of a low-pass filter to an idealized wake input	29
Figure 3.7.	Shock tube electronic data acquisition system: (a) probe output recording system; (b) shock speed measurement and probe output recording system	31

Figure 3.8.	Typical traces recorded by an oscilloscope from the response of the fast-response total-pressure probe used in this research project	32
Figure 3.9.	Probe tip designed by Junkhan (1973)	33
Figure 3.10.	Typical trace recorded by an oscilloscope from the response of Junkhan's probe: sweep time sensitivity = 100 μs/cm, vertical sensitivity = 5 mV/cm	34
Figure 3.11.	Oscillation envelopes for the amplitude frequency response of a second-order system to a unit step: (a) probe response, f_n = 94 kHz, ξ = 0.009; (b) transducer response, f_n = 94 kHz, ξ = 0.003; (c) addition of probe response and transducer response; (d) experimental response	36
Figure 3.12.	Amplitude frequency response of the measurement system	37
Figure 3.13.	Research compressor performance curve and operating point	39
Figure 4.1.	Relative velocity of wake segment fluid	44
Figure 4.2.	Plane velocity vector triangles for fluid in an interacted wake, a noninteracted wake, and free-stream for first rotor exit flow at midspan	46
Figure 4.3.	Blade-to-blade distribution of time-average total head	49
Figure 4.4.	Radial distribution of blade-to-blade-average total head	53
Figure 4.5.	Comparison of periodic-average total-head values measured by the fast-response total-pressure probe to those values calculated from hot-wire velocity data at 50% PHH	55
Figure 4.6.	Blade-to-blade distribution of periodic-average total head and time-average total head at station 3	58
Figure 4.7.	Periodic-average cascade plots for the first stage of the research compressor at 50 percent passage height	63
Figure 4.8.	Velocity triangles at station 3 and 50% PHH	64

Figure 4.9. Blade span distribution of time-average total-head loss coefficient for first rotor row 66

Figure 4.10. Blade-to-blade distribution of first rotor exit periodic-average axial flow at different radial positions for $YO_R/S_R = 0.0$ 67

Figure 4.11. Time varying blade-to-blade-average total-head values at station 3 69

Figure 4.12. Blade-to-blade distribution of periodic-average total head and time-average total head at station 4 71

Figure 4.13. Time varying blade-to-blade-average total-head values at station 4 76

Figure 4.14. Blade-to-blade distribution of periodic-average total head and time-average total head at station 5 and 50% PHH 78

Figure 4.15. Velocity triangles at station 5 and 50% PHH 79

Figure 4.16. Time varying blade-to-blade-average total-head values at station 5 and 50% PHH 80

LIST OF TABLES

		Page
Table 2.1.	Blade geometry tables for IGV, rotors, and stators at several radial locations	7
Table 2.2.	Transducer specifications	13
Table 4.1.	Blade-to-blade-average and time-average total-head values in the first stage	52
Table 4.2.	Behavior of fluid particles moving from the rotor inlet to the measurement station downstream of the rotor	68
Table 8.1.	Periodic-average total-head circumferential survey data	90

ACKNOWLEDGMENTS

The work described in this report was accomplished in the Iowa State University Engineering Research Institute/Mechanical Engineering Department Turbomachinery Components Research Laboratory under Air Force Office of Scientific Research Contract F49620-79-C-0002 with cost sharing by Iowa State. This sponsorship is gratefully acknowledged.

Our colleagues were of help to us in many ways. Professor William J. Cook and his shock tube facility were important to our program in calibrating the pressure probe. Suggestions from Dr. Gabriel A. Alarcon, Professor George H. Junkhan, Professor George K. Serovy, and Mr. Stephen L. Wells were very useful.

We appreciate the competent assistance received from those Engineering Research Institute Staff members who support our research by making reports like this one available to interested individuals through their editing, typing and illustrating skills.

SUMMARY

A fast-response, total-pressure probe was used with a periodically sampling and averaging data acquisition system to study the unsteady total-pressure field in an axial-flow turbomachine. Periodically unsteady total-pressure data were used to demonstrate some of the ways in which turbomachine blade wake transport and interaction influences the energy transfer involved. Observed trends of periodic variations in local total pressures could be explained in terms of the details of energy transfer associated with the different kinds of fluid particles (freestream, wake segment, blade surface boundary layer, mixed) moving through a blade row.

Some frequency response requirements of measurement systems used for turbomachine unsteady total-pressure research are proposed. Examples of how the system and its components (probes, filters and amplifiers) respond to idealized wakes illustrate the necessity of a system that will faithfully respond to anticipated wake forms. The importance of the harmonic content of the unsteady data being measured is demonstrated.

SYMBOLS AND NOTATION

A	Harmonic amplitude (Figure 3.3)
b	Width of the wake (Figure 3.3)
c	Blade chord length (Figure 2.3), m
f_n	Undamped natural frequency
g	Local acceleration of gravity, m/s^2
g_c	Gravitational constant, 1.0 $(kg \cdot m)/(N \cdot s^2)$
$\overline{H}$	Time-average total head with respect to barometric pressure (Eq. 3.2), $N \cdot m/kg$
$\tilde{H}_{TPP}$	Periodic-average total head with respect to barometric pressure (Eq. 3.2), $N \cdot m/kg$
HT	Periodic-average total head with respect to barometric pressure, $N \cdot m/kg$
h	Static head with respect to barometric pressure, $N \cdot m/kg$; velocity difference between wake and freestream to freestream velocity ratio (Figure 3.3)
h_d	Dynamic head with respect to barometric pressure, $N \cdot m/kg$
h_{hg}	Barometric pressure (Eq. 3.3), m of Hg
K	Blade spacing to wake width ratio
N	Number of arithmetically averaged samples involved
P	Total pressure with respect to barometric pressure (Figure 3.2), in. of H_2O
P_{atm}	Barometric pressure, N/m^2
PHH	Percent passage height from hub
R	Gas constant (Eq. 3.4), $N \cdot m/kg \cdot {}^{o}K$
S	Circumferential space between blades, blade pitch, m or deg
s	Blade spacing (Figure 3.3)
t	Temperature, ^{o}K

t_{max} Maximum blade thickness (Figure 2.3), m

V Voltage (Figure 3.2), volts; absolute velocity, m/s

W Relative velocity (Figure 4.2), m/s

Y Circumferential traversing position, deg

YO Circumferential blade-row setting position when Y is equal to zero, circumferential distance from probe-traversing measurement stations to blade stacking axis, positive in direction of rotor rotation, deg

α Absolute flow angle (Figure 4.2), deg

β Relative flow angle (Figure 4.2), deg

γ Stagger angle (Figure 2.3), deg

γ_{H_2O} Specific weight of water manometer fluid, N/m^3

γ_{hg} Specific weight of mercury (Eq. 3.3), N/m^3

κ_1 Inlet blade angle (Figure 2.3), deg

κ_2 Outlet blade angle (Figure 2.3), deg

ξ Damping ratio

ρ Density of air, kg/m^3

σ Standard deviation of the periodic sample average, N·m/kg

σ_n Standard deviation of the random fluctuations, N·m/kg

ω_b Blade passing frequency, rad/s

ω_c Cut-off frequency, rad/s

ω_n Undamped natural frequency, rad/s

Subscripts

F Freestream (Figure 4.2)

k Harmonic components (Figure 3.3)

W Wake (Figure 4.2)

1. INTRODUCTION

Further generalization of turbomachine design procedures to the extent that they more correctly reflect the inherent periodically unsteady flows involved is desirable. This kind of progress is dependent on more of the phenomenological aspects of the unsteadiness of the flow being revealed through experiment and organized by analysis. Research in this direction is important because of the improvements still to be realized in designing turbomachines that are energy efficient, quiet and able to survive the variety of aerodynamic sources of blade vibration present when the machine is in operation.

The unsteady flow of interest to the research project described in this report is the periodically unsteady flow due to rotor/stator wake production, transport and interaction in an axial-flow turbomachine. Total-head values are indicative of fluid particle energy addition, through work, and energy loss, through friction. Thus, the periodic unsteadiness of turbomachine energy transfer can be studied by observing the periodic unsteadiness of the total-head field. Advancements in measurement systems and techniques have made periodically unsteady total-head data acquisition possible. The objectives of this project were to develop further a periodically unsteady total-pressure measurement system designed earlier by Alarcon, Okiishi and Junkhan (1977) and to use this system to acquire unsteady total-pressure data in the first stage of an axial-flow turbomachine. Previously obtained velocity vector data (Schmidt et al. (1978)) and total-pressure data (Alarcon, Okiishi and Junkhan (1977)) for the same axial-flow turbomachine now used indicate

that a considerable amount of periodic unsteadiness exists downstream of embedded rotor and stator blade rows. Further, it has been concluded that this unsteadiness is largely caused by variations with rotor sampling position of the spatial distribution and proportions of different kinds of fluid particles in the measurement "window."

2. RESEARCH COMPRESSOR FACILITY

The research compressor facility of the Iowa State University Engineering Research Institute/Mechanical Engineering Department Turbomachinery Components Research Laboratory was used in this research project. This facility will be described briefly in this section. A more complete description was given previously by Schmidt and Okiishi (1976).

2.1. Axial-Flow Research Compressor

An overall schematic of the low-speed, three-stage, axial-flow research compressor apparatus is shown in Figure 2.1. The compressor was driven by an 11 kw (15 hp) variable speed DC motor. The motor speed was measured with a frequency counter/magnetic pickup/60-toothed gear arrangement and could be adjusted electronically and maintained to within $\pm$ 1 rpm with a feedback control circuit. From the compressor, air proceeded through a downstream duct consisting of a flow straightening section, a venturi flow rate meter, and a diffuser section and then past an adjustable throttle plate.

Details of the compressor section are illustrated in Figure 2.2. A smooth, gradually contracting inlet to the compressor guided the flow entering both the inlet guide vanes and the three repeating sets of rotor/stator stages. These blades were located within a constant cross-sectional area annulus with a 0.284 m (11.2 in.) hub diameter and a 0.406 m (16.0 in.) tip diameter. The blades were composed of British C4 sections reflecting a free vortex design and were constructed of a

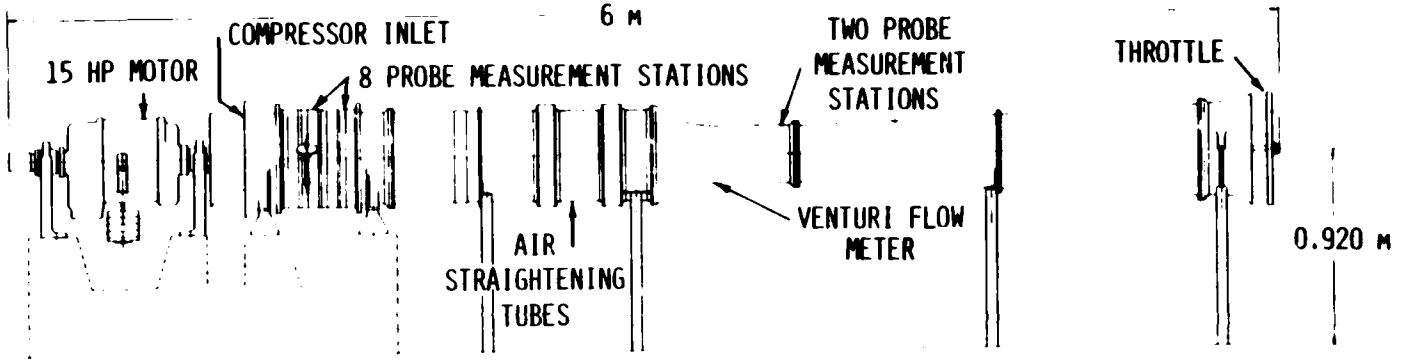

Figure 2.1. Research compressor apparatus side view.

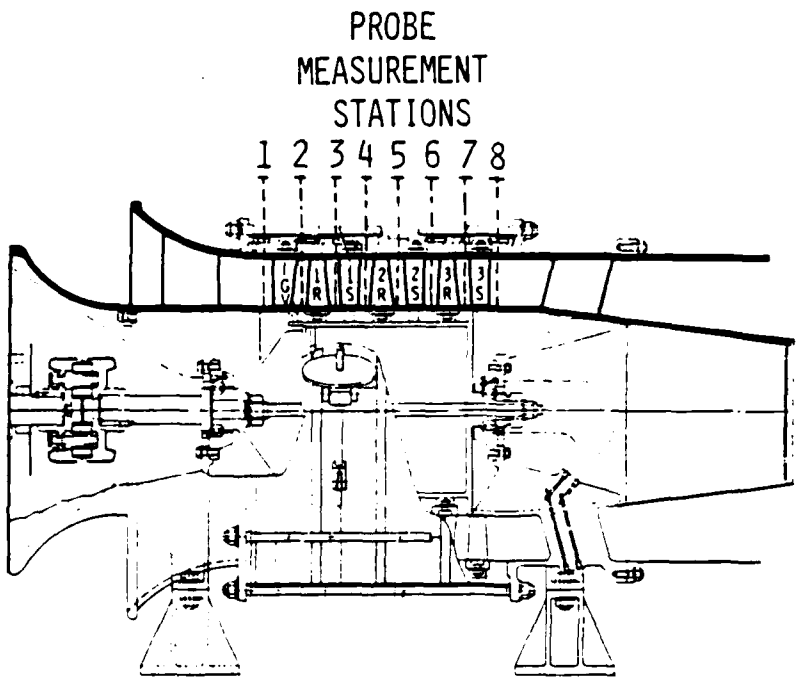

Figure 2.2. Research compressor with probe measurement stations.

Monsanto ABS plastic. General blade characteristics are summarized below:

Number of blade rows	inlet guide vane (IGV) and stator rows - 37 rotor rows - 38
Blade span (constant)	6.10 cm (2.4 in.)
Blade chord (constant)	3.05 cm (1.2 in.)
Blade section maximum thickness/chord ratio	10%

Blade section geometry details are listed in Table 2.1 with the nomenclature defined in Figure 2.3. The rotor blade rows were aligned so that corresponding blade stacking axes for each rotor row were in line when viewed along the compressor axis. The stationary blade rows, which could be moved individually or simultaneously by a motor-driven circumferential-motion carriage, were positioned to yield minimum noise. The minimum noise circumferential settings of the stationary blade rows were determined from sound-pressure level measurements by Schmidt and Okiishi (1976).

Probe measurement stations were located axially approximately midway between the blade rows as shown in Figure 2.4. For the first stage only, Figure 2.5 shows the circumferential extent of the measurement stations. Some important measurement position nomenclature is also explained in Figure 2.5. Circumferential traversing of the flow was accomplished by moving all blades (including sampled reference rotor blades) together past a stationary probe. Sampling was performed with the help of a photoelectric pickup, triggered by a disk with one slot per revolution. Unsteady flow data were obtained for circumferential

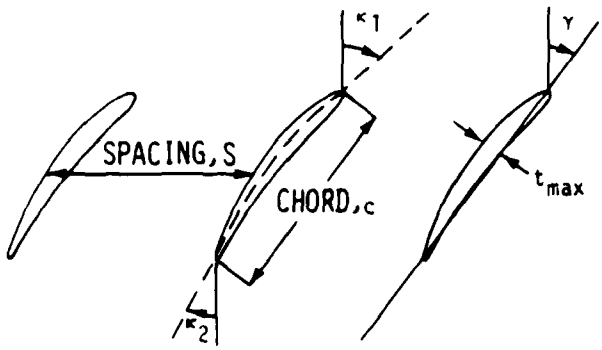

Figure 2.3. Blade nomenclature.

Table 2.1. Blade geometry tables for IGV, rotors, and stators at several radial locations

Blade Row	Percent Passage Ht. From Hub PHH	Solidity c/S	Blade Angles: Stagger degrees	Inlet κ_1 degrees	Outlet κ_2 degrees	Camber $\kappa_1 - \kappa_2$ degrees
IGV	0	1.263	20.35	0.00	42.10	-42.10
	10	1.211	20.05	0.00	40.77	-40.77
	20	1.164	19.69	0.00	39.47	-39.47
	30	1.121	19.25	0.00	38.23	-38.23
	40	1.080	18.65	0.00	37.08	-37.08
	50	1.041	18.15	0.00	36.05	-36.05
	60	1.004	17.63	0.00	35.02	-35.02
	70	0.971	17.05	0.00	33.93	-33.93
	80	0.940	16.45	0.00	32.92	-32.92
	90	0.913	15.65	0.00	32.10	-32.10
	100	0.887	14.15	0.00	31.40	-31.40
Rotor	0	1.299	-20.54	-42.40	3.90	-46.30
	10	1.250	-24.39	-44.76	- 2.84	-41.92
	20	1.205	-28.11	-46.85	- 9.51	-37.34
	30	1.164	-31.70	-48.53	-15.96	-32.57
	40	1.123	-35.15	-49.82	-21.88	-27.94
	50	1.078	-38.47	-50.81	-27.06	-23.75
	60	1.035	-41.66	-51.77	-31.64	-20.13
	70	0.999	-44.71	-52.90	-35.78	-17.12
	80	0.968	-47.63	-53.98	-39.26	-14.72
	90	0.939	-50.41	-54.82	-41.91	-12.91
	100	0.909	-53.07	-55.50	-44.10	-11.40
Stator	0	1.263	40.24	54.80	26.70	28.10
	10	1.211	39.32	53.48	25.67	27.81
	20	1.164	38.39	52.36	24.68	27.68
	30	1.121	37.46	51.43	23.74	27.69
	40	1.080	36.54	50.25	22.77	27.48
	50	1.041	35.61	48.56	21.72	27.84
	60	1.004	34.68	47.13	20.76	26.37
	70	0.971	33.75	46.65	20.01	26.64
	80	0.940	32.83	46.36	19.34	27.02
	90	0.913	31.90	45.59	18.62	26.97
	100	0.887	30.97	44.50	17.85	26.65

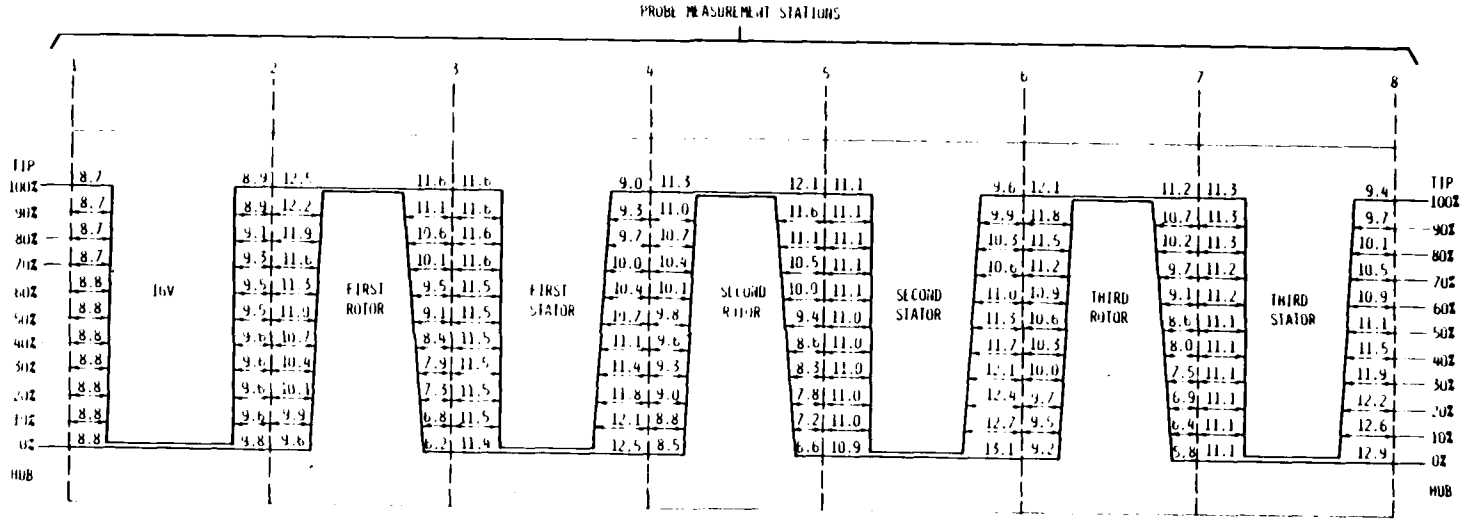

Figure 2.4. Schematic diagram showing axial location of probe measurement stations (dimensions in mm).

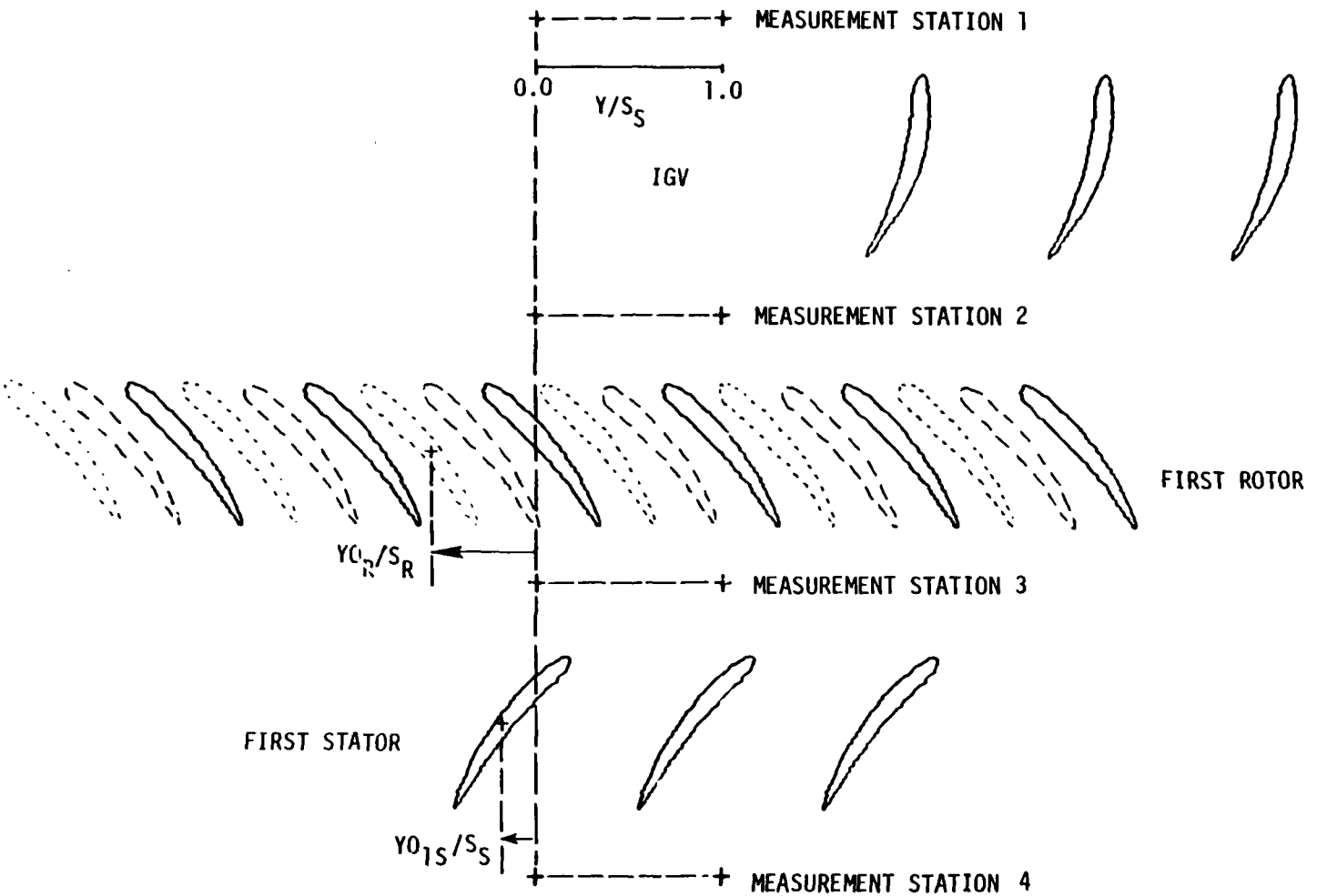

Figure 2.5. Blade cascade showing relative positions of blades for several rotor sampling positions. (S_R is rotor blade spacing; S_S is stator spacing; Y is measurement circumferential location; YO_R is reference rotor blade circumferential location; YO_{1S} is reference first stator blade circumferential location.)

position values of Y/S_s from 0.0 to 1.0 for different values of YO_R/S_R, the circumferential sampling position of a reference rotor blade.

2.2. Stationary Blade Row and Probe Actuators

A circumferential-motion carriage was used to move the stationary blades and the periodically sampled rotor blades past the stationary probe in twenty-one steps over the circumferential distance between two adjacent stator blades. A calibrated potentiometer was used to monitor the circumferential position.

A probe actuator (L. C. Smith Company model 6180) and related control indicator (L. C. Smith Company model DI-3R) and switch box (L. C. Smith Company model DI-4R-SB) were used to position the measuring probes to the radial position and yaw angle desired in the compressor. The radial position, specified in terms of percent of annulus passage height from the hub (PHH), could be measured to within 0.15 mm. The yaw angle could be measured to within 0.05 degrees. Calibrated potentiometers indicating immersion and yaw angle were used to set probe radial position and yaw angle.

2.3. Pressure and Temperature Measurement Instrumentation

Unsteady total-pressure measurements were obtained with a fast-response probe similar to the one designed by Alarcon, Okiishi, and Junkhan (1977). The probe, shown in Figure 2.6, was equipped with a KULITE model XCS-062-5 pressure transducer. The transducer consisted of a miniature silicon diaphragm on which a fully active four-arm

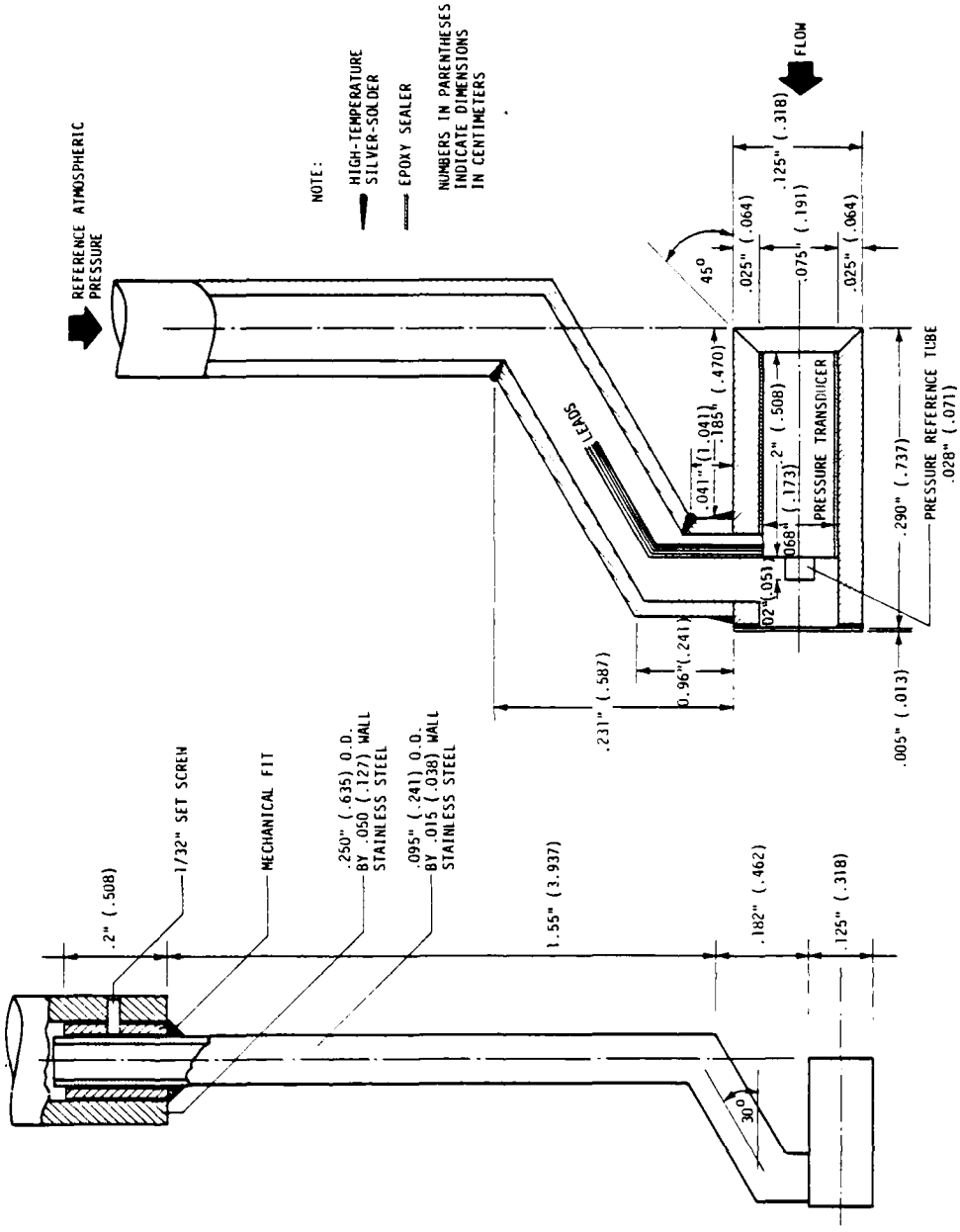

Figure 2.6. Fast-response total-pressure probe details.

Wheatstone bridge had been atomically bonded using solid state diffusion. A 15-volt power supply was used to provide an excitation voltage to the bridge. A metal screen, designed by Boeing Company engineers for protecting a transducer diaphragm without seriously decreasing frequency response, was installed in front of the diaphragm. Basically, the metal screen consisted of one hole in the center surrounded by seven smaller holes. The volume between the screen and the transducer diaphragm was filled with a silicon seal material. To keep the probe's frequency response high, the volume between the transducer and the probe hole opening was minimized. Some connecting volume was necessary to include an internal chamber intended to extend the flow direction range over which the probe is insensitive. A temperature compensation device was added to the original transducer electrical circuit. The probe was designed so that the pressure reference tube of the transducer was exposed to atmospheric pressure. The transducer specifications are summarized in Table 2.2.

Time-average total-pressure measurements were made earlier by Schmidt and Okiishi (1976) with a slow-response cobra probe (United Sensor type CA)/water-in-glass manometer system.

Barometric pressure was measured using a mercury-in-glass barometer (Princo Instruments, Inc. model B-222).

Copper-constantan thermocouples and a precision millivolt potentiometer (Leeds and Northrup Company model 8686) were used to measure working fluid temperatures. Several mercury-in-glass thermometers were employed for room air temperature measurements.

Table 2.2. Transducer specifications

Rated pressure	5 psig
Maximum pressure	25 psig
Maximum reference pressure	25 psig
Sensitivity	16.754 mV/psig
Maximum excitation	20 VDC
Thermal effect on zero	< 3.00% PS/100°F
Thermal effect on sensitivity	< 3.00% FS/100°F
Output impedance	1110 ohms
Input impedance	2390 ohms
Natural frequency (approx)	125 kHz

2.4. Fast-Response Measurement System

A schematic setup diagram of the fast-response measurement system used to make unsteady total-pressure measurements is shown in Figure 2.7. The measurement system was composed of the following components:

(1) Fast-response total-pressure probe.

(2) 15-volt probe power supply (Burr-Brown model 558).

(3) 1000-gain differential voltage amplifier.

(4) Amplifier power supply (Burr-Brown model 503).

(5) Band-pass filter (General Radio Co. model 1952 universal filter).

(6) Capacitor (0.01 $\pm$ 10% pf).

(7) Periodic sample-and-hold circuit.

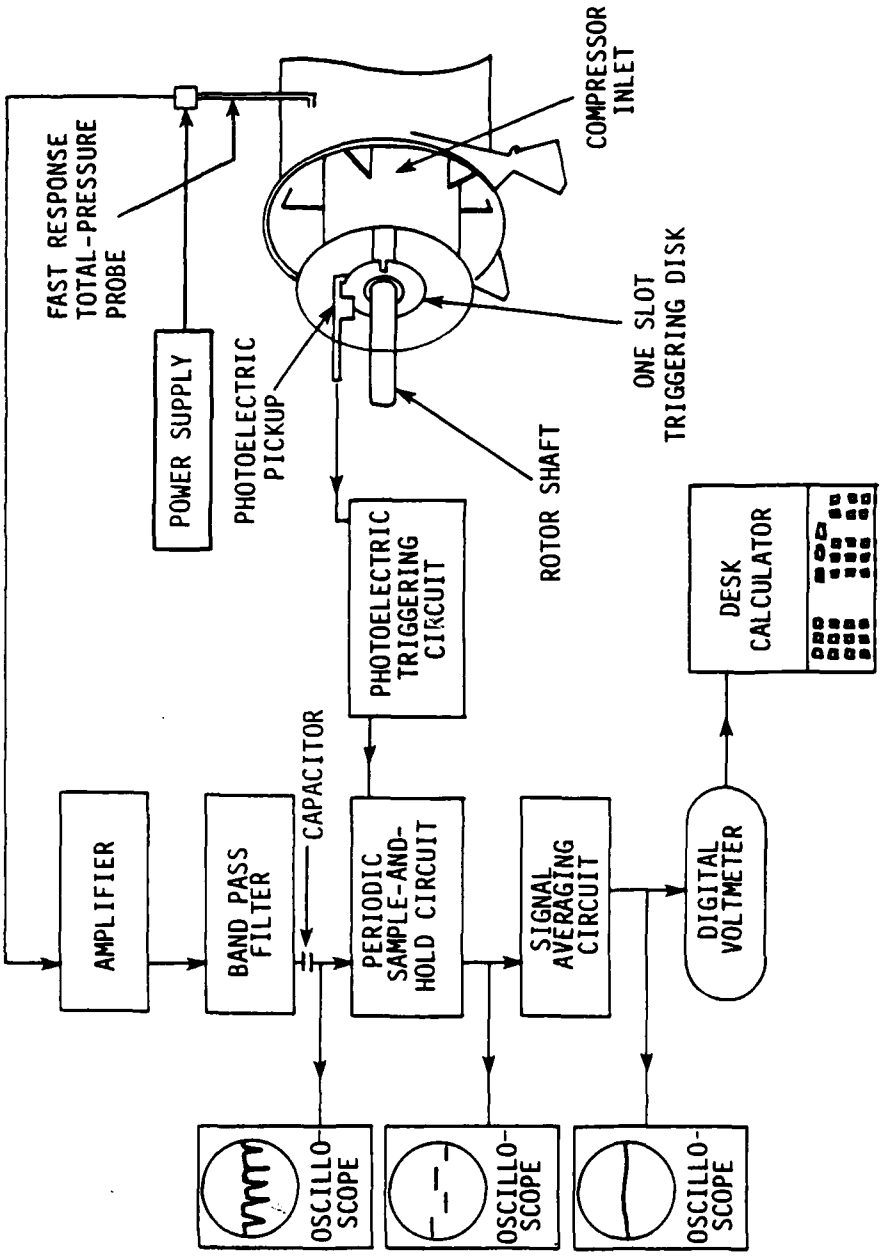

Figure 2.7. Periodic-average total-pressure measurement system.

(8) Photoelectric triggering circuit.

(9) Signal averaging circuit.

(10) Digital scanning voltmeter (Hewlett-Packard model 3480D).

(11) Desk-top calculator (Hewlett-Packard model 9821A).

(12) Oscilloscopes (Tektronix, Inc. model R564B).

The signal from the fast response total-pressure probe was enlarged by a 1000-gain differential amplifier to enhance the output voltage. A band-pass filter was used to attenuate 60 cycle noise from the surroundings and high frequency noise from the amplifier. A 0.01 pf capacitor was placed in the circuit to eliminate the drifting DC voltage from the filter.

The periodic sample-and-hold circuit and the photoelectric triggering circuit made it possible to synchronize data acquisition with the periodic sampling position of a reference rotor blade. A 5 μsecond sample could be obtained during each revolution of the rotor since a one slot per revolution disk rotating with the compressor shaft was used to interrupt the photoelectric circuit. The photoelectric pickup was attached by an adjustable arm to the circumferential motion carriage so that the periodic rotor sampling position did not change in relation to the stationary blades when the stationary blades were moved circumferentially. The position of the adjustable arm could be changed to obtain any desired rotor sampling position (YO_R). The rotor sampling position was measured from the reference line of the probe measurement station as shown in Figure 2.5.

The signal averaging circuit consisted of a low-pass filter with a 1.0 second time constant that electronically averaged the periodic

sample-and-hold signal. A specified number of these electronically averaged signals were read by the digital voltmeter and arithmetically averaged and stored by the calculator. The resulting data were called periodic-average data.

2.5. Calibration Equipment

An air nozzle was used for the static calibration of the fast-response total-pressure probe. The nozzle has a throat diameter of 25.4 mm (1.0 in.) and a contraction ratio of 144 to 1. Values of velocity from 0.0 to 50 m/s were provided by a regulated compressor air supply. The temperature of the nozzle air was controlled with a variable-current heater, blower, and heat exchanger system.

The Iowa State University Engineering Research Institute/Mechanical Engineering Shock Tube Facility was used to generate a step input in total pressure for dynamic calibration of the fast-response total-pressure probe. The equipment used included the shock tube, the trigger and time delay circuits, and the output recording equipment. A more detailed description of the shock tube facility is given by Chaney (1977).

3. EXPERIMENTAL PROCEDURE

The measurement of unsteady total pressures in the research compressor involved two types of total-pressure measurements. Weyer (1976) pointed out that because of the inherent zero thermal drift of semiconductor pressure transducers, absolute pressure measurements made with these transducers could involve large uncertainties. He recommended that absolute unsteady total-pressure values should be determined by adding time-average (DC) and fluctuating (AC) pressure measurement components. Since compressibility effects in the present compressor were negligibly small, the slow-response cobra probe pressure measurements of Schmidt and Okiishi (1976) were considered to represent correct values of time-average total pressure. The procedure used to determine the fluctuating total-pressure data will be discussed in this section.

3.1. Periodic Sampling and Averaging Technique

The flow field in a turbomachine generally involves two types of unsteady flows, namely, a periodically unsteady flow and a turbulent flow. In order to measure the periodically unsteady total pressure, the fast-response total-pressure probe signal was periodically sampled (once per revolution) and averaged. As more electronically averaged periodic signals are arithmetically averaged, the influence of the turbulent component will be reduced because of its random nature. A relation between the standard deviation of the periodic sample average, σ, and the standard deviation of the random fluctuations, σ_n, given by Hirsch and Kool (1977) is

$$\sigma^2 = \frac{1}{N} \sigma_n^2 \qquad (3.1)$$

where N is the number of arithmetically averaged samples involved. An experiment was designed to yield a value of N that would give sufficient accuracy. The results of the experiment appear in Figure 3.1. A sample size of 250 was chosen since only small improvements on accuracy were seen for larger sample sizes. Therefore, the calculator/DVM sampled the electronically averaged periodic signal 250 times, once every 0.12 second, and then arithmetically averaged these 250 values to obtain one periodic-average value. This process took approximately 30 seconds during which time about 700 fast-response total-pressure samples were taken to produce the electronically averaged signal.

3.2. Static Calibration

The relationship between the fast-response probe transducer output voltage and a steady probe input pressure was determined by a static calibration using the air nozzle described earlier. The plenum pressure measured by a precision water-in-glass manometer was used as the total pressure at the nozzle exit since no measurable difference could be found between the two. The probe sensitivity data were then obtained by placing the probe 0.25 nozzle orifice diameters downstream from the nozzle exit with zero pitch and yaw angle. A voltage step was measured for a sudden change in input pressure by a circuit similar to the fast-response measurement system already described. The band-pass filter was replaced by a low-pass filter with a cut-off frequency of 20 Hz and the

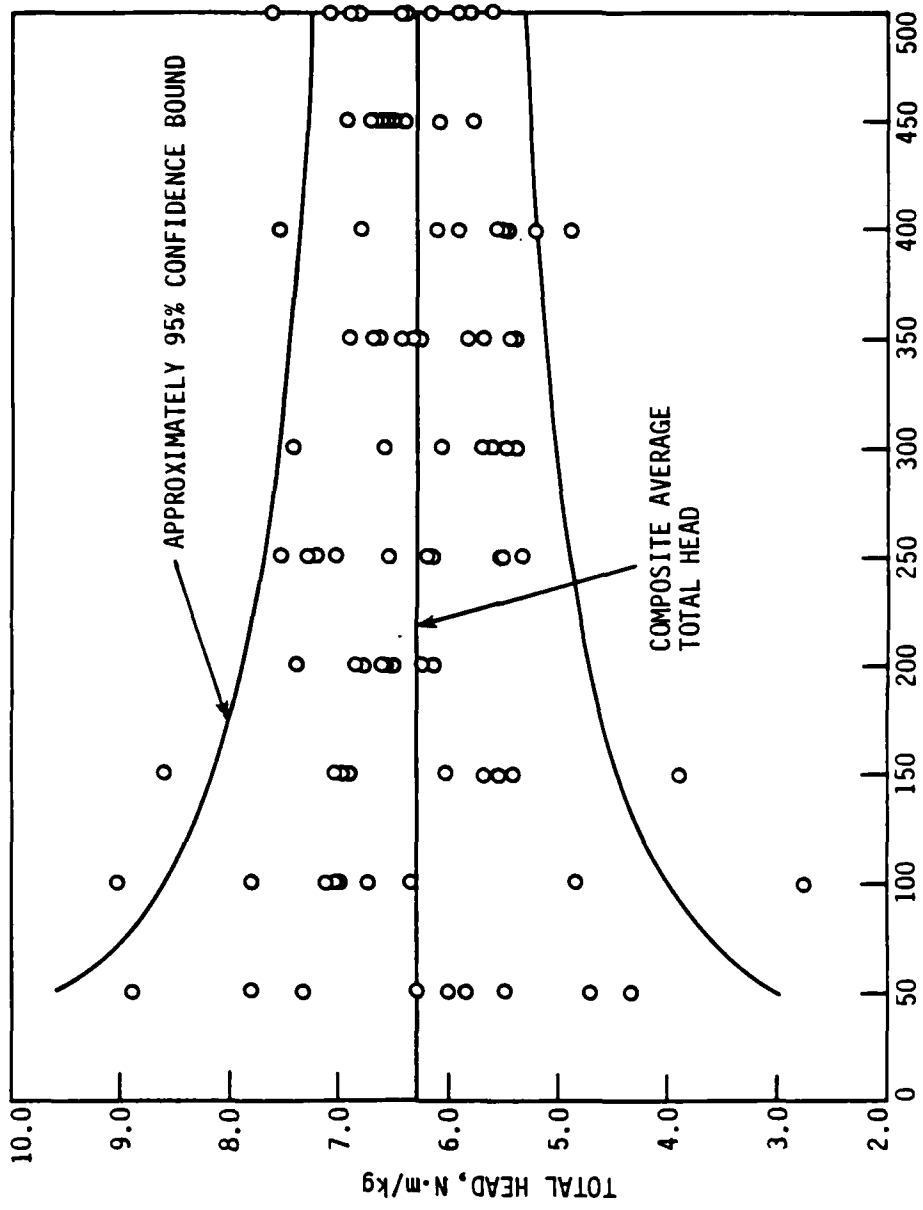

Figure 3.1. Variation of periodic-average values of total head for different sample sizes.

0.01 pf capacitor was removed to allow the DC voltage to be measured. The signal averaging low-pass filter was also removed since it attenuated the change in DC voltage. By using changes in pressure and voltage with constant nozzle air temperature, the long-term zero drift problem was completely avoided. Figure 3.2 shows a linear calibration for a nozzle air temperature of 21.7°C.

3.3. Dynamic Calibration

The measurement of high frequency, time varying, total-pressure fluctuations requires the knowledge of the frequency response characteristics of the measurement system involved. The fast-response probe should be able to respond to the fluctuations it is required to measure. Other electronic components in the system, such as amplifiers and/or filters, should also be able to respond to the fluctuations.

The fast-response total-pressure probe used presently may be considered to respond approximately as a lightly damped second-order system. Using the second-order system equations of Beckwith and Buck (1973), an undamped second-order system can be shown to have an amplitude ratio with an error greater than 5% (about 0.42 db) when the frequency is over 21.8% of the natural frequency. Therefore, an undamped or very lightly damped fast-response total-pressure probe should not be used in measurements where frequencies greater than 20% of the probe's natural frequency are important. Some efforts have been made to extend this useful frequency limit by increasing the natural frequency of a probe. For example, Delio, Schwent, and Cesaro (1949), in an effort to increase the

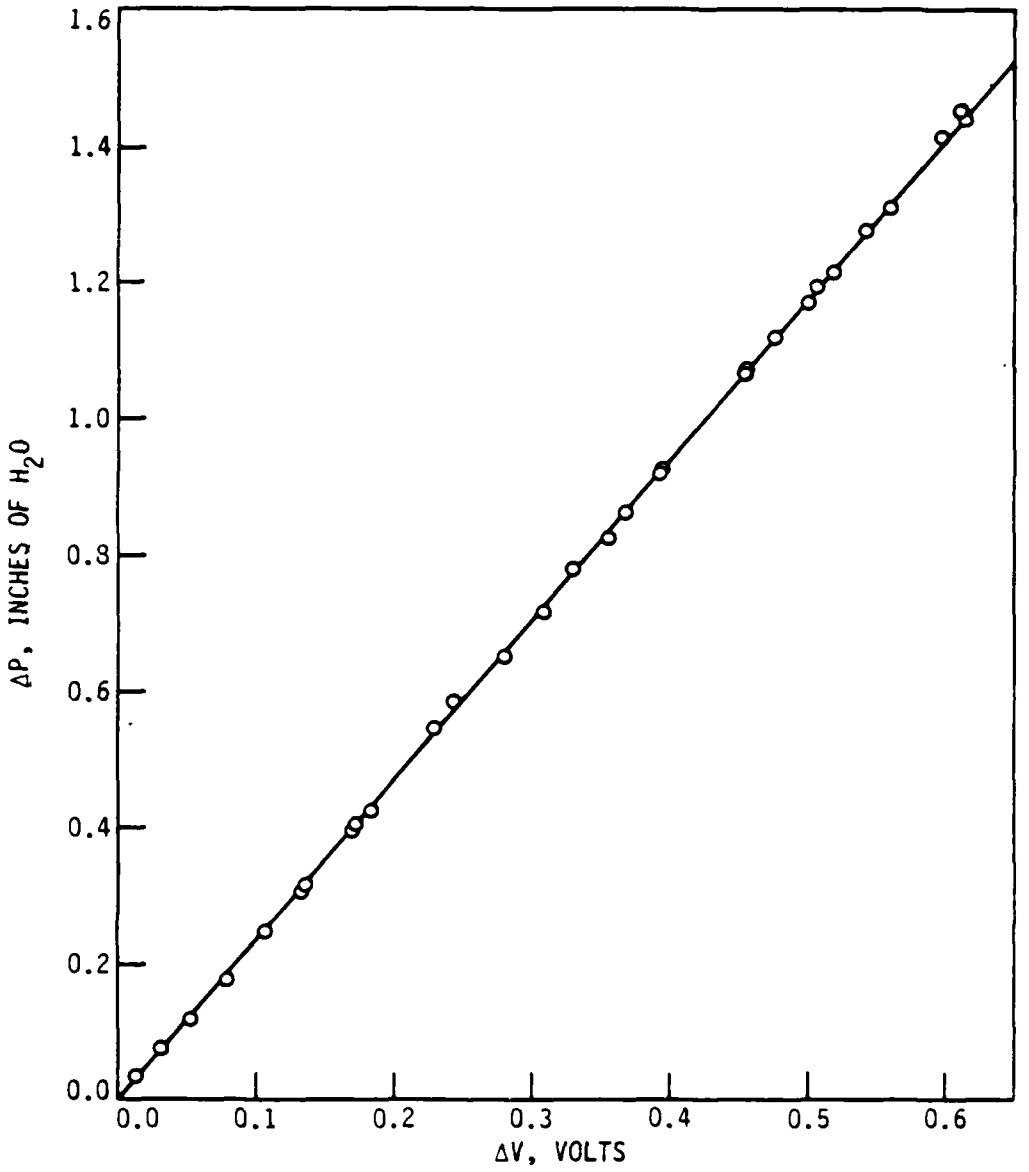

Figure 3.2. Typical sensitivity calibration curve.

natural frequency of their probe, increased the radius of the tube upstream of the pressure-sensing transducer. This effort, however, resulted in a lower damping ratio.

Another important method of extending the useful frequency range of the probe involves increasing the damping of the probe. Assuming an allowable 5% error in amplitude, calculations show that the useful frequency range of a second-order system can be extended to 57.3% of the natural frequency with an optimum damping ratio of 0.707. This agrees with the assertion of Fleeger and Seyb (1975) that the useful frequency range can be extended to 50% of the natural frequency if care is taken to dampen the transducer properly. With this in mind, Delio, Schwent, and Cesaro (1949) claimed that the insertion of an orifice, a wire mesh, or some other fluid restriction would enable them to increase the damping ratio without decreasing the natural frequency. Methods of changing the probe geometry in order to increase damping may decrease the natural frequency and actually decrease the useful frequency range. One successful method of changing the probe geometry to extend the useful frequency range was used by Atkins (1974). This method was to decrease the ratio of cavity volume to tube volume. Siddon (1969) used loose cotton plugs in front of his pressure transducer to provide some viscous damping in his static-pressure probe.

Siddon (1969) found that mechanical damping was insufficient to reduce resonance. The remaining resonance effect was eliminated using a simple tuned L-C rejection filter. Low-pass filtering to remove diaphragm resonance has also been used successfully by Fischer (1971), Robinson (1972), and Junkhan (1973). Cook and Rabinowicz (1963) suggest

a method of designing a properly matched, compensating "notch filter" to extend or improve the frequency response of a second-order system. They caution that a poorly matched electronic second-order compensating network could produce poorer response characteristics. Further problems can occur if mechanical or electronic damping is used to extend the useful frequency range of a second-order system. Nyland and Anderson (1971) and Atkins (1974) point out that damping introduces a higher phase shift which may not be acceptable. Fischer (1971) further points out that waveform distortion might accompany this phase shift. He also claims that it may be hard to maintain a constant damping ratio when damping is added to probes being used in turbomachines.

Knowledge of the probe's natural frequency and damping ratio is essential in order to obtain the useful frequency range of the probe. However, this is not sufficient information for determining if a probe can accurately respond to a particular wake form. Junkhan (1974) pointed out that the minimum required natural frequency for a total-pressure probe can be estimated as a function of the pressure difference, the ratio of blade spacing to wake width, and the blade passing frequency. He further said that the slope of the pressure-time input to the probe has a strong effect on the transient error for a fast-response probe. Siddon (1969) felt that transducers must have a frequency response compatible with the dominant spectral content of the unsteady components of the instantaneous values of pressure and velocity.

Our research on probe response indicates that the ability of a fast-response total-pressure probe to respond to a particular turbomachine blade wake total-pressure distribution is a function of the natural

frequency of the probe, the damping ratio of the probe, the blade passing frequency, and the harmonic content of the wake. The harmonic content is consistent with the parameters mentioned by Junkhan (1974). Gallus, Lambertz, and Wallmann (1979) suggest that the harmonic content of a wake is primarily a function of the wake width to blade spacing ratio and the wake to freestream pressure difference as shown in Figure 3.3. Their model shows that only the first few harmonics diminish slowly. The frequency of the largest important harmonic of a wake should be within the useful frequency range as determined by the natural frequency and the damping ratio of the probe.

Figure 3.4 shows how a fast-response probe would respond to some idealized wakes if it were modeled by a second-order system on an analog computer. Calculations involved ratios of natural frequency to blade passing frequency, ω_n/ω_b, of 50, 25, 10, 5, and 2 for a ratio of blade spacing to wake width, K, of 2.21. When the damping ratio, ξ, is 0.005 -- or in other words, when the system is nearly undamped -- the response becomes entirely unacceptable for $\omega_n/\omega_b \leq 10$. For this case only two harmonics lie in the useful frequency range (about $\omega_n/\omega_b \geq 5$) which is not enough for the probe to respond adequately. When the probe damping ratio is increased to $\xi = 0.100$, the useful frequency range is not altered significantly. However, the amount of amplification occurring at resonance is not as great and the response is still tolerable in this case for $\omega_n/\omega_b = 10$. If the probe damping ratio could be increased to the optimum value of $\xi = 0.707$, the useful frequency range would be extended to $\omega_n/\omega_b \geq 2$. The response is acceptable for $\omega_n/\omega_b \geq 2$ where all the harmonics except the first are attenuated. Figure 3.5 shows the

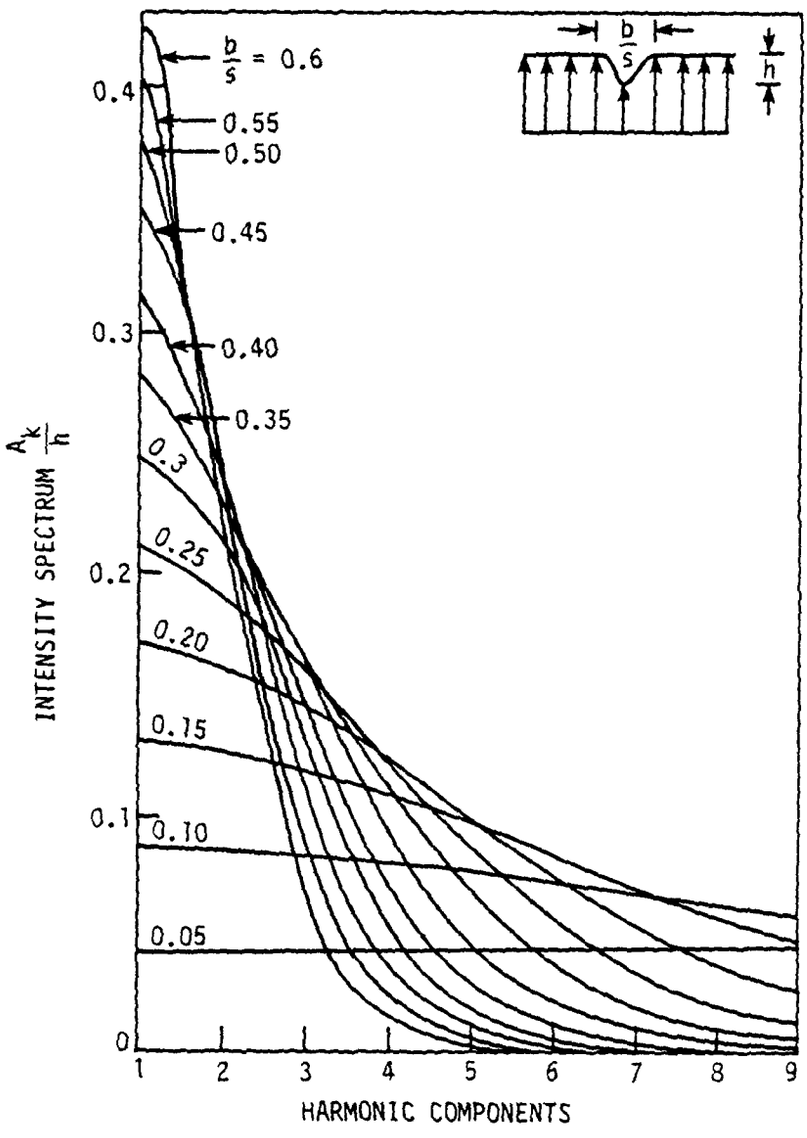

Figure 3.3. Harmonic analysis of a wake given by an idealized functio- of the two parameters h and b/s (from Gallus, Lambertz, and Wallmann (1979)).

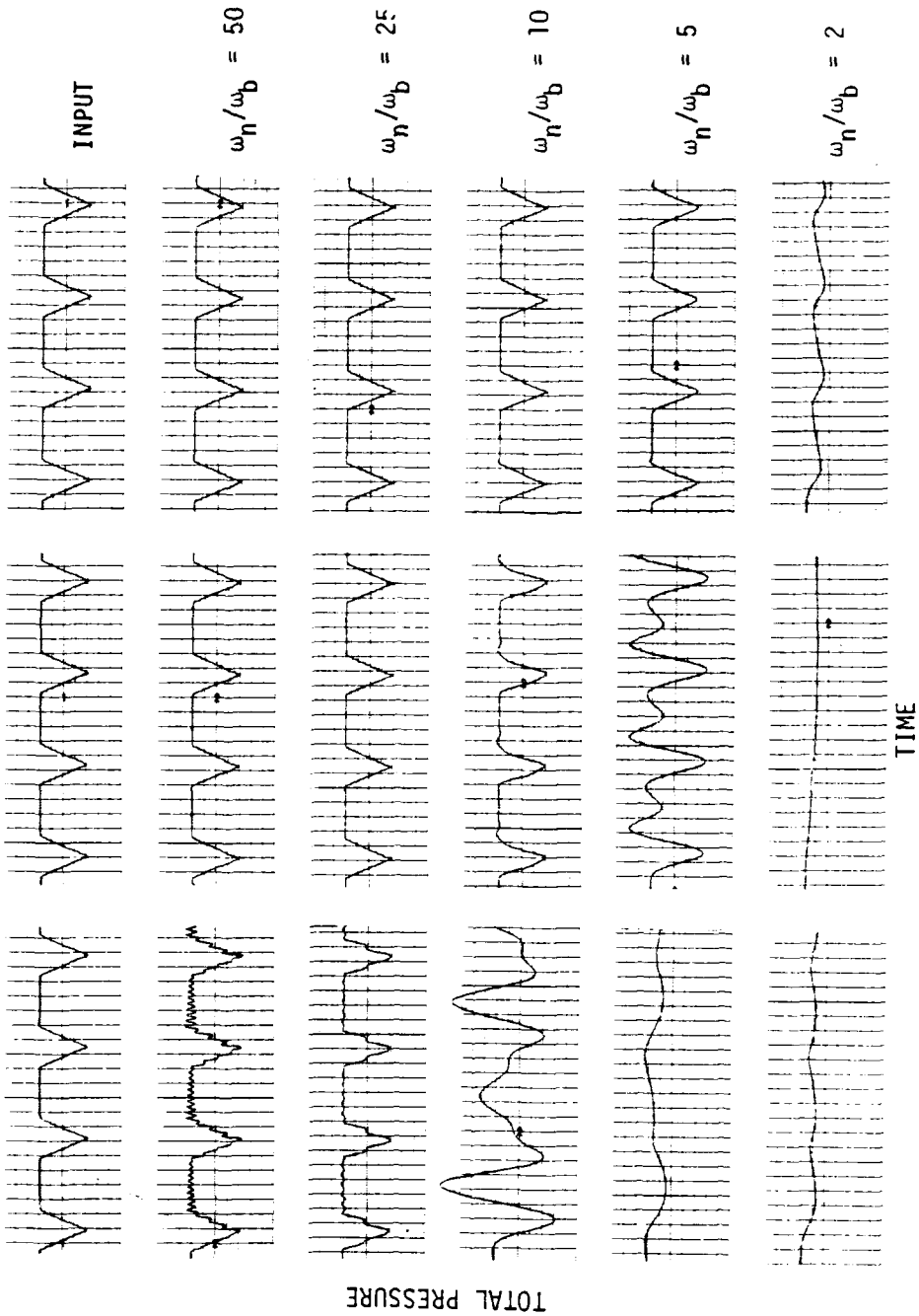

(a) ξ = 0.005. (b) ξ = 0.100. (c) ξ = 0.707.

Figure 3.4. Response of a second-order system to an idealized wake input with K = 2.21.

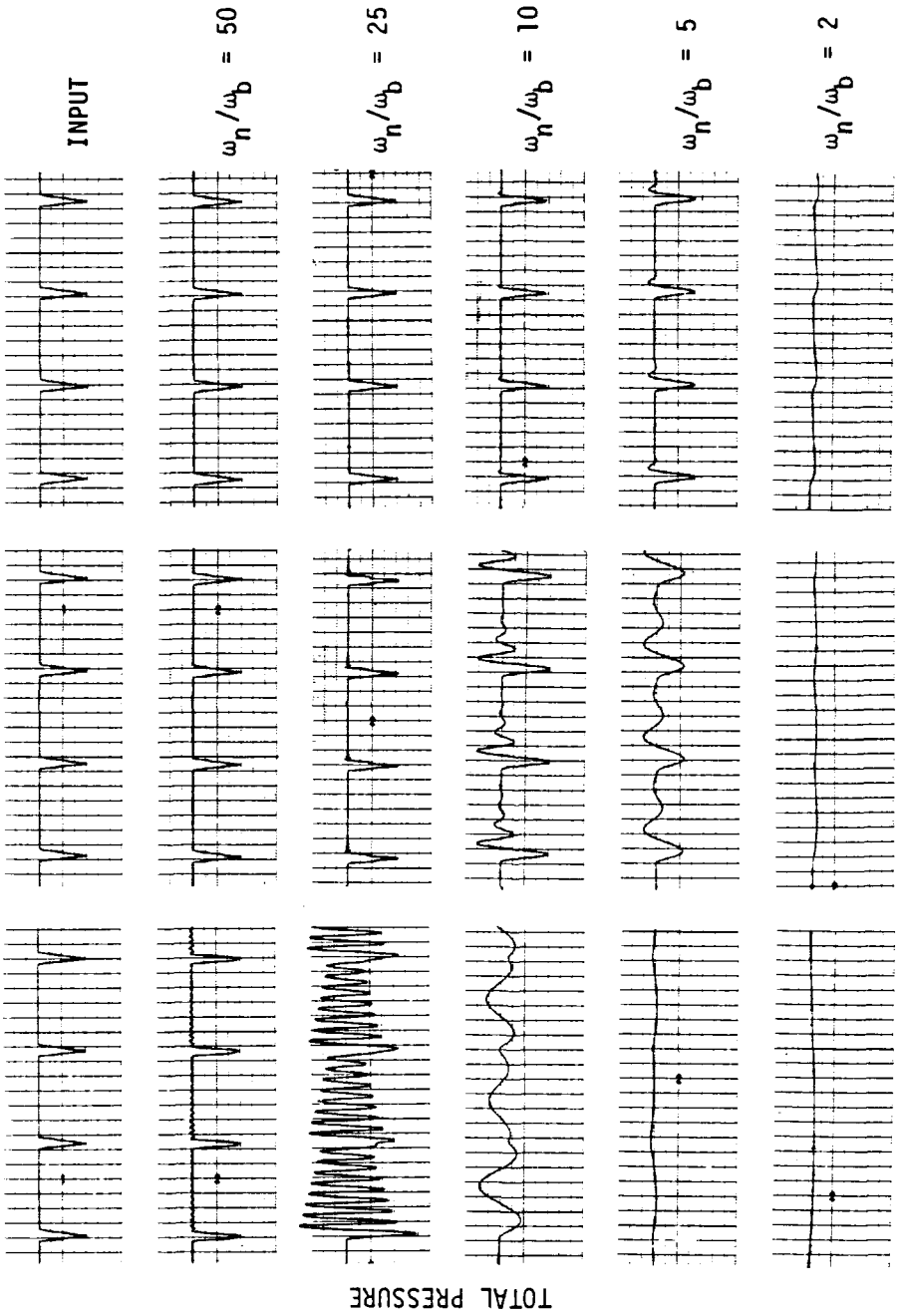

(a) ξ = 0.005. (b) ξ = 0.100. (c) ξ = 0.707.

Figure 3.5. Response of a second-order system to an idealized wake input with K = 7.29.

same sequence of responses for a blade spacing to wake width ratio of 7.29. This type of wake involves more harmonics than the one in Figure 3.4. The frequency response curve is required to be flatter since more harmonics are important. This results in the responses for K = 7.29 being worse than those for K = 2.21. Responses that were tolerable for $\xi = 0.005$ and $\omega_n/\omega_b = 25$ and for $\xi = 0.100$ and $\omega_n/\omega_b = 10$ when K = 2.21 are no longer tolerable when K = 7.29.

After a probe has been found that will adequately respond to the type of wakes to be measured, it is important to check the response of the rest of the measurement system. When amplifiers are added to multiply the transducer output voltage and/or when filters are added to remove noise or help dampen the probe response, the response curves of these devices must be checked to insure that the useful frequency range has not been altered to the point where the important harmonics of the wakes are being severely amplified or attenuated. Figure 3.6 shows how a low-pass filter responds to an idealized wake. The cut-off frequency (the frequency where the relative amplitude is -3 db) is set at each of the first eight harmonics. As the cut-off frequency setting is increased, the resulting amplitude, phase angle, and wave shape are improved because fewer harmonics are being attenuated.

The frequency response characteristics of the probe used in this research project were approximated from a dynamic calibration using a shock tube to approximate a step input of total pressure. A shock moving at a Mach number of 1.08 provided a sudden total-pressure ratio of 1.208 to the transducer. Two thin film gages were used to measure the speed of the shock. The second gage was also used to trigger an

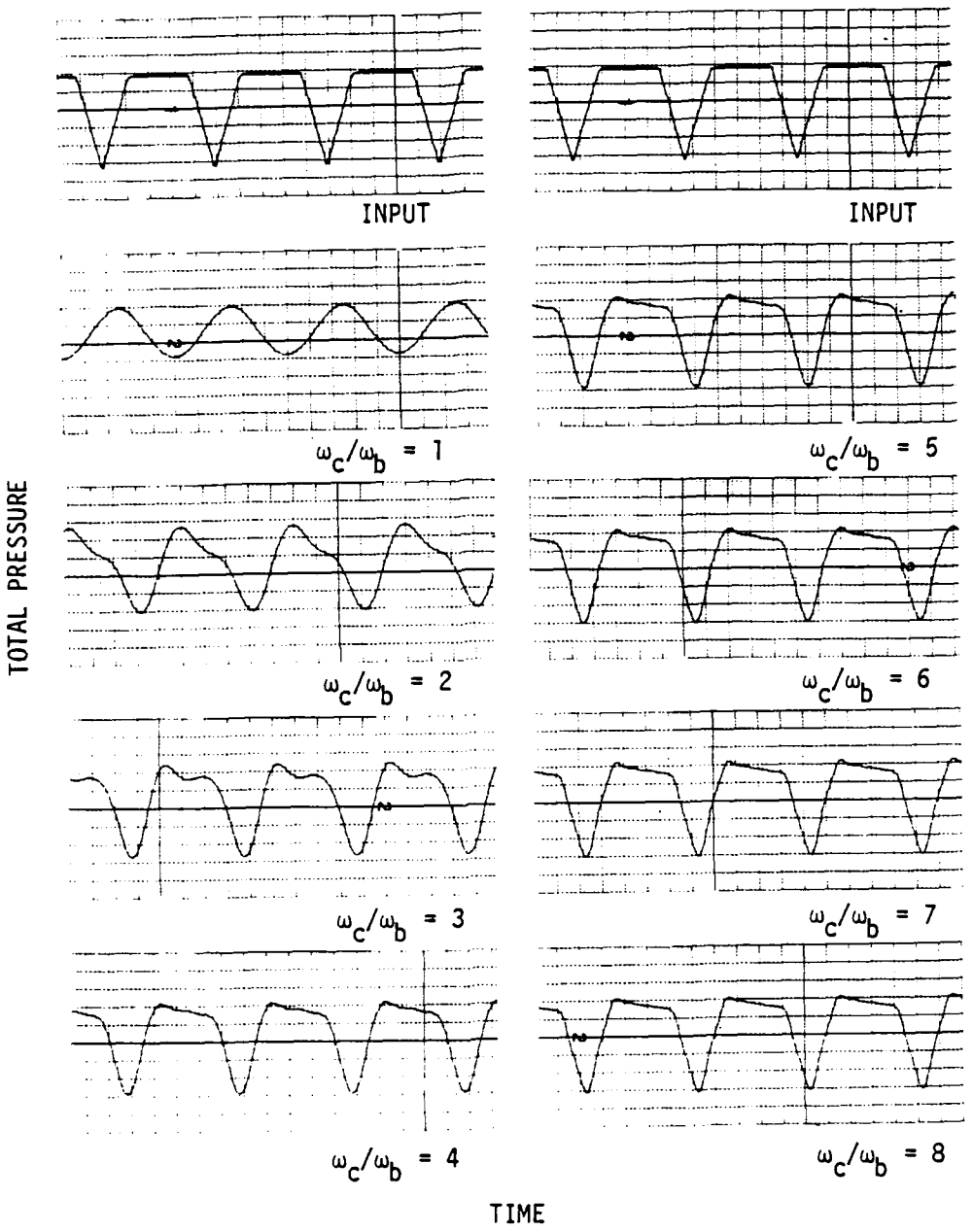

Figure 3.6. Response of a low-pass filter to an idealized wake input.

oscilloscope fitted with a camera. A time delay circuit was used to insure that the recording equipment was started a few μseconds before the shock reached the probe. A photographic record of the probe's response to the shock was then obtained by holding the camera shutter open and setting the oscilloscope to give a single sweep when triggered. A schematic of the electronic data acquisition system is shown in Figure 3.7. In order to obtain the frequency response of the probe itself, the oscilloscope recorded only the output from the probe alone without the amplifier and the filter normally used.

Typical voltage-time traces of the probe response to a step input are shown in Figure 3.8. These traces pose a problem in calculating the probe response characteristics through approximation as a second-order system. Although in the limiting case of an undamped second-order system the largest overshoot possible is twice the size of the step, the overshoot observed was even larger. The frequency response data of a fast-response total-pressure probe designed by Junkhan (1973) suggest a means for explaining this apparent inconsistency. The position of the transducer in Junkhan's probe tip, as shown in Figure 3.9, resulted in the natural frequency of the probe system being much less than the natural frequency of the transducer. The response of this probe to a step input shows the relationship of the probe system natural frequency to the transducer natural frequency (see Figure 3.10). This voltage-time trace reflects the addition of the low probe system natural frequency (about 8 kHz) to the high transducer natural frequency (about 125 kHz). The design of the probe used in this research project resulted in the natural frequency of the present probe system being nearly the same as

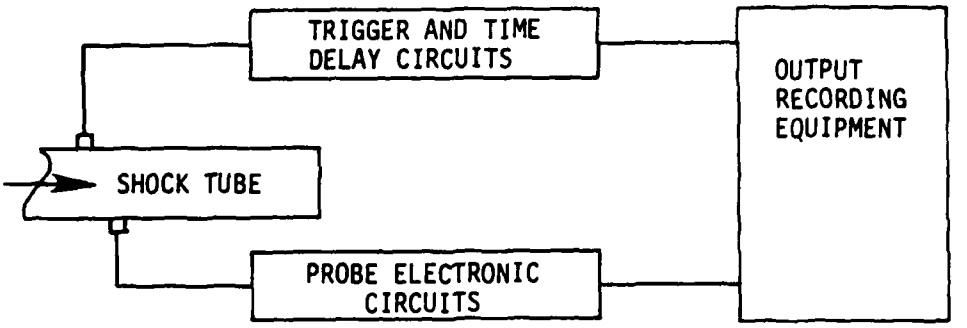

(a)

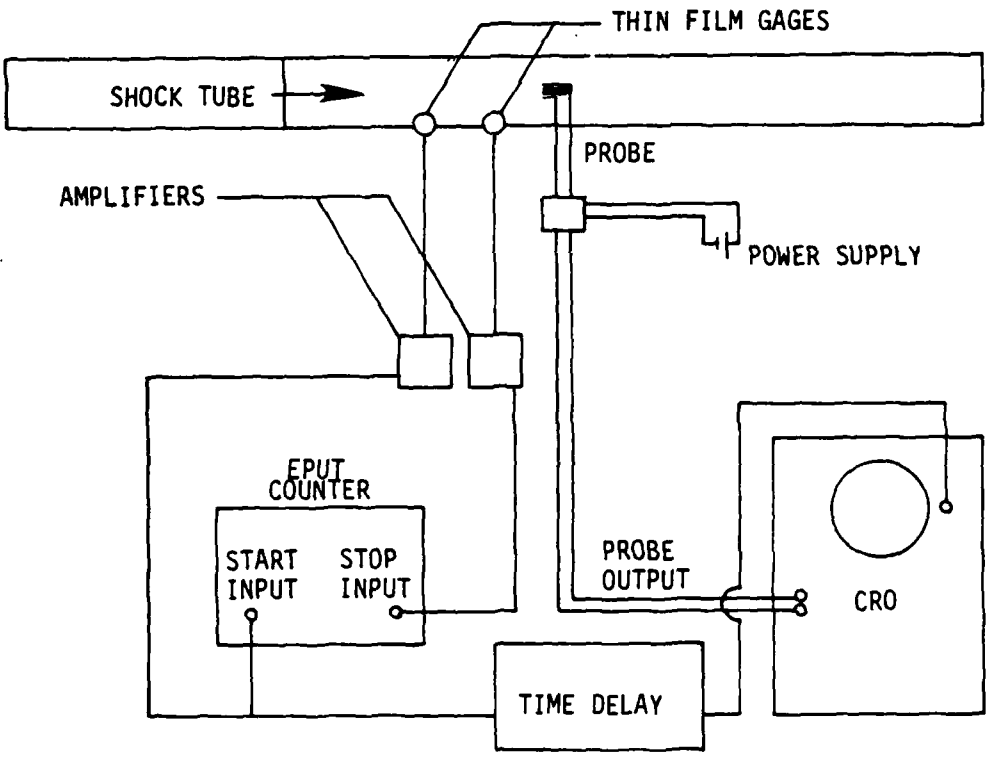

(b)

Figure 3.7. Shock tube electronic data acquisition system: (a) probe output recording system; (b) shock speed measurement and probe output recording system.

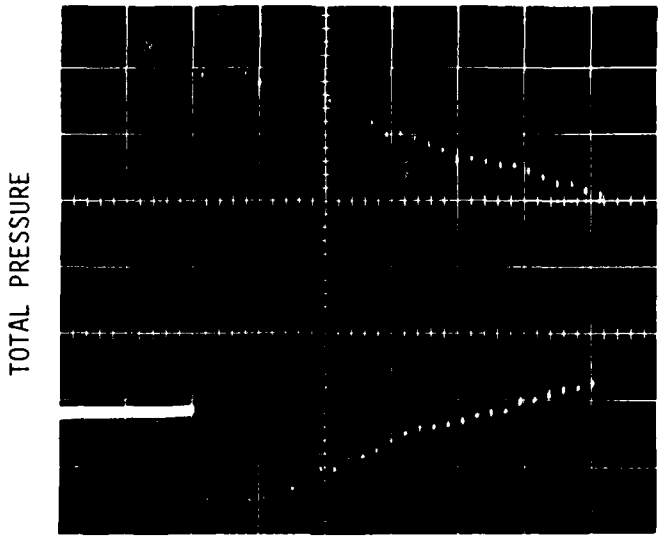

(a) Sweep time sensitivity = 50 μs/ cm, vertical sensitivity = 20 mV/cm.

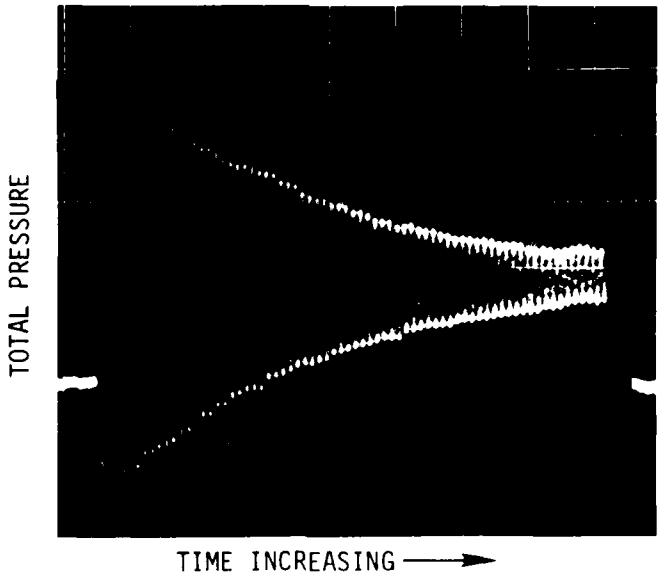

(b) Sweep time sensitivity = 100 μs/cm, vertical sensitivity = 20 mV/cm.

Figure 3.8. Typical traces recorded by an oscilloscope from the response of the fast-response total-pressure probe used in this research project.

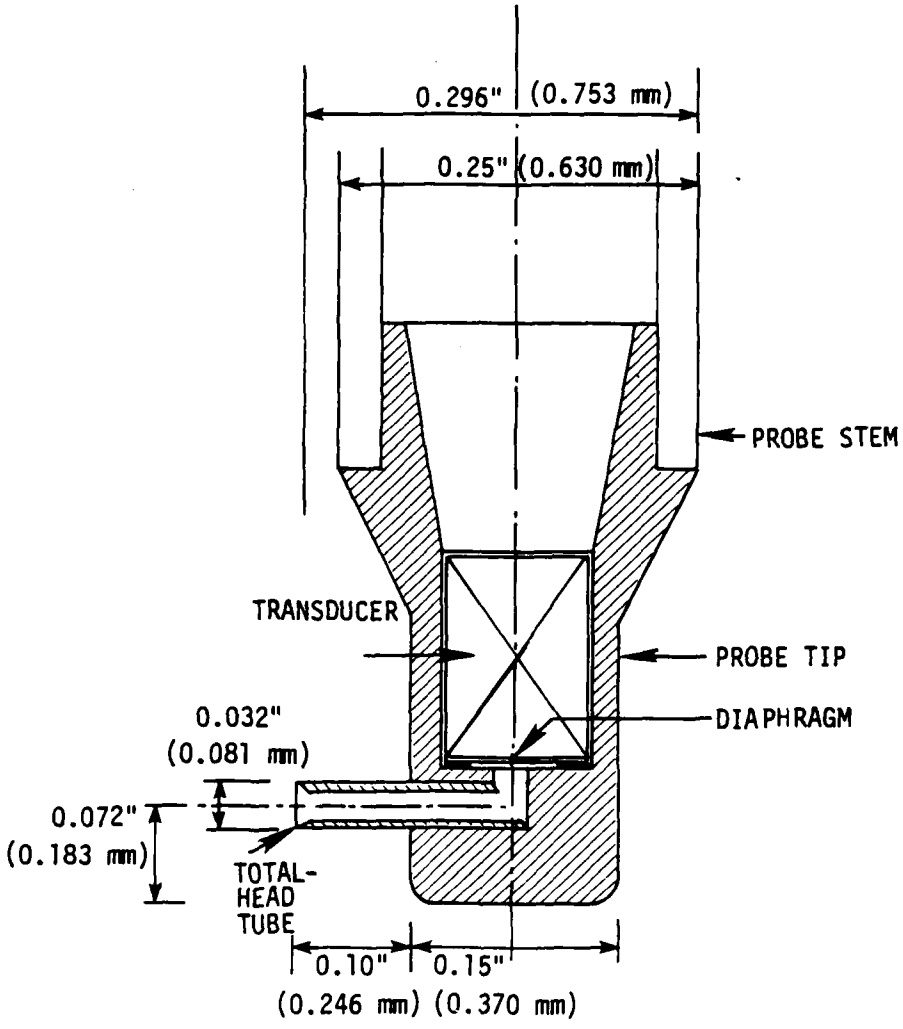

Figure 3.9. Probe tip designed by Junkhan (1973).

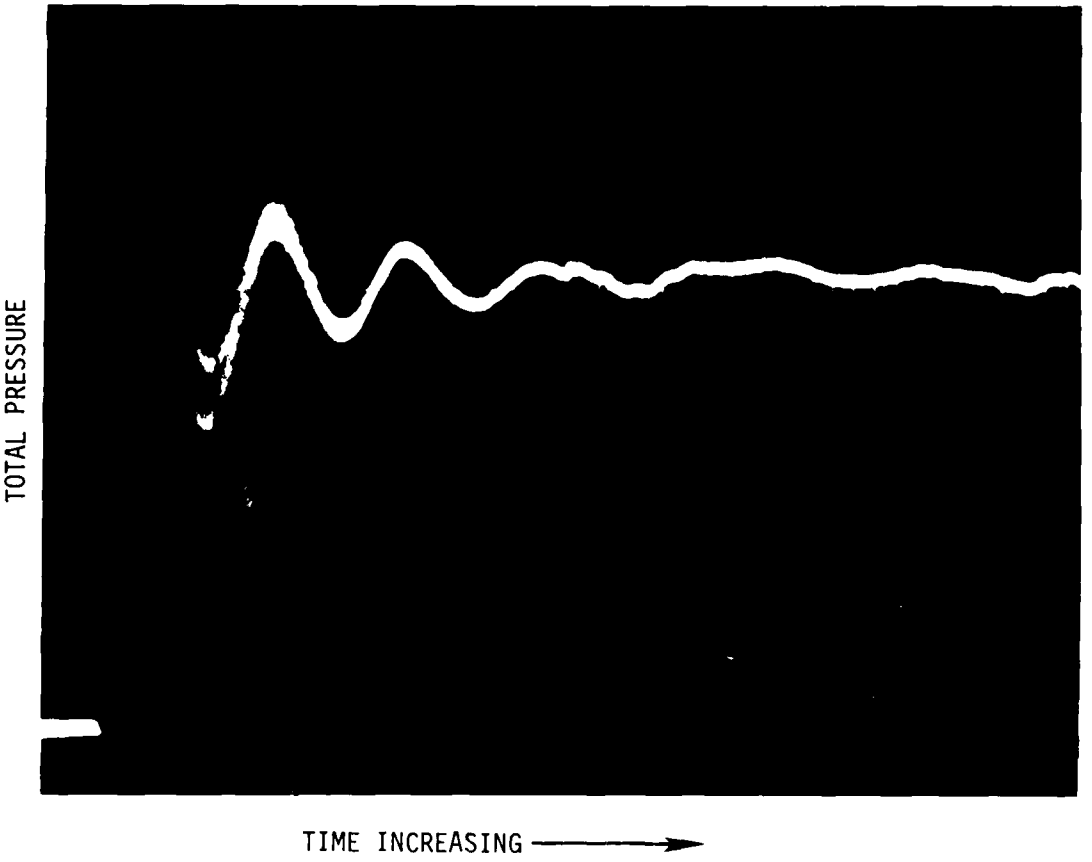

Figure 3.10. Typical trace recorded by an oscilloscope from the response of Junkhan's probe: sweep time sensitivity = 100 μs/cm, vertical sensitivity = 5 mV/cm.

the natural frequency of the transducer. The addition of the two waveforms having similar frequencies can look like the traces in Figure 3.8.

The damping ratio of the probe was difficult to estimate because the observed traces contained two similar waveforms. After an initial estimation using the logarithmetic decrement method and some speculation on how the two waveforms might be summed, a reasonable solution was obtained. It was found that a probe with a damping ratio of 0.009 and a natural frequency of 94 kHz and a transducer with a damping ratio of 0.003 and a natural frequency of 94 kHz would combine to give a result quite similar to the one obtained experimentally. Figure 3.11 shows the envelopes of the ringing for the probe and for the transducer. Since the natural frequencies are the same, the ringing envelopes can be added. The results of this addition and the similar ringing envelopes of the experimental data are also shown in Figure 3.11.

Finally, the response curves of the differential amplifier and the band-pass filter were obtained. These response curves are shown with the response curve for the fast-response probe in Figure 3.12. The amplifier response attenuates all of the harmonics of the wake except the first. The total-pressure data taken in this project were measured far enough from the trailing edge of the blades that the first harmonic should have been dominant. Ravindranath and Lakshminarayana (1979) show that the first harmonic is clearly more significant than the larger harmonics in their wake measurements.

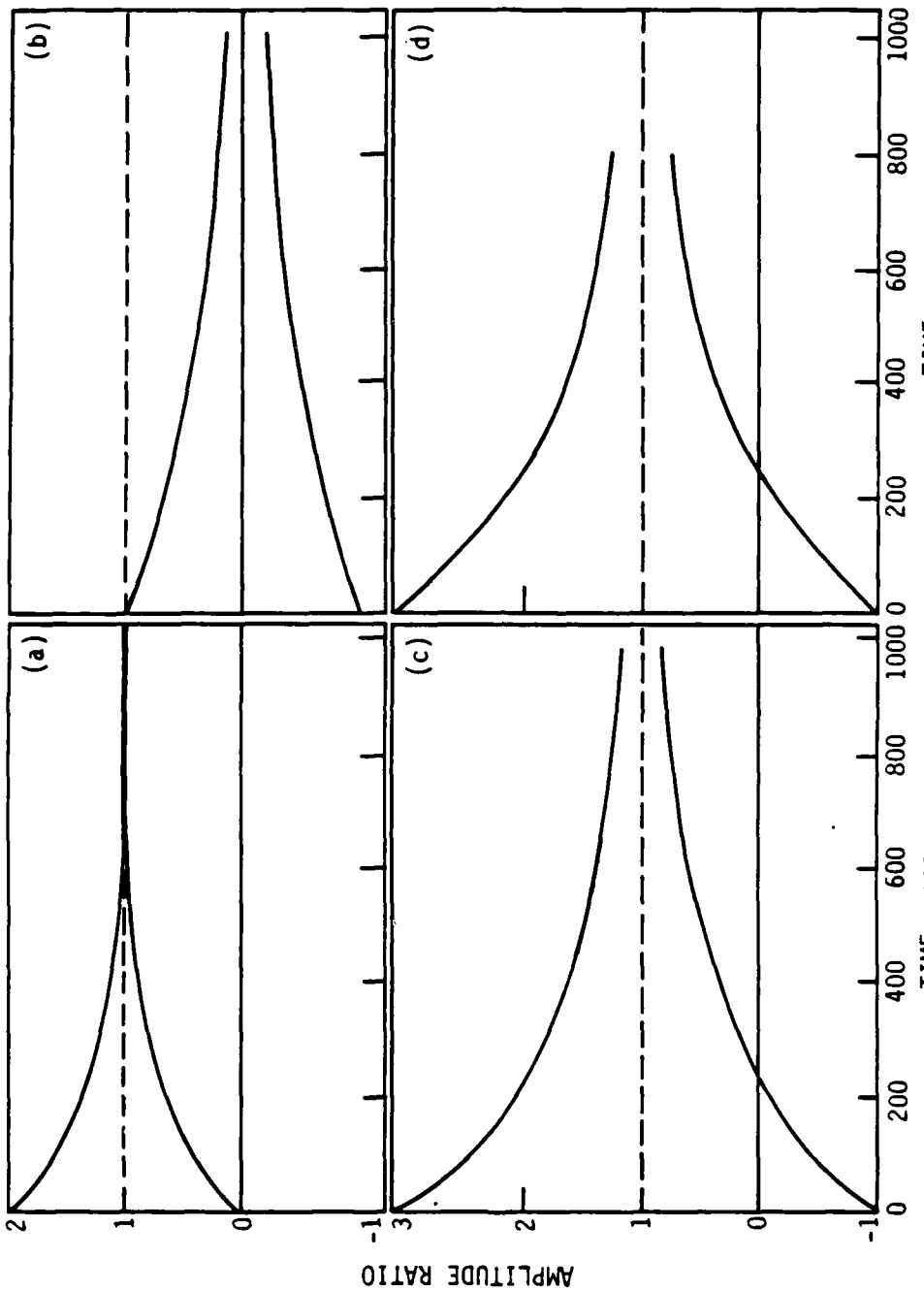

Figure 3.11. Oscillation envelopes for the amplitude frequency response of a second-order system to a unit step: (a) probe response, f_n = 94 kHz, ξ = 0.009; (b) transducer response, f_n = 94 kHz, ξ = 0.003; (c) addition of probe response and transducer response; (d) experimental response.

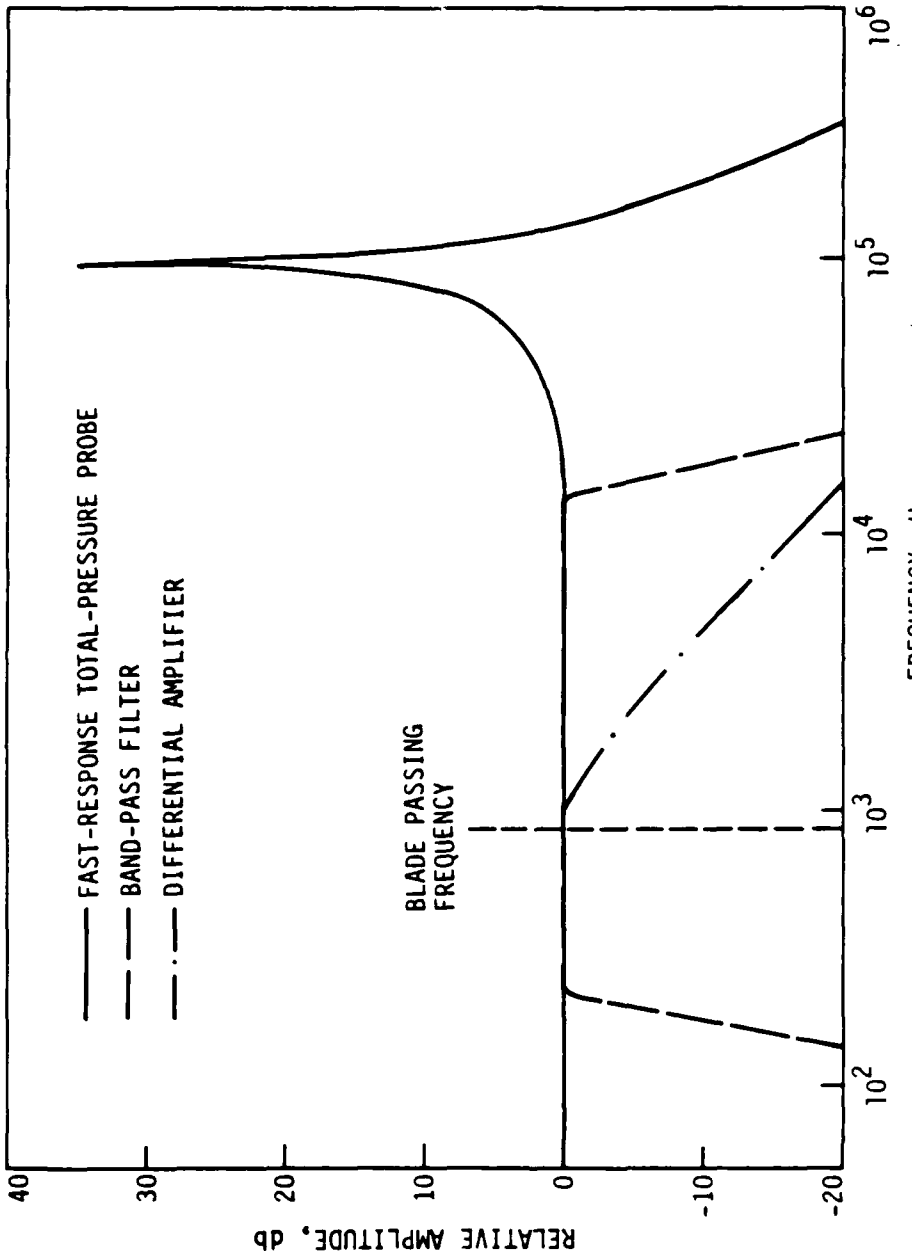

Figure 3.12. Amplitude frequency response of the measurement system.

3.4. Data Acquisition

Periodic-average total-pressure data were acquired at six rotor sampling positions (over one rotor blade-to-blade spacing) for each of five spanwise locations (10%, 30%, 50%, 70%, and 90% passage height from hub) behind the first rotor and stator rows and one spanwise location behind the second rotor row. For each one of these rotor sampling positions, data were obtained at twenty-one circumferential positions over one spacing between two adjacent stator blades. All of the data were obtained with the compressor operating at 1400 rpm with a flow coefficient of 0.42. This operation point can be seen on the research compressor performance map in Figure 3.13.

Several preliminary steps were needed in order for measurements to be made in the compressor. All of the instruments were allowed to warm up for thirty minutes. The manometer used to measure the pressure difference across the venturi flow meter was zeroed. The probe yaw angle and circumferential position potentiometers were calibrated and the flow coefficient was set. Finally, the probe was immersed into the compressor at the proper radial position. In order to zero the periodic rotor sampling position, it was necessary to position the photoelectric pickup at zero and then adjust the variable triggering delay. The desired rotor sampling position was then set.

Initial testing of the fast-response total-pressure probe showed that despite the internal chamber the probe did show some sensitivity to changes in flow direction. These tests showed that for changes of ten degrees in the yaw angle, the probe readings varied about 5 N·m/kg.

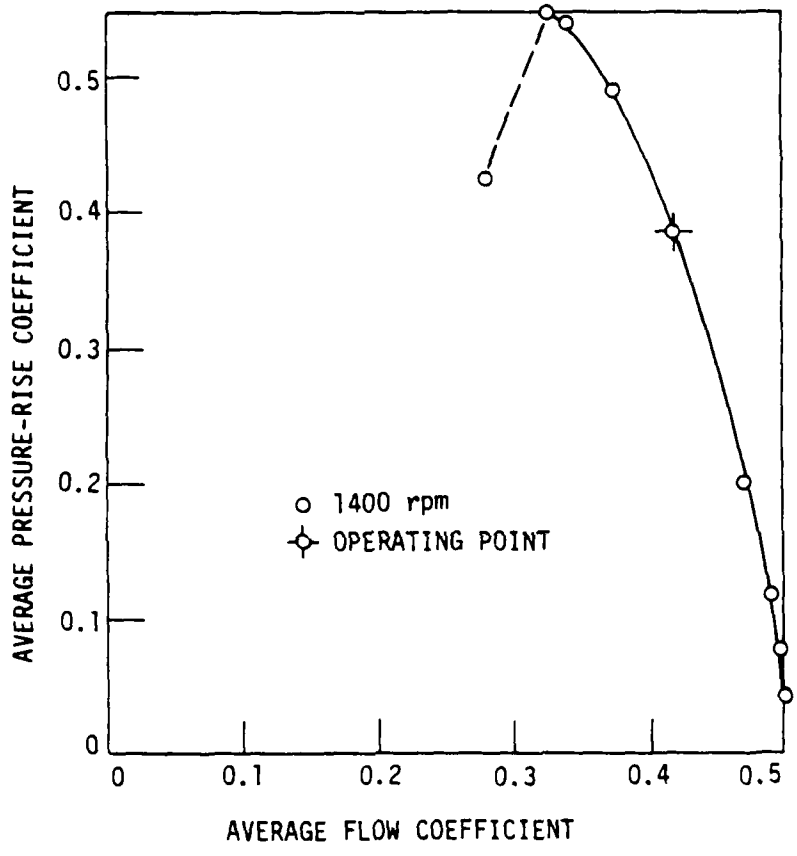

Figure 3.13. Research compressor performance curve and operating point.

Since time-average flow angles could vary by as much as twenty-five degrees from the periodic-average flow angles, periodic-average flow angles were needed for each circumferential position. The periodic-average flow angles were obtained from the hot-wire measurements of Schmidt et al. (1978).

The periodic-sampling and averaging technique was then used to measure the fluctuating total pressure as explained previously.

3.5. Data Reduction

The alternating output voltage of the fast-response total-pressure probe represented the fluctuating total pressure. This voltage, which is actually the difference between the absolute values of alternating voltage and time-average voltage, was related to the difference between the fluctuating total pressure and the time-average total pressure by the probe sensitivity determined in the static calibration. The absolute total-pressure values were obtained by adding the fluctuating total-pressure and the time-average total-pressure values. All of the total-pressure values were expressed in terms of total-head units, N·m/kg. The final values of absolute total head were thus found by the following equation:

$$\tilde{H}_{TPP} = \tilde{H}_{tH_2OYH_2O} \Big/ \rho_{air} g + \overline{H} \qquad (3.2)$$

Equations for basic fluid properties are given below:

Barometric pressure, N/m^2

$$P_{atm} = h_{hg@t_{baro}}\left[1.0 - 0.00018(t_{baro} - 273.5)\right]\gamma_{hg@273^oK} \quad (3.3)$$

Density of air, kg/m^3

$$\rho = P_{atm}/Rt \quad (3.4)$$

Specific weight of water, N/m^3

$$\gamma_{H_2O} = g/g_c\left[996.86224 + 0.1768124\left(\frac{9}{5}\,t - 459.67\right) - 2.64966 \times 10^{-3}\left(\frac{9}{5}\,t - 459.67\right)^2 + 5.00063 \times 10^{-6}\left(\frac{9}{5}\,t - 459.67\right)^3\right] \quad (3.5)$$

During the analysis of the data, which will be presented in the next section, it proved useful to compare the measured data to data obtained by calculation from hot-wire data (Schmidt et al. (1978)) taken in the same compressor at the same operating conditions. The hot-wire data were used to calculate a periodic-average total-head value by addition of the dynamic head, h_d, and the static head, h, assuming constant static pressure at any radial location. The dynamic head could be obtained from the hot-wire data as follows:

$$h_d = \frac{1}{2}\,V^2/g_c \quad (3.6)$$

Schmidt and Okiishi (1976) determined the static head values at each axial station by using outer wall static pressure tap data and the radial equilibrium equation. This assumes that the static head was constant circumferentially at a particular radial position, which is not necessarily correct. The method does provide some data for comparison purposes, however.

4. PRESENTATION AND DISCUSSION OF DATA

The periodically unsteady total-pressure data will be presented and discussed in this section. The discussion of these data involves the consideration of flow in wake, wake segment, and wake-free (free-stream) flow regions. Therefore, a review of how flow field variables are affected as chopped wake segments move through downstream blade rows and interact with downstream blade wakes will be presented first.

4.1. Turbomachine Wake Transport and Interaction

When the wakes of an upstream blade row are periodically chopped by a downstream blade row, the fluid in these chopped wake segments is subsequently transported through the downstream blade row. The kinematics of wake transport and interaction has been established through the work of Meyer (1958), Lefcort (1965), Smith (1966), Kerrebrock and Mikolajczak (1970), Brandone and Bernard (1971), Walker and Oliver (1972), Lockhart and Walker (1974), Wagner and Okiishi (1977), and Gallus, Lambertz, and Wallmann (1979). As a wake segment impinges onto the pressure surface of a chopping blade, its motion relative to the chopping blade results in a tendency for the wake segment fluid to move toward the impacted pressure surface as the segment is transported downstream. This tendency of the wake segment fluid to move toward the pressure side of a chopping blade can also be seen in terms of a so-called "slip velocity" (Kerrebrock and Mikolajczak (1970)) as demonstrated in the simple velocity polygons in Figure 4.1. It should be understood that these polygons are somewhat idealized. For example,

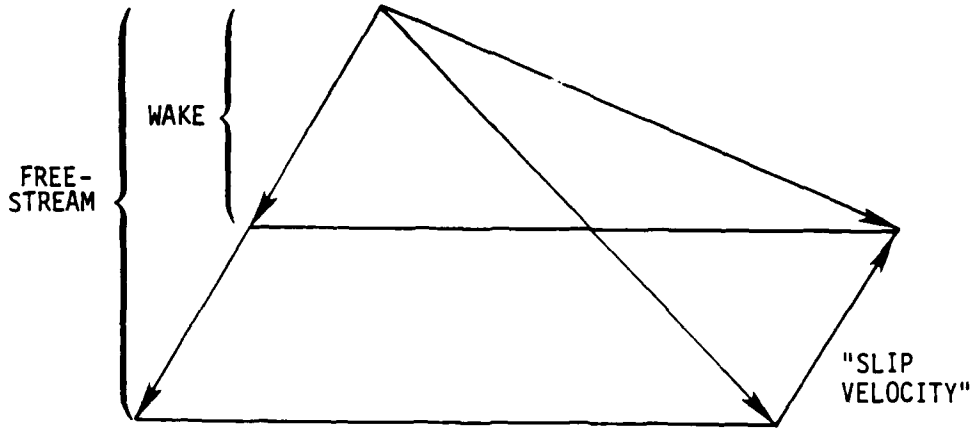

(a) "Slip velocity" of IGV wake fluid at rotor entrance (IGV exit).

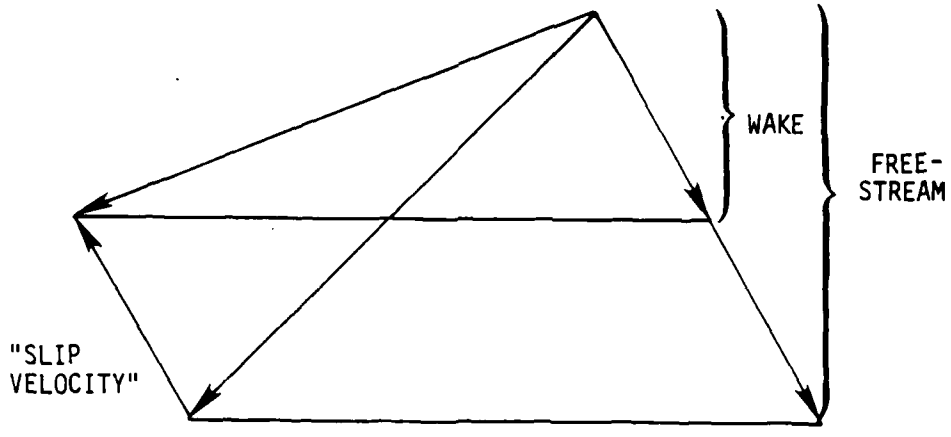

(b) "Slip velocity" of rotor wake fluid at stator entrance (rotor exit).

Figure 4.1. Relative velocity of wake segment fluid.

the velocity polygon in Figure 4.1b is simplified in that it suggests that the relative flow angles for rotor wake and freestream flow particles are the same. These rotor exit relative flow angles can actually vary when the rotor is not the first blade row in the machine as shown by Wagner and Okiishi (1977). Their data indicate that as chopped IGV wake segments left the rotor blades, they interacted with the rotor wakes. Using the same terminology as Wagner and Okiishi (1977), an "interacted wake situation" occurs when the rotor wake/IGV wake interaction takes place slightly upstream or at the measurement plane. Similarly, a "noninteracted wake situation" occurs when the rotor wake/IGV wake interaction takes place downstream of the measurement plane. As the rotor blade moves tangentially, the chopped IGV wake segments move tangentially and axially, thus resulting in periodic occurrences of interacted and noninteracted rotor wake situations in the measurement window. Figure 4.2 shows how these wake interactions affected the rotor exit velocity polygons. The rotor wake velocity polygon is for a particle of fluid at the center of the rotor wake, while the freestream velocity polygon is for a fluid particle in a region of flow not affected by either rotor wakes or IGV wakes. In the case of a noninteracted rotor wake, the relative flow angle was smaller in the wake region than in the freestream, while the absolute velocity was larger in the wake region. For an interacted rotor wake, the results were just the opposite. In this case, the relative flow angle was larger in the wake region than in the freestream, while the absolute velocity was smaller in the wake region. Ravindranath and Lakshminarayana (1979) have taken data behind a rotor row with an IGV row farther (several

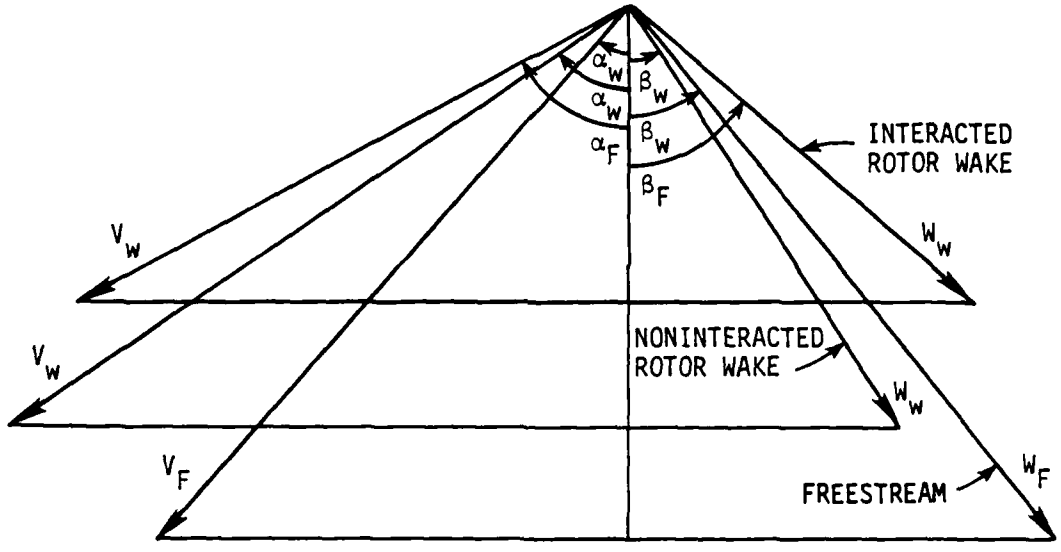

Figure 4.2. Plane velocity vector triangles for fluid in an interacted wake, a noninteracted wake, and freestream for first rotor exit flow at midspan.

chord lengths) upstream. In their situation, the effects of the IGV wakes were small behind the rotor row and wake interactions were almost nonexistent. Their data showed that the absolute velocities were larger and that the relative flow angles were smaller in the wake region as would be predicted from the noninteracting case mentioned above.

Fluid in chopped IGV wakes being transported through a rotor row resides in the blade row longer than the fluid in the freestream region. Thus, more energy is transferred to the wake region fluid than to the freestream fluid. More energy is also added to the slower moving rotor boundary layer fluid than to the freestream fluid. As this higher enthalpy IGV wake fluid is transported through the rotor blade row, it tends to pile up on the pressure surface of the rotor blades. The IGV wake fluid then appears with the higher enthalpy rotor boundary layer fluid in the rotor wakes giving the rotor wakes a definitely higher value of stagnation temperature than the freestream fluid. In a similar manner, this higher enthalpy rotor wake fluid tends to pile up on the pressure surface of stator blades as the rotor wakes are chopped and transported through a stator blade row. The rotor wake fluid then appears in the stator wakes giving them a higher value of stagnation temperature than the freestream fluid. The idea of high enthalpy wakes from an upstream rotor blade row appearing in the wakes of a downstream stator blade row was developed by Kerrebrock and Mikolajczak (1970). They used this wake transport model to explain the shape of measured transonic compressor stator exit stagnation-temperature profiles.

Kerrebrock and Mikolajczak (1970) also attempted to calculate the shape of stagnation-pressure profiles in a compressor. They found that

these profiles could not be easily determined. However, they did state that rotor wakes may have either an excess or a deficiency of stagnation pressure in comparison to freestream values. The difficulty in predicting total-pressure levels in a compressor is related to the fact that while total temperatures are dependent on work and heat transfer amounts but are not dependent on loss, total pressures depend on work, heat transfer, and loss. The total-pressure data in the remaining sections show how wakes and their interactions affect local total-pressure values.

4.2. Data Uncertainty

The uncertainty levels associated with this total pressure data are discussed first. Periodic-average total-pressure data were obtained for six rotor sampling positions at each of several selected radial positions between blade rows in the first stage of the research compressor and at one radius only behind the second rotor. For any one radial and axial location combination, the arithmetic average of the six measured periodic-average total-pressure profiles should compare favorably with the time-average total-pressure profile as measured with a slow-response probe system (Schmidt and Okiishi (1976)). Figure 4.3 shows such comparisons at midspan (PHH = 50%) for the first rotor and first stator flows. Another method was employed to compare fast-response and slow-response total-pressure probe data. At each radial and axial location combination, periodic-average total-pressure profiles for each rotor sampling position were numerically integrated to yield blade-to-blade-average values of total pressure. The blade-to-blade-average values of

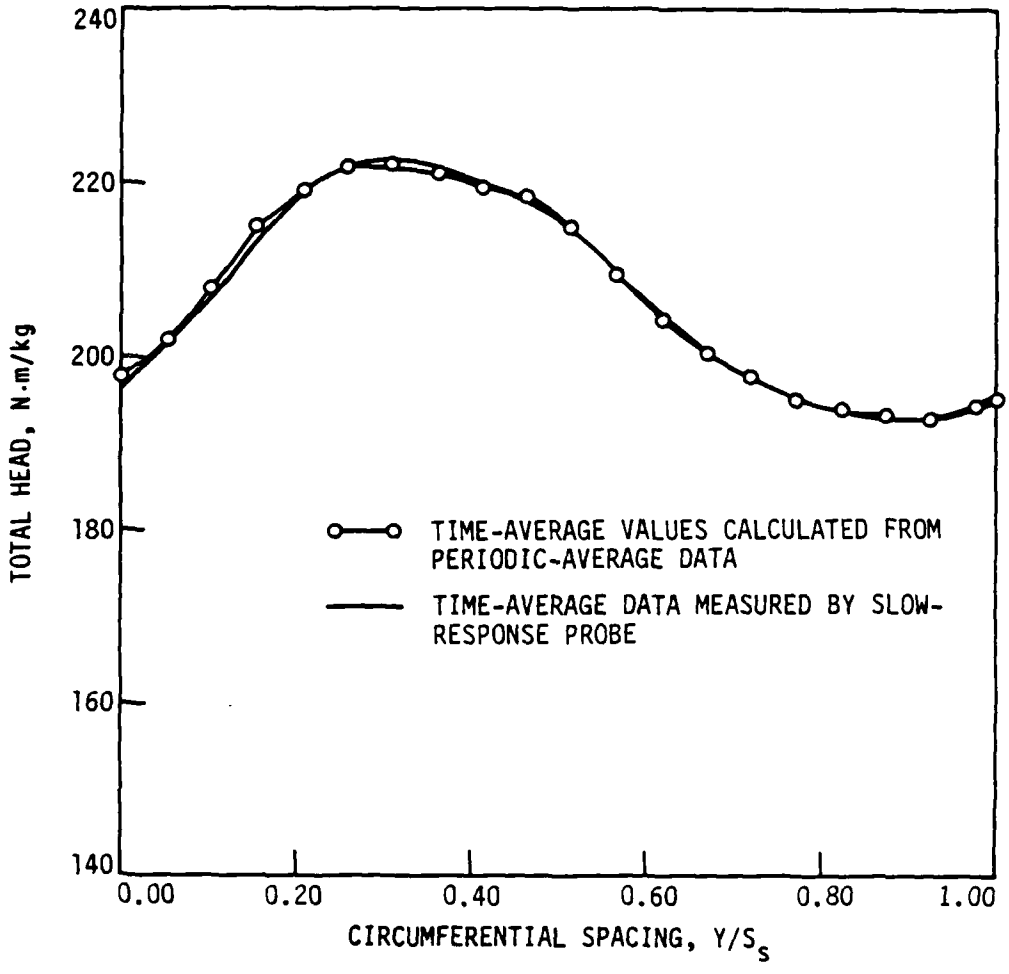

(a) Station 3.

Figure 4.3. Blade-to-blade distribution of time-average total head.

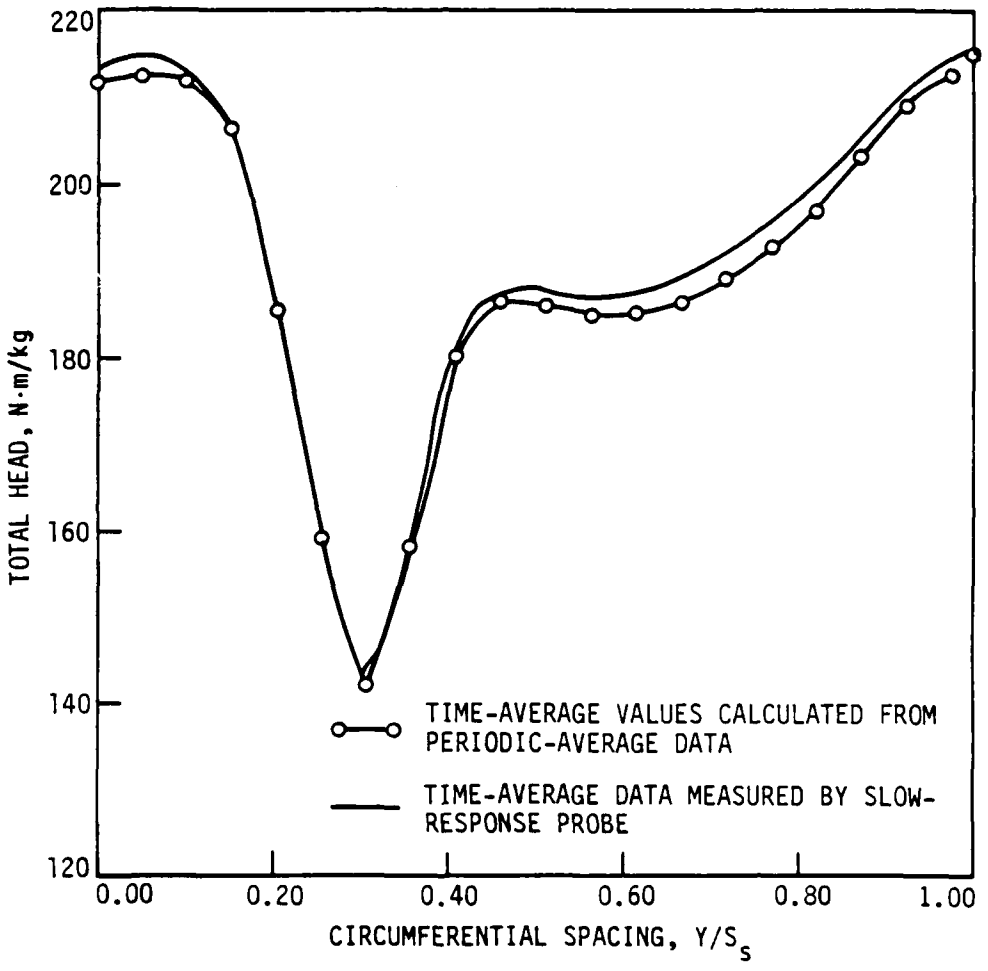

(b) Station 4.

Figure 4.3. Continued.

periodic-average total pressures corresponding to each of the six rotor sampling positions were then arithmetically averaged and compared with the blade-to-blade-average values of time-average total pressures obtained by numerically integrating the measured time-average total-pressure profile. Once again, these comparisons showed excellent agreement. All of the blade-to-blade-average value and time-average value comparisons are shown in Table 4.1 and Figure 4.4. These comparisons suggest an uncertainty of 3 N·m/kg in the periodic-average total-head data.

As explained previously, hot-wire velocity data taken in the research compressor configuration now employed were used to calculate total-head values assuming constant static pressure circumferentially at any radial location. These calculated data were compared to the total-head data taken with the fast-response total-pressure probe. In making this comparison, it is important to realize that the static pressure is not necessarily constant at any radial position. Ravindranath and Lakshminarayana (1979) have taken data which show that the static pressure can vary circumferentially in a turbomachine. The amount of static-pressure variation depends on the distance downstream of the blade row. This variation should be small at the measurement stations used in this research compressor. The comparison of hot-wire based and measured total-head values, shown in Figure 4.5 for first rotor and first stator exit flows at midspan (PHH = 50%), indicates similar trends for the two types of curves.

Table 4.1. Blade-to-blade-average and time-average total-head values in the first stage

	YO_R deg.	HT N·m/kg	YO_R deg.	HT N·m/kg	YO_R deg.	HT N·m/kg	YO_R deg.	HT N·m/kg	YO_R deg.	HT N·m/kg
	PHH = 10%		PHH = 30%		PHH = 50%		PHH = 70%		PHH = 90%	
Station 3	0.00	207.01	0.00	205.00	0.00	213.40	0.00	206.15	0.00	198.54
	1.60	206.92	1.60	207.67	1.60	215.49	1.60	206.39	1.60	198.30
	3.20	203.59	3.20	212.05	3.20	213.68	3.20	205.47	3.20	194.56
	4.70	197.98	4.70	205.66	4.70	204.77	4.70	197.45	4.70	191.60
	6.50	197.95	6.50	198.87	6.50	196.63	6.50	191.67	6.50	196.01
	7.90	200.81	7.90	200.67	7.90	199.76	7.90	197.60	7.90	198.10
Arith. avg.		202.39		204.99		207.29		200.79		196.19
Time-avg.		200.61		205.09		207.29		202.26		196.12
Station 4	0.00	181.33	0.00	188.46	0.00	190.85	0.00	193.98	0.00	173.54
	1.60	180.49	1.60	186.50	1.60	189.46	1.60	194.46	1.60	171.52
	3.20	179.33	3.20	190.67	3.20	189.15	3.20	192.89	3.20	172.16
	5.00	179.69	4.70	190.22	4.70	190.84	4.70	189.10	4.70	173.22
	6.50	181.00	6.50	188.98	6.50	187.77	6.50	185.00	6.50	174.11
	8.10	181.52	7.90	188.46	7.90	188.42	7.90	186.85	7.90	175.53
Arith. avg.		180.56		188.88		189.42		190.38		173.38
Time-avg.		180.41		188.52		191.15		190.62		174.24

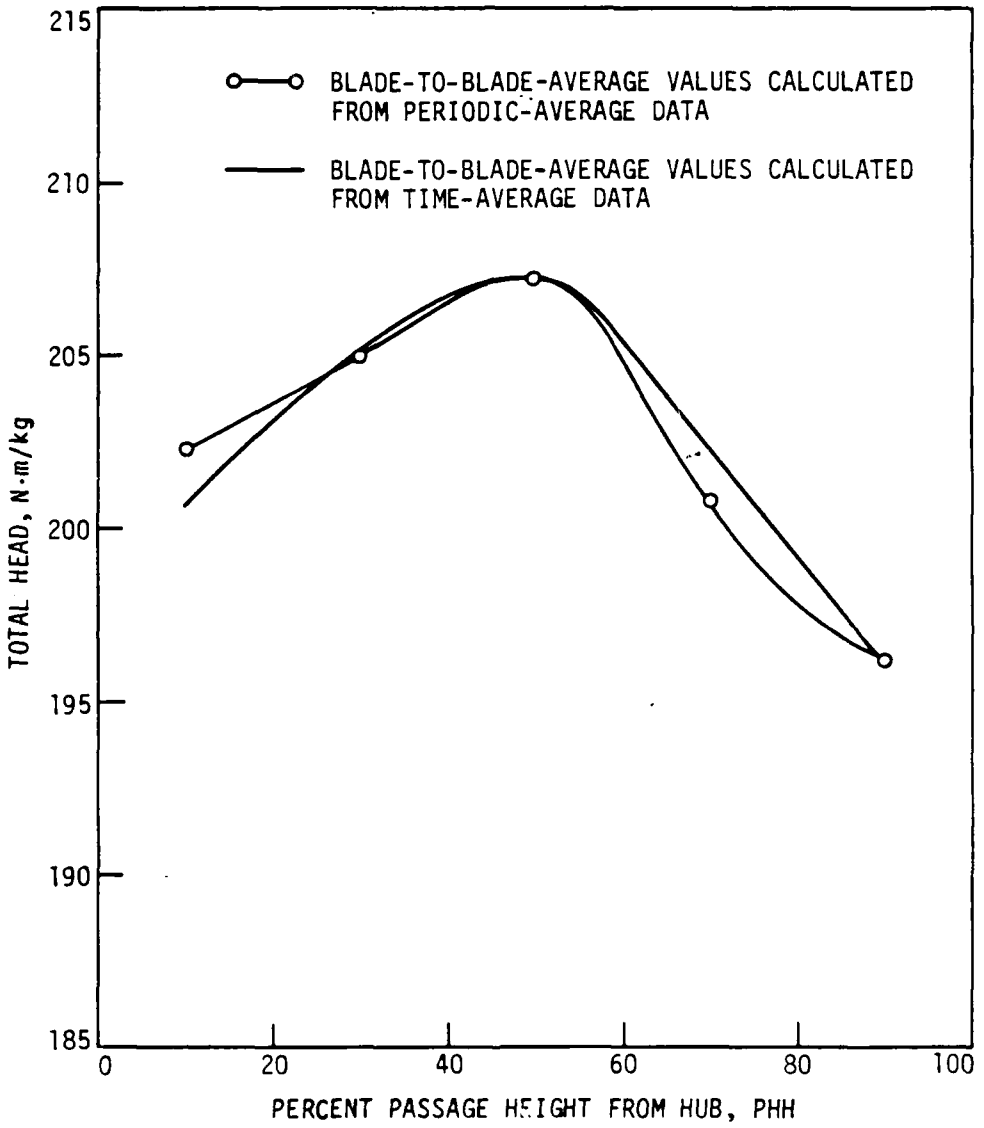

(a) Station 3.

Figure 4.4. Radial distribution of blade-to-blade-average total head.

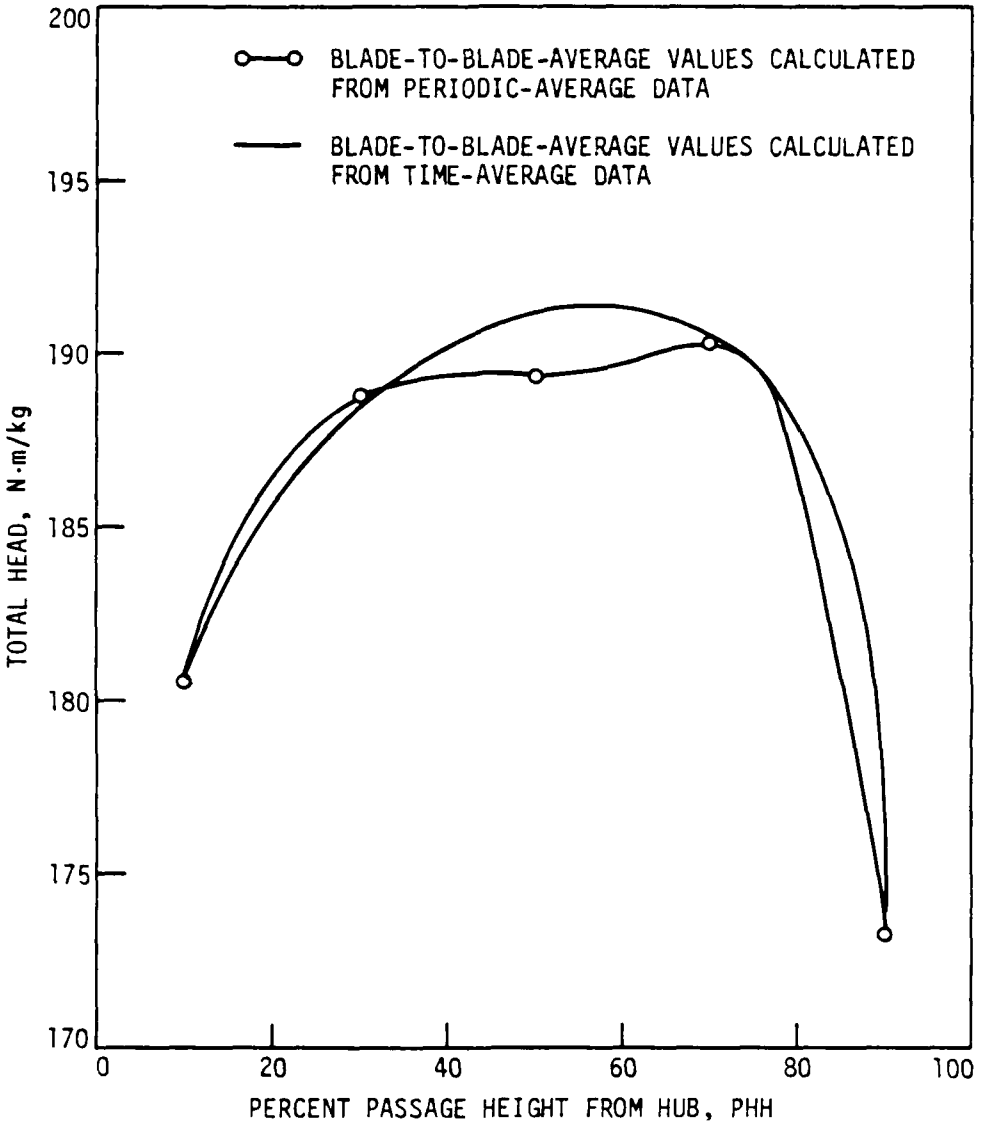

(b) Station 4.

Figure 4.4. Continued.

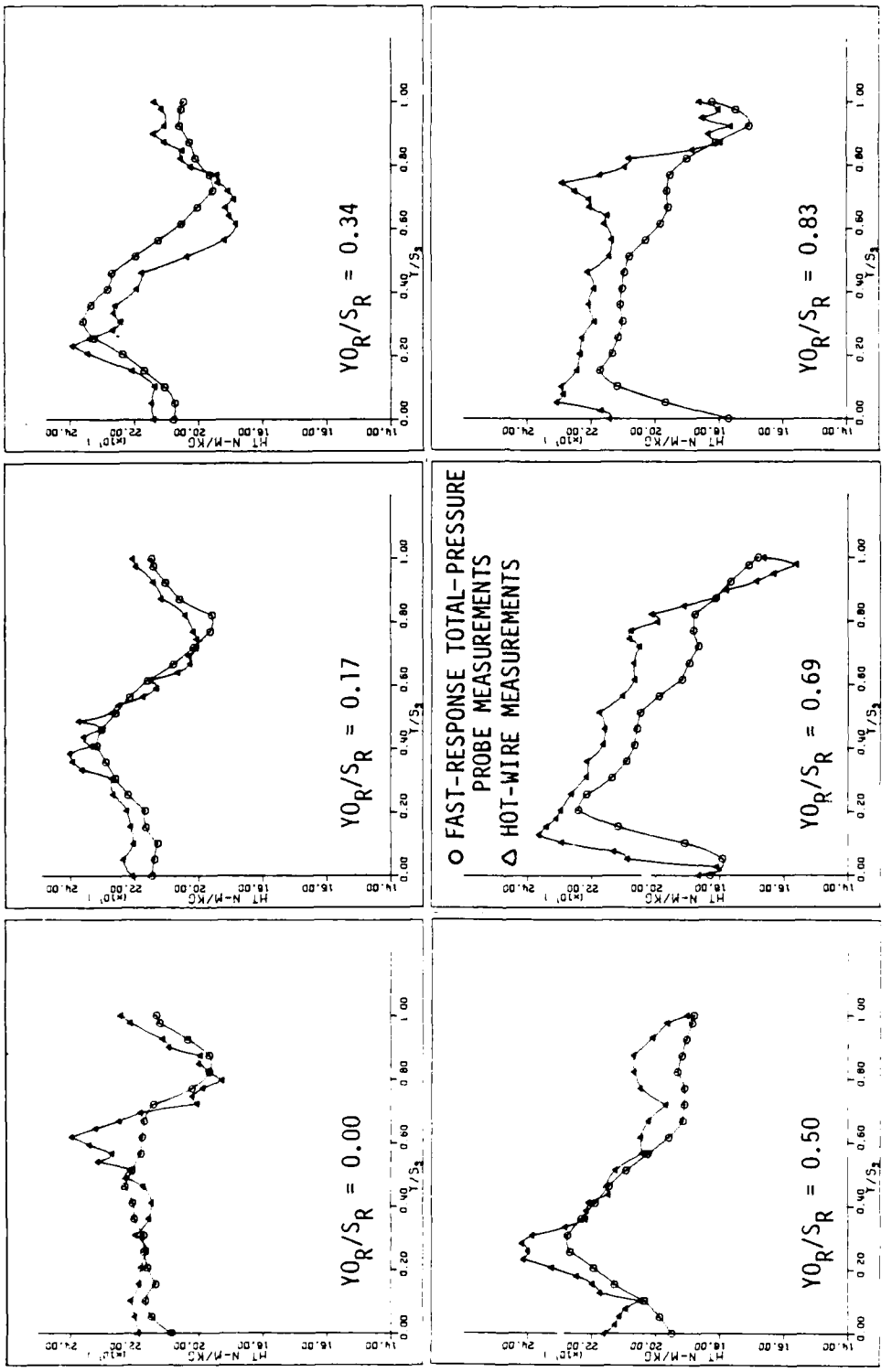

(a) Station 3.

Figure 4.5. Comparison of periodic-average total-head values measured by the fast-response total-pressure probe to those values calculated from hot-wire velocity data at 50% PHH.

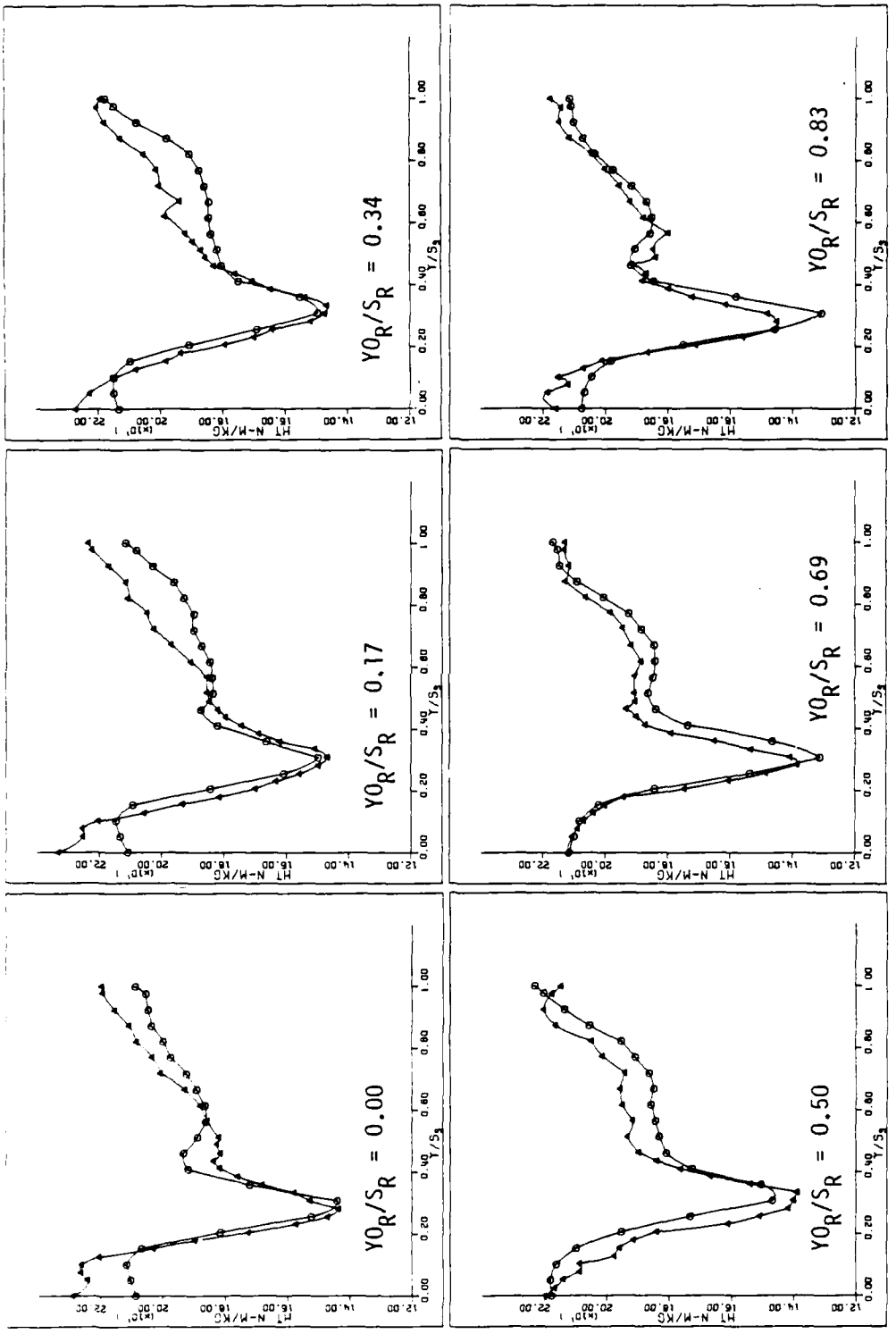

(b) Station 4.

Figure 4.5. Continued.

4.3. First Rotor Exit Flow Data

4.3.1. Local Total-Head Data

First rotor exit time-average and periodic-average local total-head data are compared in Figure 4.6. The IGV wake avenues are characterized by lower time-average total-head values. The vertical line passing through each of the plots represents the approximate circumferential location of the rotor wakes as indicated by hot-wire data. An "I" label indicates an interacted wake while an "N" is used for noninteracted wake. Note that the periodic-average rotor wake local total-head values vary considerably with rotor sampling position. It was concluded that this unsteady behavior was related to the periodically varying spatial distribution and proportions of the different kinds of fluid particles (freestream, IGV wake, segment, noninteracted rotor wake, interacted rotor wake) present in the measurement window for the different rotor positions (see Figure 4.7). This reasoning was used earlier (Wagner and Okiishi (1977)) to explain observed periodic variations in local velocities. The velocity polygons shown in Figure 4.8 in combination with the periodically varying cascade plots of Wagner and Okiishi (1977) shown in Figure 4.7 and the observed location of the rotor wakes relative to the IGV wake avenues suggest, as might be expected, that interacted wakes generally involve lower total-head values than noninteracted wakes. This conclusion was made for data at midspan, but it also proved to be valid elsewhere in the passage. At all span locations, the interacted rotor wake total-head values are less than the chopped IGV wake segment total-head values and much less than the freestream total-head

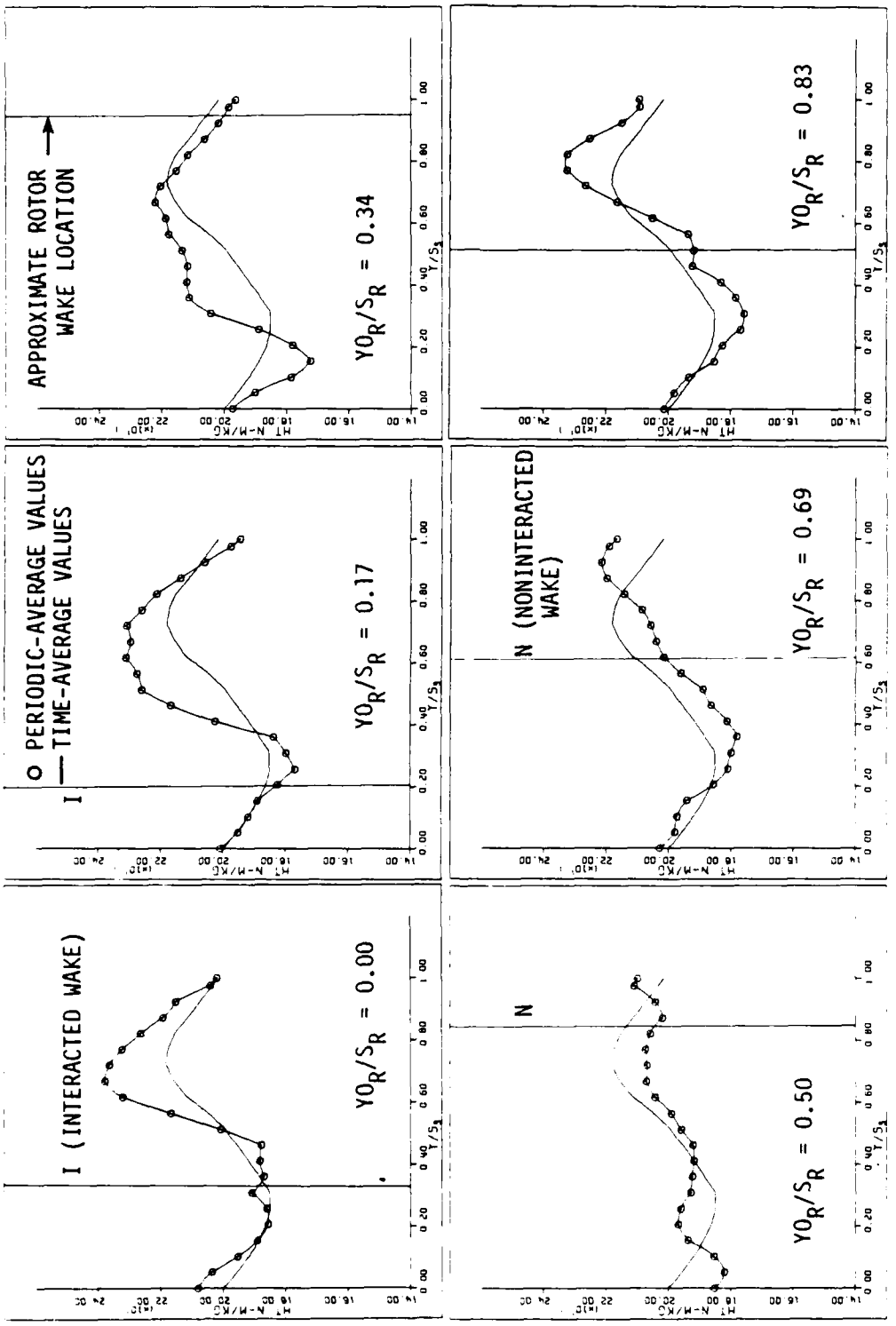

(a) PHH = 10%.

Figure 4.6. Blade-to-blade distribution of periodic-average total head and time-average total head at station 3.

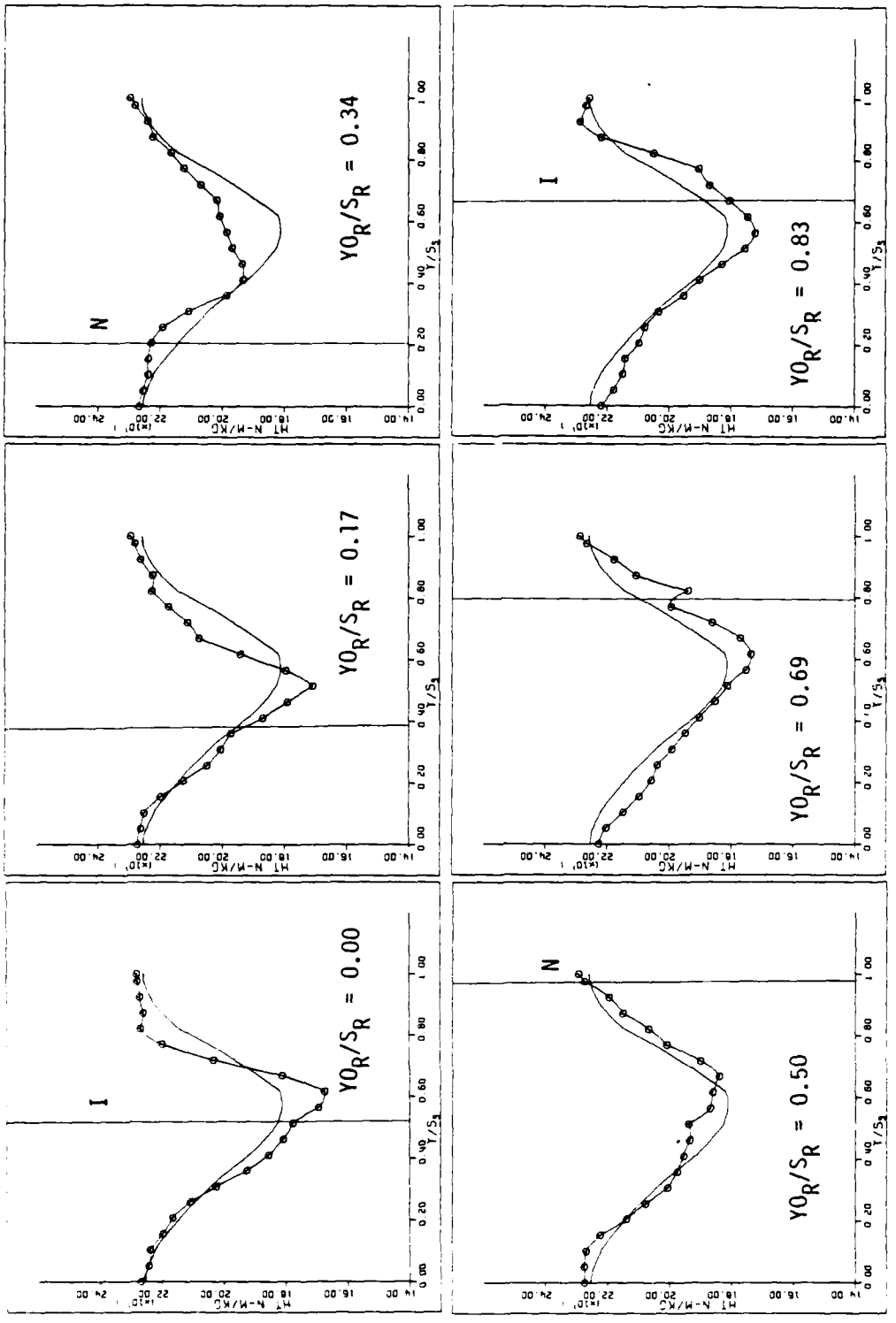

(b) PHH = 30%.

Figure 4.6. Continued.

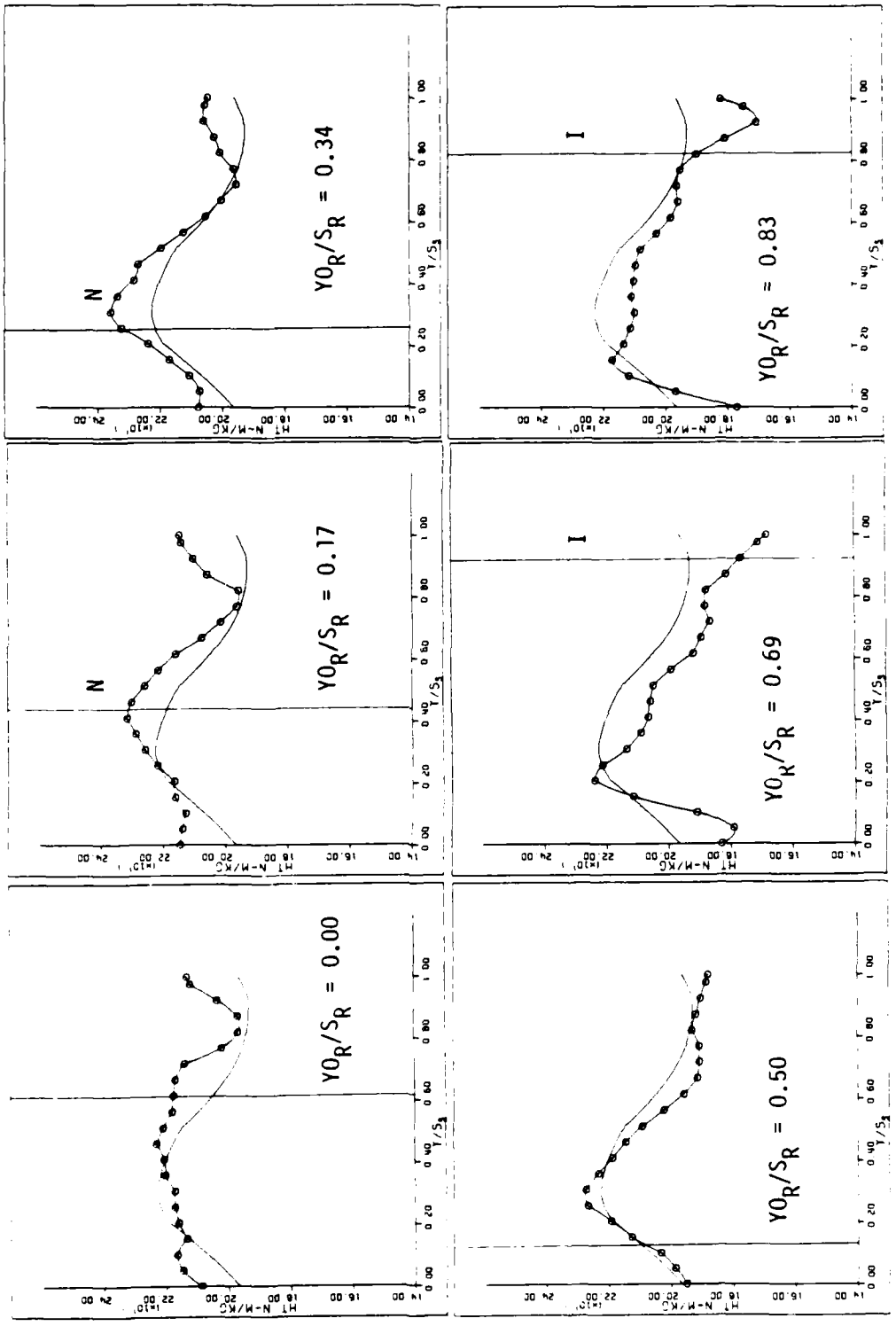

(c) PHH = 50%.

Figure 4.6. Continued.

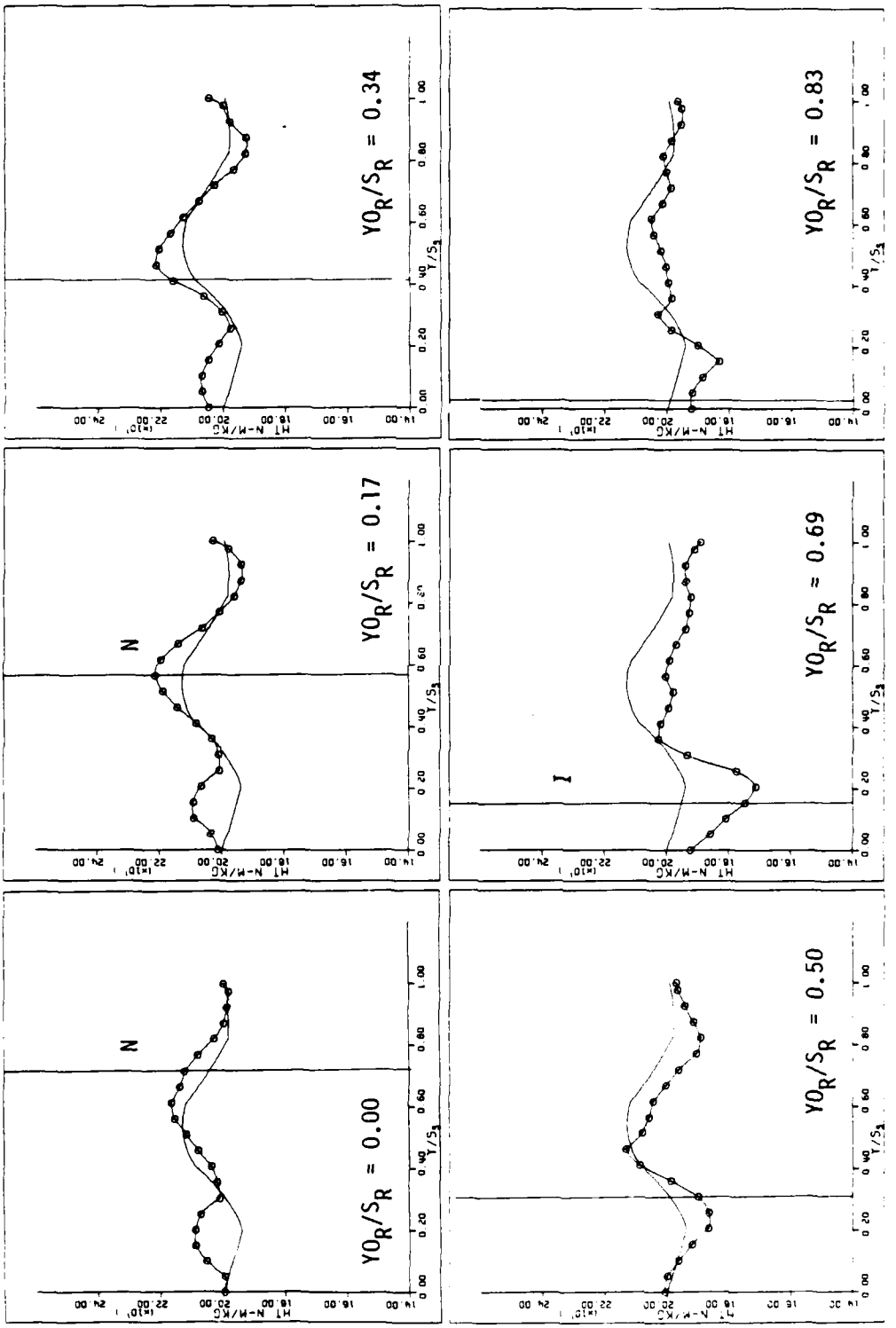

(d) PHH = 70%.

Figure 4.6. Continued.

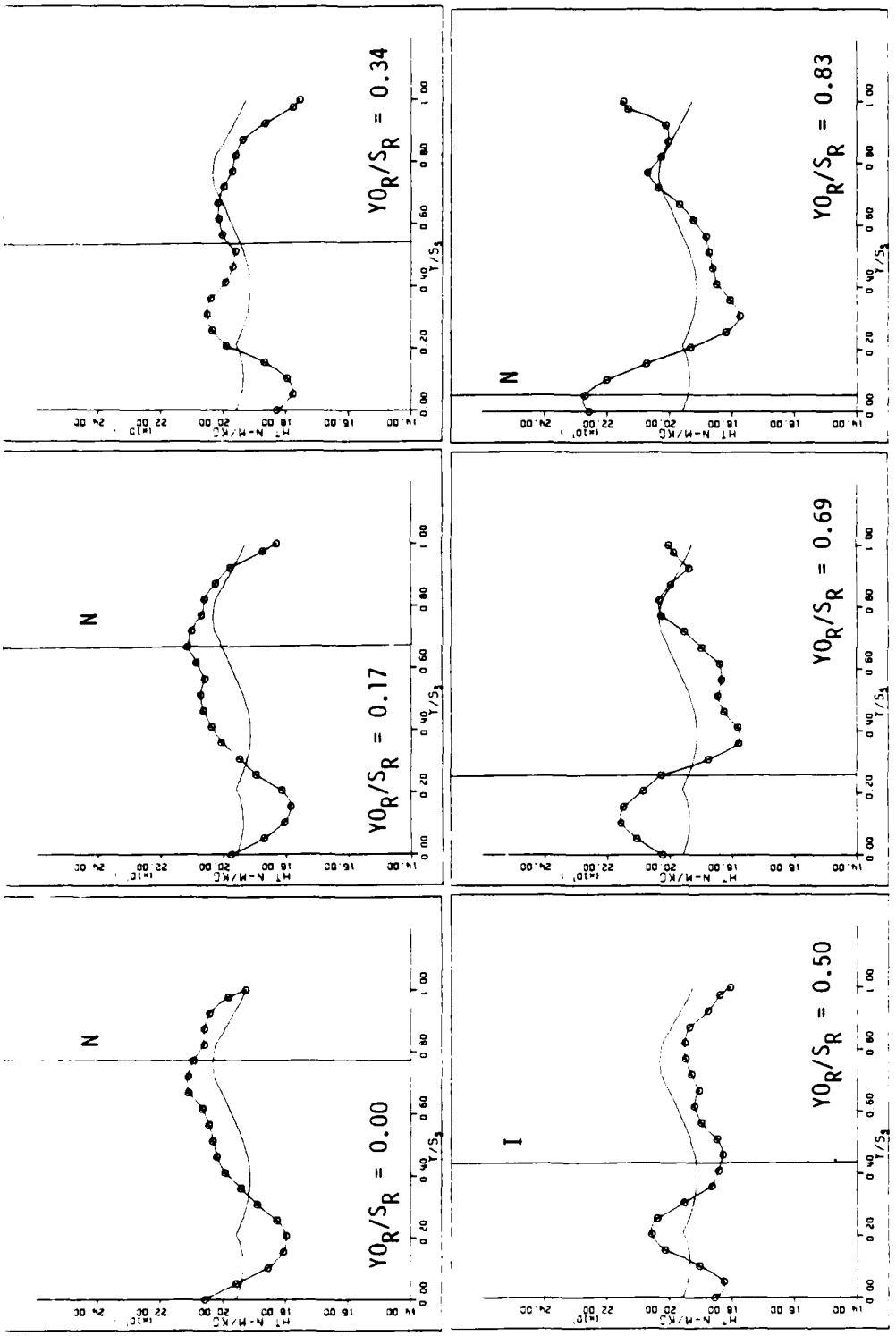

(e) PHH = 90%.

Figure 4.6. Continued.

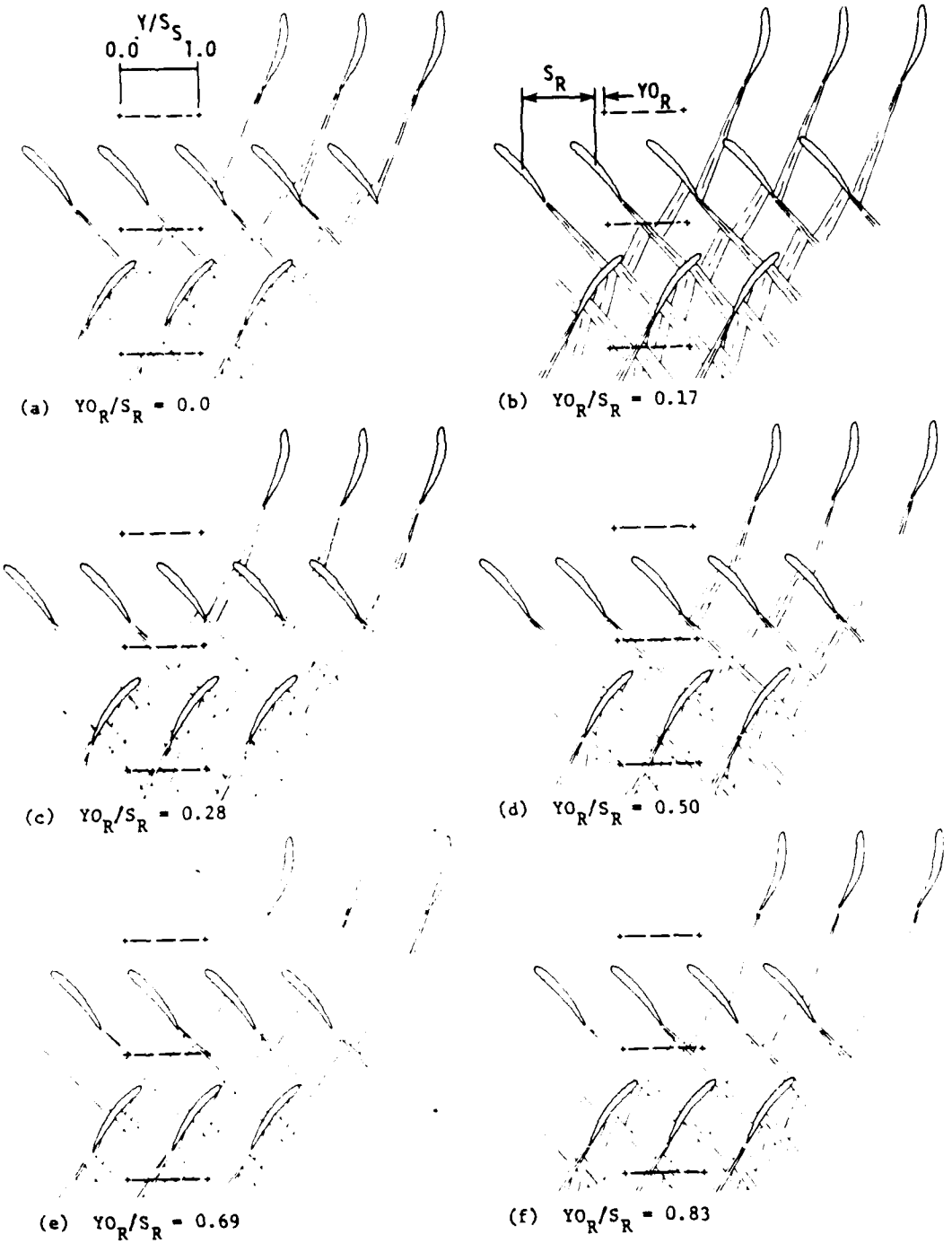

Figure 4.7. Periodic-average cascade plots for the first stage of the research compressor at 50 percent passage height (from Wagner and Okiishi (1977)).

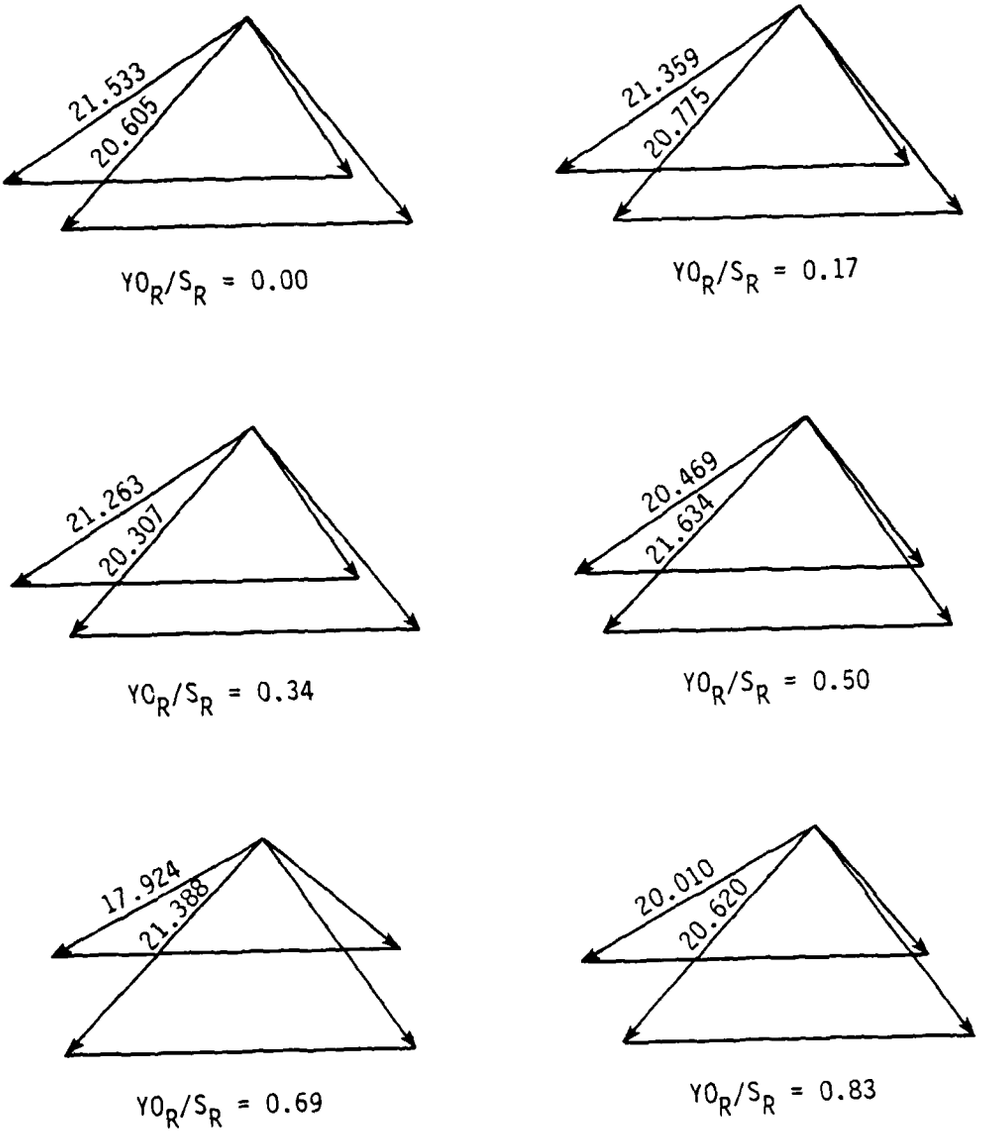

Figure 4.8. Velocity triangles at station 3 and 50% PHH.

values. Further, the data indicate that except at 10% and 30% span from the hub, the noninteracting wake total-head values are larger than the total-head values measured at that circumferential location in the absence of any wake material (i.e., when freestream flow particles occupy that portion of the measurement window). For example, at 50% span (Figure 4.6c), the total-head at circumferential position $Y/S_S = 0.411$ is 231.78 N·m/kg for a noninteracting wake fluid particle ($YO_R/S_R = 0.17$) and 206.58 N·m/kg for a freestream fluid particle ($YO_R/S_R = 0.69$). At 10% span the opposite trend is true: the noninteracting total-head values are smaller than the total-head values measured at that circumferential location in the absence of any wake material. For example, at 10% span (Figure 4.6a), the total-head at circumferential position $Y/S_S = 0.617$ is 201.56 N·m/kg for a noninteracting wake fluid particle ($YO_R/S_R = 0.69$) and 232.06 N·m/kg for a freestream fluid particle ($YO_R/S_R = 0.00$). At 30% span, both kinds of behavior are noted. These observations appear to be related to blade profile loss levels. As indicated by the data in Figure 4.9 the blade-element loss level near the hub is very high compared to the level elsewhere in the passage. The periodic-average velocity data in Figure 4.10 show that the large loss near the hub is associated with a very deep wake and is thus indicative of a large profile loss. Elsewhere in the passage, the wakes are shallower. The larger loss observed near the tip is partly due to a tip clearance leakage effect.

All of these observations about the details of the local total-head variations prompted the organization of the information in Table 4.2. In summary form, the processes proposed in Table 4.2 suggest what local total-head levels will be observed at the measurement window when certain

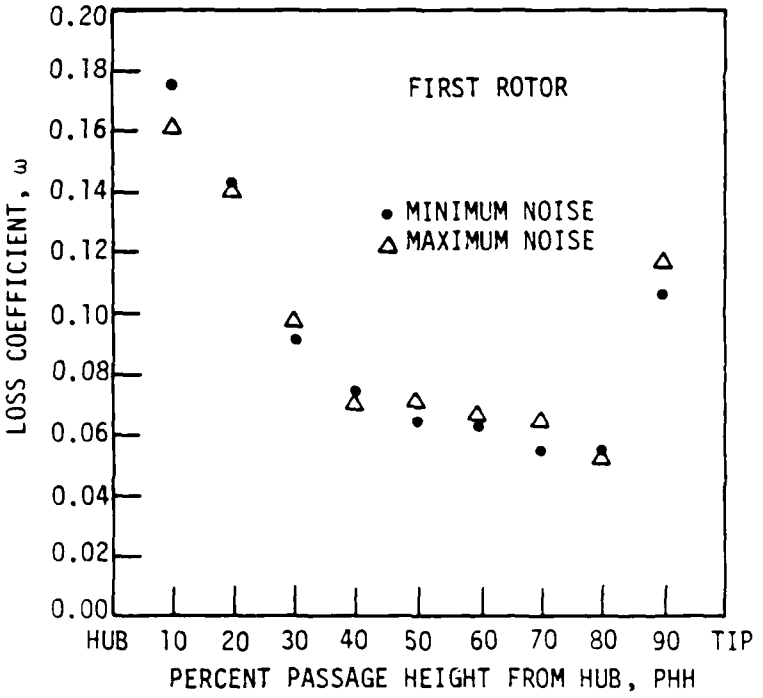

Figure 4.9. Blade span distribution of time-average total-head loss coefficient for first rotor row (from Schmidt and Okiishi (1977)).

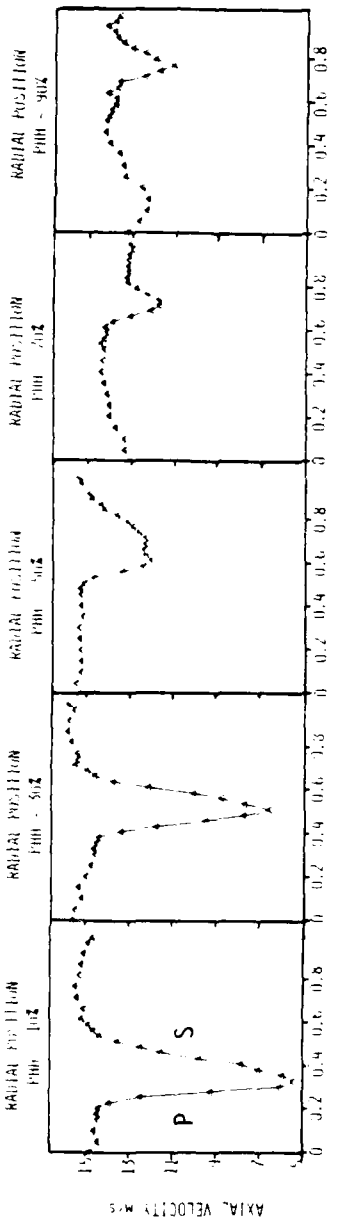

Figure 4.10. Blade-to-blade distribution of first rotor exit periodic-average axial flow at different radial positions for YO_R/S_R = 0.0 (from Schmidt and Okiishi (1977)).

Table 4.2. Behavior of fluid particles moving from the rotor inlet to the measurement station downstream of the rotor

Type of fluid particle	Total pressure at the rotor inlet	Energy added	Losses	Total pressure at the rotor exit measurement station
Freestream	A	B	C	D
Chopped IGV wake	<A	>B	>C	<D
Noninteracted rotor wake	A	>>B	>C(50%-90% PHH)	>D
			>>C(30%)	D
			>>>C(10%)	<D
Interacted rotor wake	<A	>>B	>>>C	<<D

The freestream values are set arbitrarily at levels A, B, C, and D. Other values are estimated in terms of being less than, equal to, or greater than these reference values.

kinds of fluid flow particles are there. It is clear that the changing spatial distribution and proportions of the different kinds of particles present at the measurement station with rotor sampling position will lead to differing total-head profiles.

4.3.2. Blade-to-Blade-Average Data

The blade-to-blade periodic-average and time-average total-head profiles of Figure 4.6 were integrated and the blade-to-blade-average results are compared in Figure 4.11. The periodic unsteadiness of the

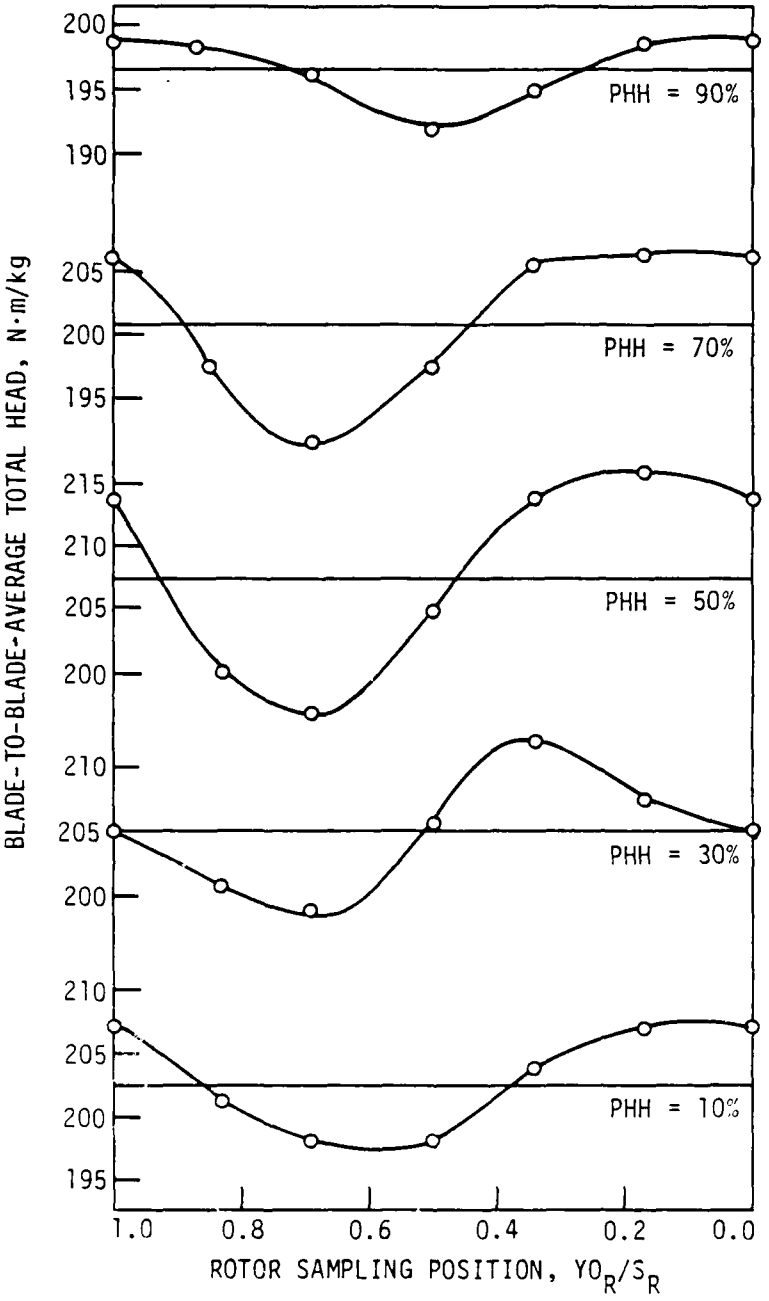

Figure 4.11. Time varying blade-to-blade-average total-head values at station 3.

blade-to-blade-average total head is large everywhere but appears to be greatest in the center portion of the blade span and less at either end. At 10% span from the hub, the interacting wake blade-to-blade-average total head is greater than the noninteracting wake value. Also, the interacting wake total-head value is greater than the time-average value while the noninteracting wake value is less than the time-average value. The opposite is true from 50% span on out to near the tip. The local effects mentioned and explained previously were influential enough to affect blade-to-blade-average results appreciably.

4.4. First Stator Exit Flow Data

Local total-head data taken behind the first stator row for different rotor sampling positions are presented in Figure 4.12.

Since energy was not added to the fluid flowing through the stator blade passage, and because the flow was approximately adiabatic, the total-head values in the stator wakes are indicative of the losses only, and the stator data are easier to interpret than the rotor data. Stator wake and chopped rotor and inlet guide vane wake fluid particles dominate the field at the measurement window downstream of the stator and result in mainly low levels of total pressure in the stator exit flow. The variation of the blade-to-blade-average total-head values with rotor sampling position is shown in Figure 4.13. While the first rotor exit total-head values varied considerably with rotor sampling position because of the energy transfer and wake interaction effects, the first stator exit total-head values varied little with rotor sampling position.

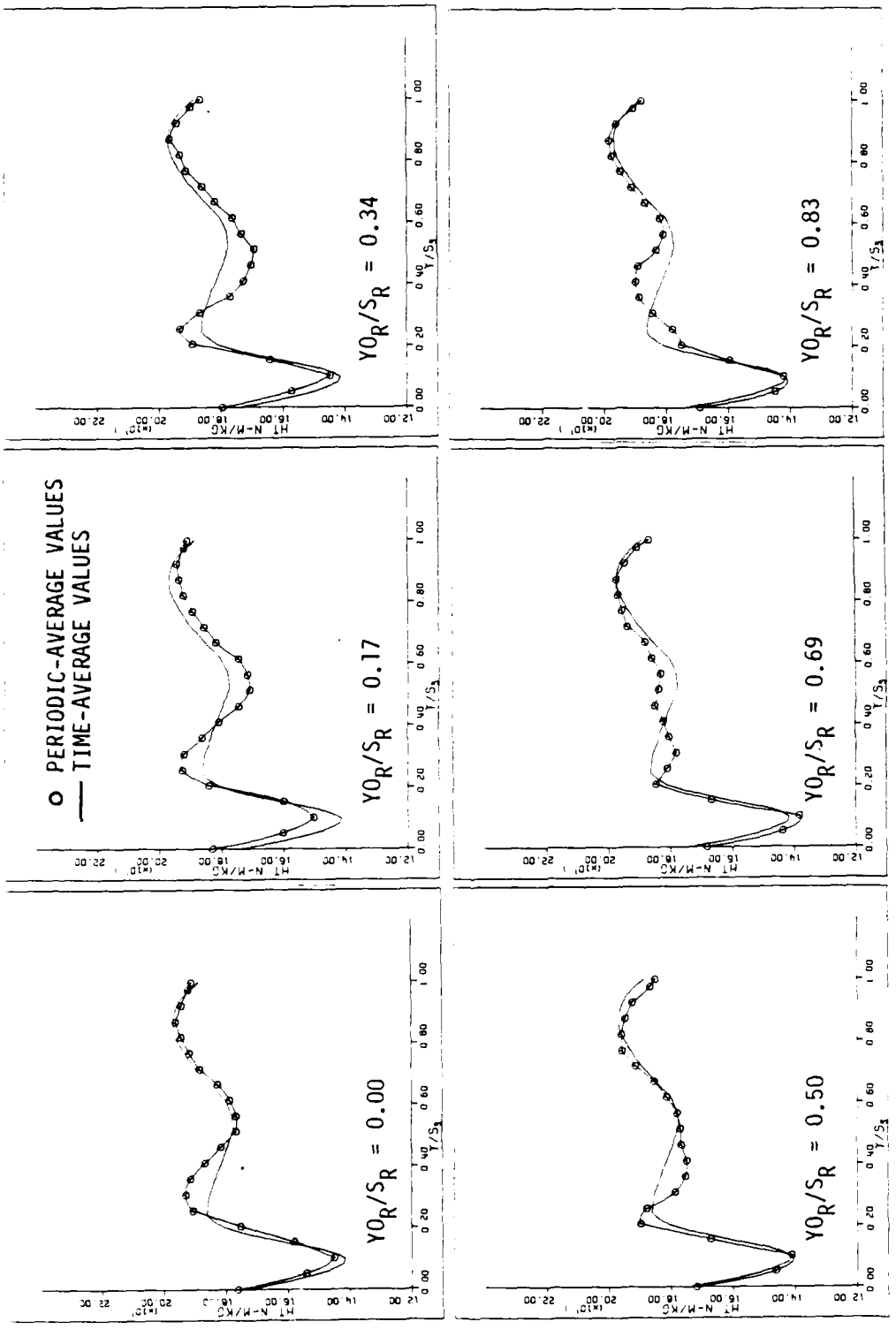

(a) PHH = 10%.

Figure 4.12. Blade-to-blade distribution of periodic-average total head and time-average total head at station 4.

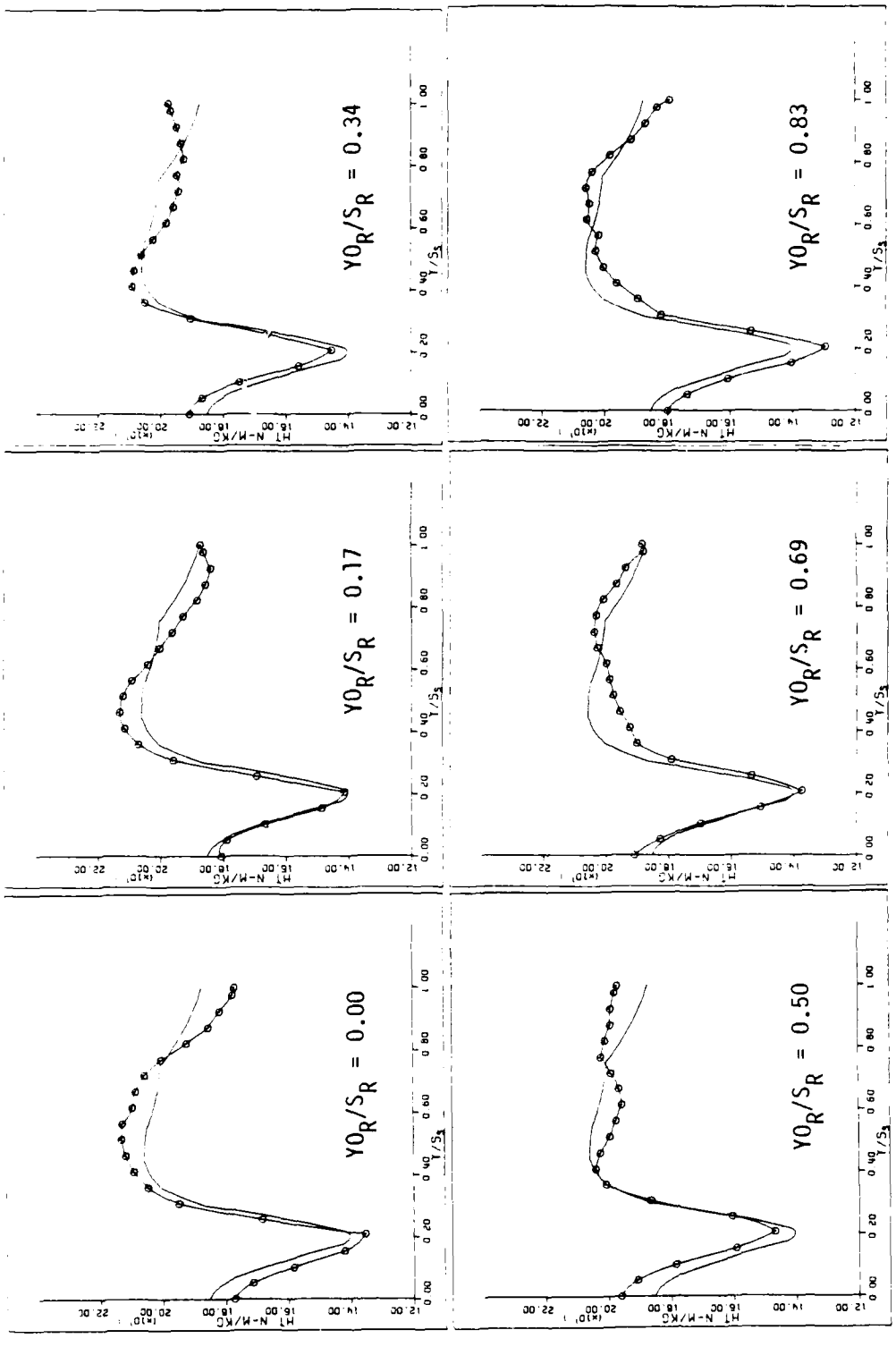

(b) PHH = 30%.

Figure 4.12. Continued.

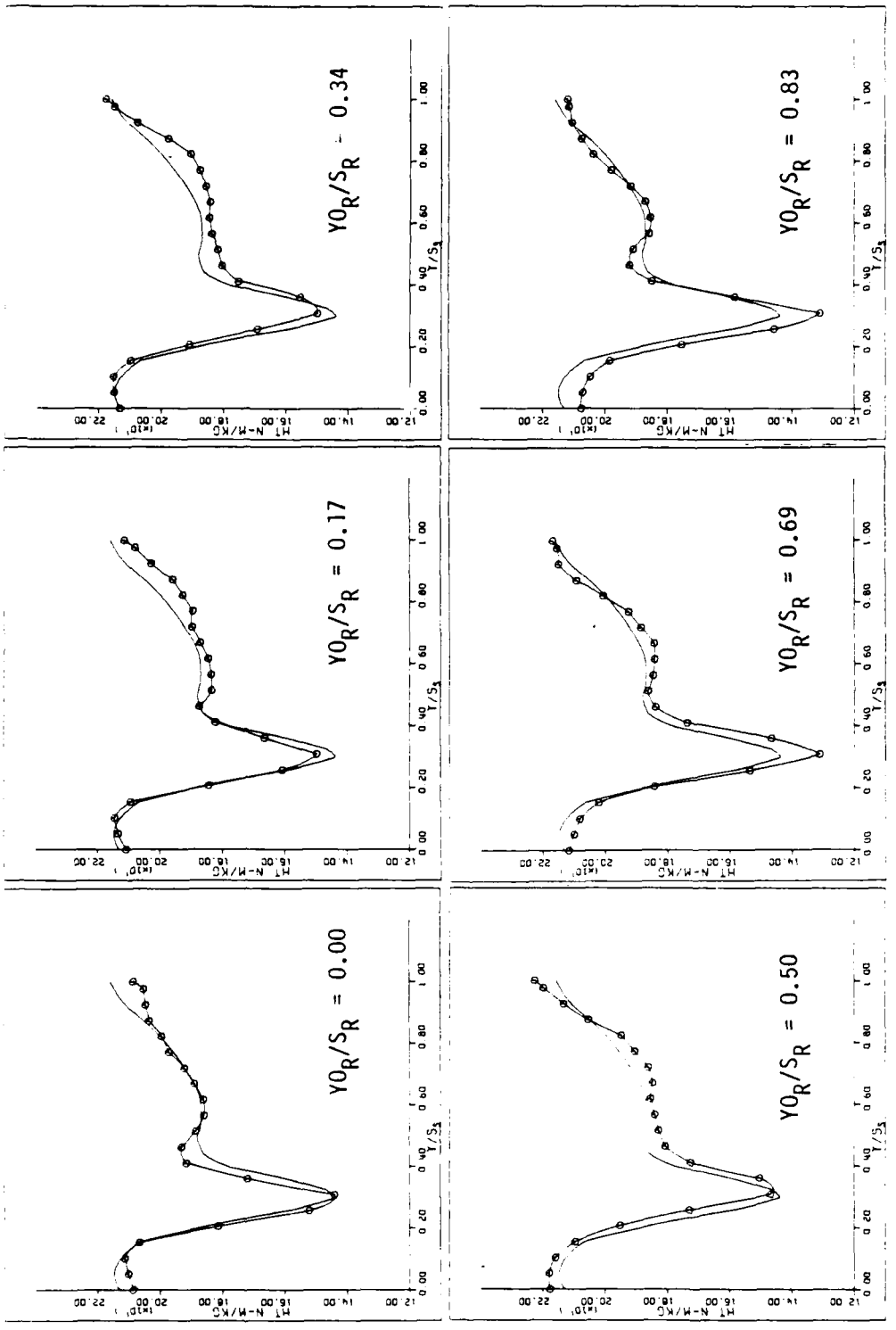

(c) PHH = 50%.

Figure 4.12. Continued.

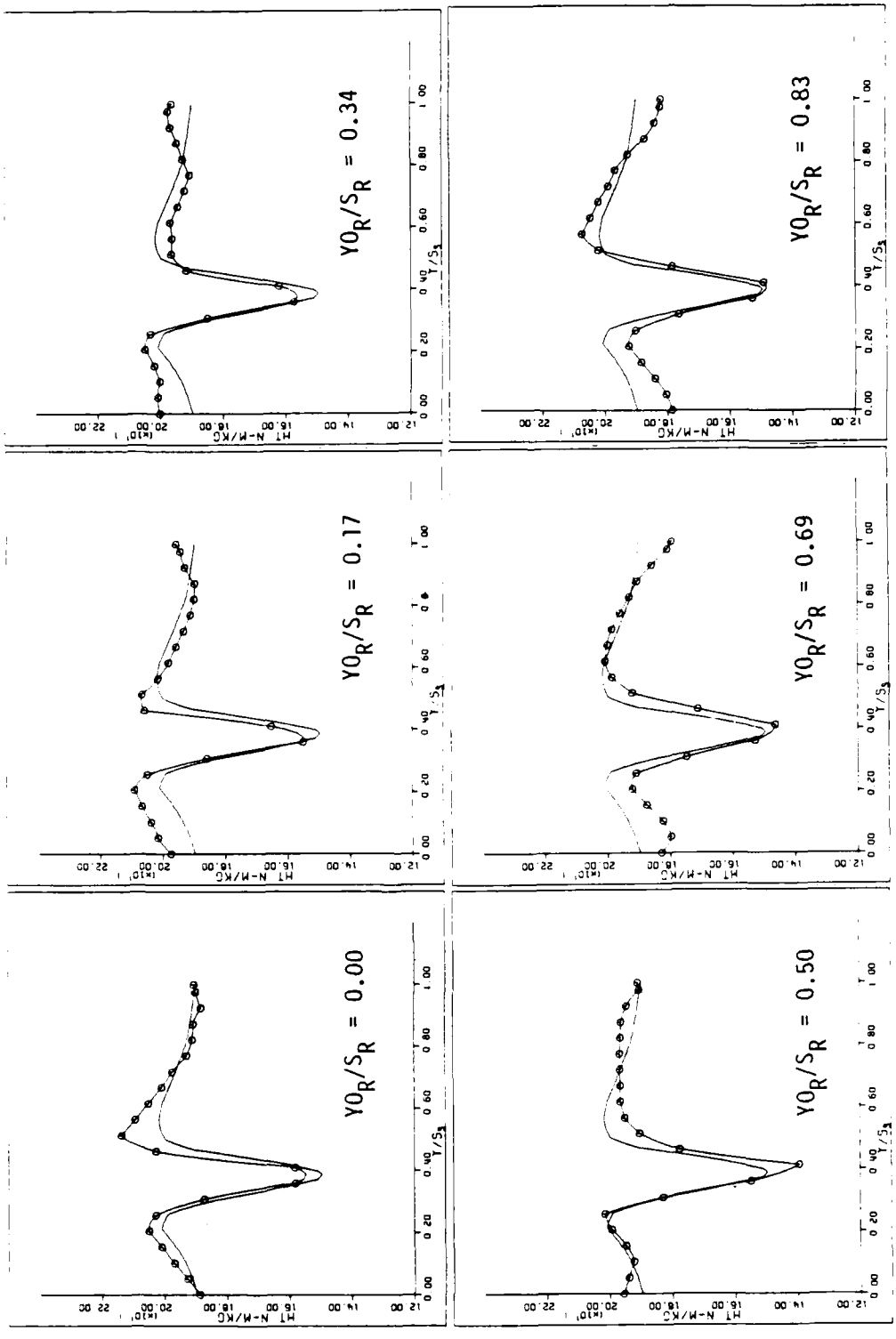

(d) PHH = 70%.

Figure 4.12. Continued.

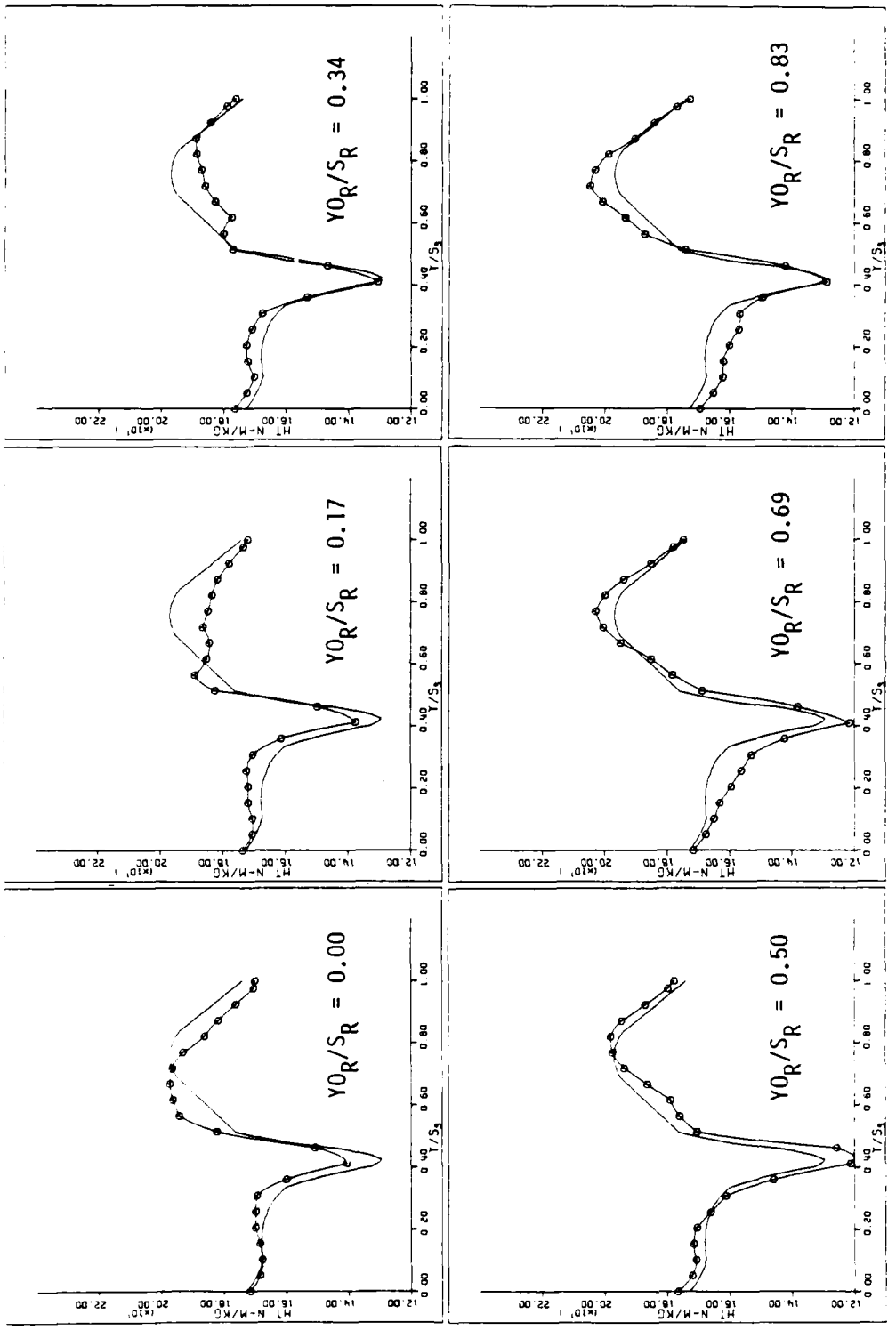

(e) PHH = 90%.

Figure 4.12. Continued.

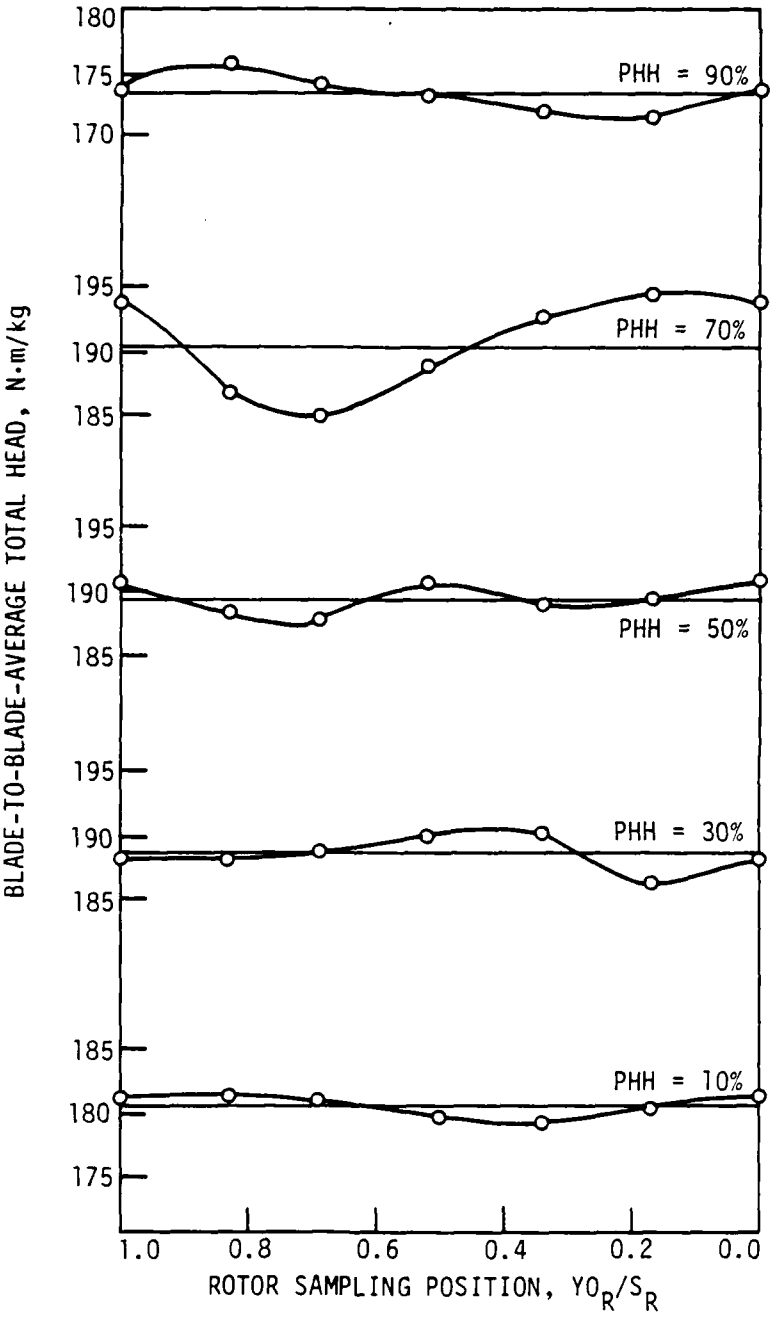

Figure 4.13. Time varying blade-to-blade-average total-head values at station 4.

The absence of energy addition in the stator row appears to be the main reason for the smaller variation of stator exit total pressure of the different kinds of fluid particles involved.

4.5. Second Rotor Exit Flow Data

Data were taken at the exit of the second rotor at one radial position (PHH = 50%) to gain an impression of how much rotor exit total-pressure levels would vary with rotor sampling position in a downstream stage. The time-average, periodic-average total-pressure comparison for the second rotor exit flow data appears in Figure 4.14. As observed with the first rotor exit data, total-head values in the rotor wake regions are larger and smaller than freestream values depending on rotor sampling position. The velocity diagrams in Figure 4.15 show that the larger rotor wake total heads occur for noninteracted rotor wakes and the smaller total heads occur for interacted rotor wakes. The variation in blade-to-blade-average rotor exit total-head values with rotor sampling position is not as great for the second rotor (see Figure 4.16) as it is for the first rotor. The second rotor exit flow data also show less difference in the shape of the total-head profiles from one rotor sampling position to another, and the corresponding velocity polygons of Figure 4.15 show less difference between interacted rotor wakes and noninteracted rotor wakes. Wake segments from more than one blade row are being transported through the second rotor row and thus through the measurement window at station 5. This would tend to smooth the variations with rotor sampling position of fluid properties such as total pressure and lead to smaller changes in that property.

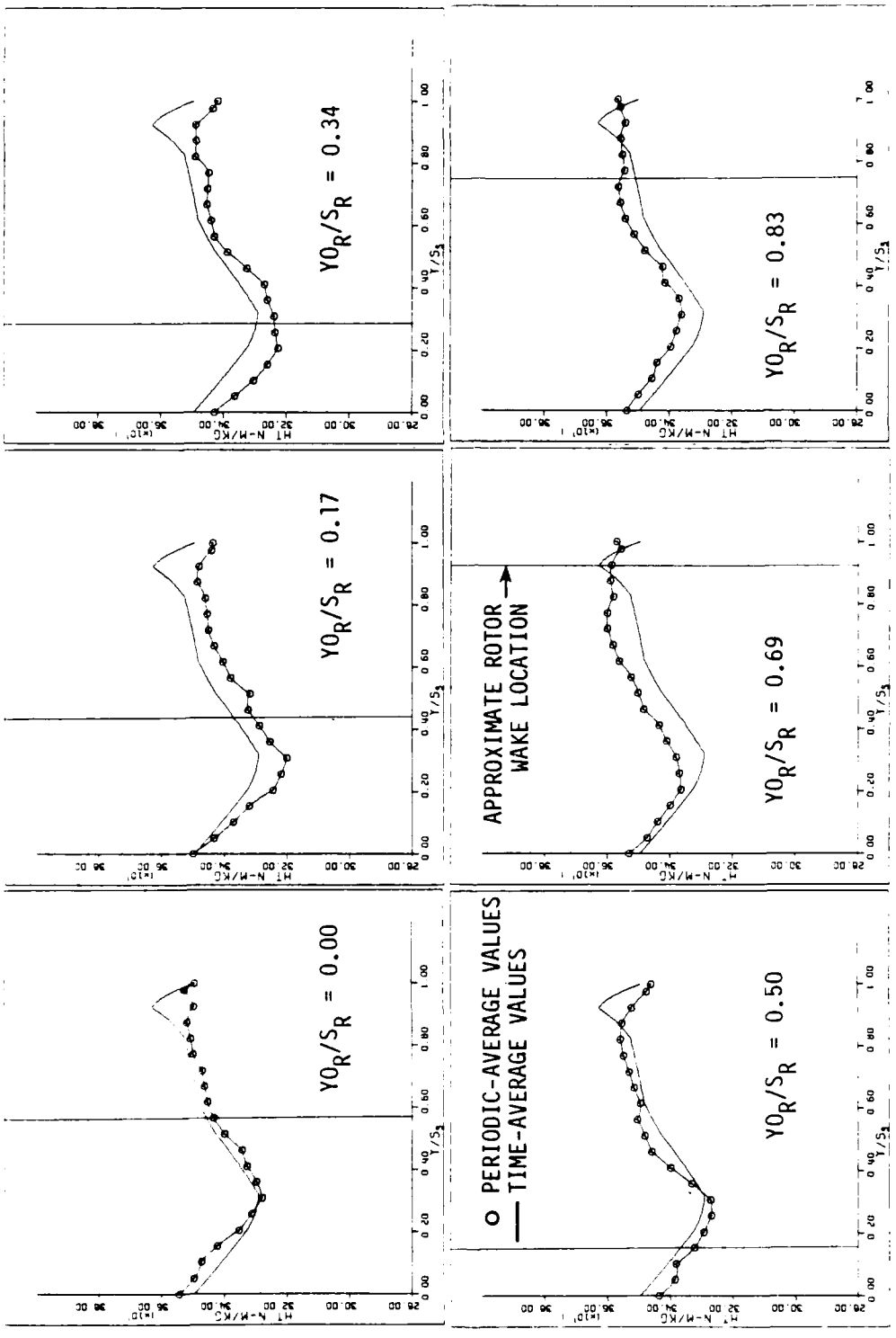

Figure 4.14. Blade-to-blade distribution of periodic-average total head and time-average total head at station 5 and 50% PHH.

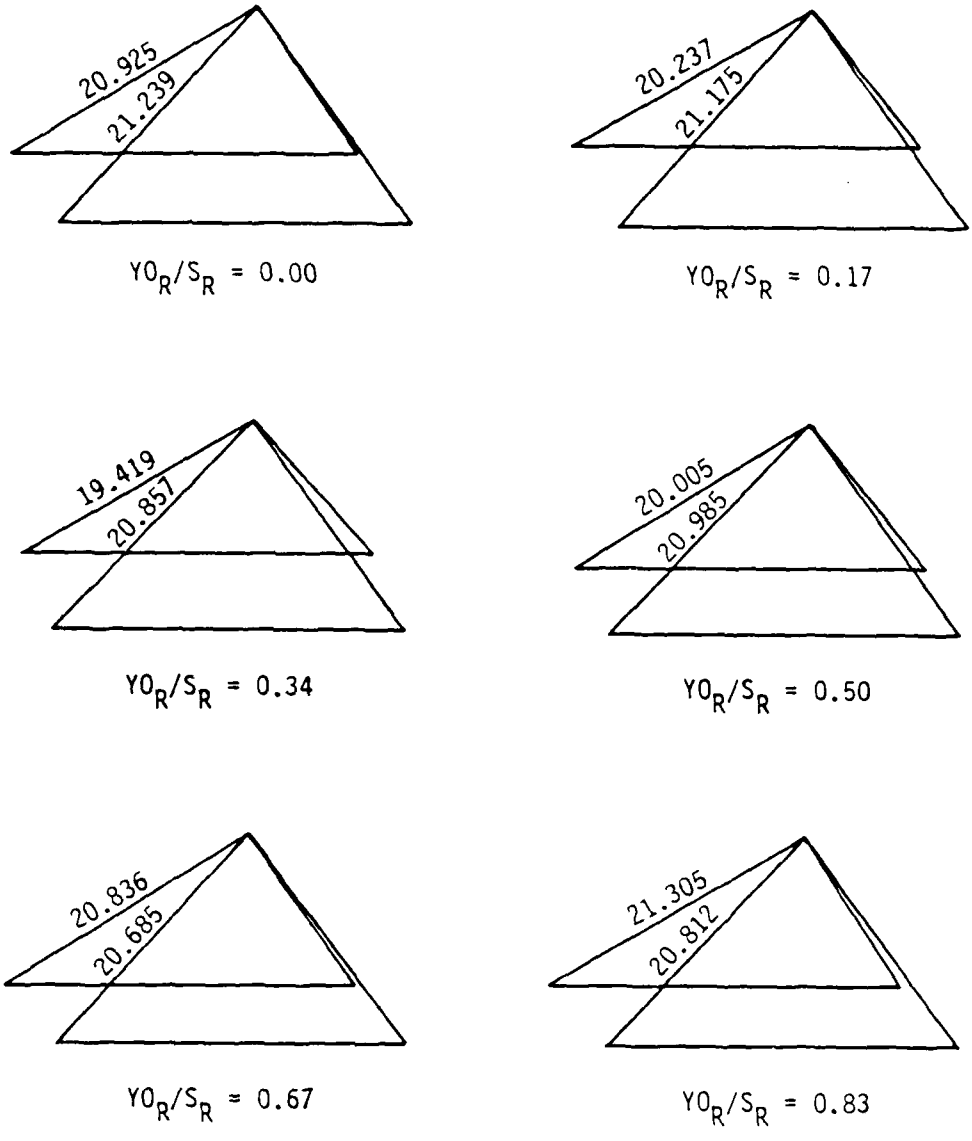

Figure 4.15. Velocity triangles at station 5 and 50% PHH.

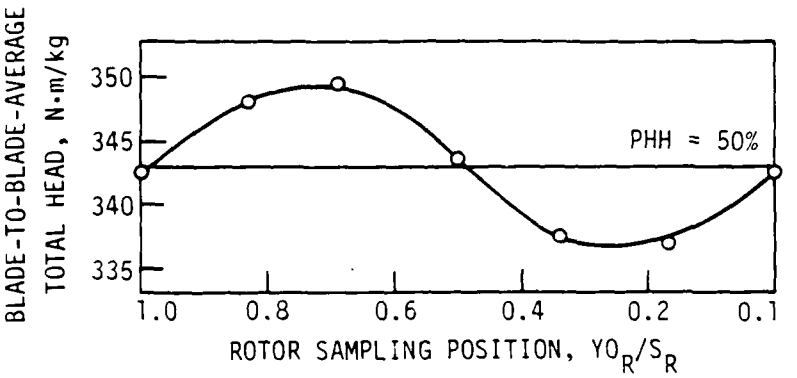

Figure 4.16. Time varying blade-to-blade-average total-head values at station 5 and 50% PHH.

5. CONCLUSIONS

Turbomachine flow total-pressure data are valuable because they are indicative of the amounts of energy gained and lost by the fluid particles involved. Rotor wake/stator or IGV wake interactions behind a rotor blade row have a strong effect on local total-pressure values. Rotor wakes that have interacted with stator of IGV wakes involve lower total pressures than rotor wakes that have not interacted with stator of IGV wakes. This effect is stronger in the first stage than in later stages.

The extent of total-pressure variation with rotor sampling position behind the first stator row was appreciably less than the amount behind the first and second rotor rows. Periodic unsteadiness of total pressure is considerable downstream of a blade row that involves energy addition and loss and is minimal downstream of a blade row that involves energy loss only.

Determination of the frequency response characteristics of the entire measurement system is necessary before measuring high-frequency, time-varying, total-pressure fluctuations. From these frequency response characteristics, the useful frequency range (within which the error in the relative amplitude is less than 5%) of the measurement system can be determined. The phase response should also be considered. The harmonic content of the flow to be measured should be determined to insure that all the important harmonics are within the useful frequency range of the measurement system. Hot-wire data and a Fast Fourier Transform could aid in determining wake harmonic content.

6. RECOMMENDATIONS FOR FUTURE RESEARCH

The results of this research project indicate that further research would be helpful in confirming the observations already made about how turbomachine energy transfer is affected by blade wake interactions. Complete surveys of periodically unsteady total pressures in the second and third stages of an axial-flow compressor should be obtained. Data for other operating points would be useful. The axial development of the periodically unsteady total-pressure field should be measured. Static-pressure values should be obtained from the total-pressure probe and hot-wire probe data and analyzed. Finally, further improvements in the measurement system should be made. For example accommodation of more harmonics within the system's useful frequency range might be considered.

AD-A097 296 IOWA STATE UNIV AMES ENGINEERING RESEARCH INST F/G 20/4
MEASUREMENT AND ANALYSIS OF THE PERIODIC VARIATION OF TOTAL PRE--ETC
NOV 80 W C ZIERKE, T H OKIISHI F49620-79-C-0002
UNCLASSIFIED ISU-ERI-AMES-81121 AFOSR-TR-81-0327 NL

END
DATE FILMED
8-81
DTIC

7. REFERENCES

Alarcon, G. A., Okiishi, T. H., and Junkhan, G. H. December 1977. "Design and Application of a Fast Response Total-Pressure Probe for Turbomachinery Flow Measurement." Iowa State University Engineering Research Institute Technical Report TCRL-9, ISU-ERI-Ames-78205.

Atkins, G. B. 1974. "Development and Calibration of a Probe/Sensor System to Measure Instantaneous Total Pressures." B.S. Thesis. The Pennsylvania State University.

Beckwith, T. G., and Buck, N. L. 1973. Mechanical Measurements. Second Edition. Reading, Mass.: Addison-Wesley.

Brandone, B., and Bernard, P. 1971. "Visualisation par Analogie Hydraulique de L'Ecoulement dans une Grille D'Aubes Plane Mobile." La Recherche Aerospatiule 141: 125-128.

Chaney, M. J. 1977. "Effect of Driver-Created Disturbances on Shock Tube Sidewall Boundary Layer Transition." M.S. Thesis. Iowa State University, Ames, Iowa.

Cook, N. H., and Rabinowicz, E. 1963. Physical Measurements and Analysis. Reading, Mass.: Addison-Wesley.

Delio, G. J., Schwent, G. V., and Cesaro, R. S. 1949. "Transient Behavior of Lumped-Constant Systems for Sensing Gas Pressures." NACA TN 1819.

Fischer, J. E. 1971. "Fluctuating Pressure Measurements from DC to Over 100 kHz in Jet Engine Testing." Instrumentation in the Aerospace Industry. Vol. 17. Edited by B. Washburn. Las Vegas, Nevada: Instrument Society of America.

Fleeger, D. W., and Seyb, N. J. April 1975. "Aerodynamic Measurements in Turbomachines." In "Modern Methods of Testing Rotating Components of Turbomachines (Instrumentation)." AGARD-AG-207.

Gallus, H. E., Lambertz, J., and Wallmann, Th. 1979. "Blade-Row Interaction in an Axial-Flow Subsonic Compressor Stage." ASME Paper No. 79-GT-92.

Hirsch, Ch., and Kool, P. 1977. "Measurement of the Three-Dimensional Flow Field Behind an Axial Compressor Stage." Transactions of the ASME, Journal of Engineering for Power, 99A: 168-179.

Junkhan, G. H. 1973. "Preliminary Investigation of Rapid Response Total-Pressure Measurements in a Turbomachine." Internal Note 43. Von Karman Institute for Fluid Dynamics.

Junkhan, G. H. 1974. "Analysis of Simulated Axial-Flow Turbomachine Wakes for Estimation of Frequency Response Requirements for Fast-Response Pressure Probes." ASME Paper 74-GT-102.

Kerrebrock, J. L., and Mikolajczak, A. A. 1970. "Intra-Stator Transport of Rotor Wakes and Its Effect on Compressor Performance." Transactions of the ASME, Journal of Engineering for Power, 92A: 359-368.

Lefcort, M. D. 1965. "An Investigation into Unsteady Blade Forces in Turbomachines." Transactions of the ASME, Journal of Engineering Power, 87A: 345-354.

Lockhart, R. C., and Walker, G. J. 1974. "The Influence of Viscous Interactions on the Flow Downstream of an Axial Compressor Stage." In Proceedings of the 2nd International Symposium on Air Breathing Engines, University of Sheffield, Royal Aeronautical Society, London.

Meyer, R. X. 1958. "The Effect of Wakes on the Transient Pressure and Velocity Distributions in Turbomachines." Transactions of the ASME 80: 1547-1552.

Nyland, T. W., and Anderson, R. C. 1971. "Some Limitations on the Use of Damping in Short Pressure Probes." NASA TND-6526.

Ravindranath, A., and Lakshminarayana, B. 1979. "Mean Velocity and Decay Characteristics of the Near- and Far-Wake of a Compressor Rotor Blade of Moderate Loading." ASME Paper No. 79-GT-202.

Robinson, R. E. April 1972. "Dynamic Response of High-Frequency Pressure Transducers to Large Amplitude Sinusoidal Pressure Oscillations." NASA CR-2000.

Schmidt, D. P., and Okiishi, T. O. 1976. "Multistage Axial-Flow Turbomachine Wake Production, Transport, and Interaction." Iowa State University Engineering Research Institute Interim Report TCRL-7, ISU-ERI-Ames-77130.

Schmidt, D. P., Wagner, J. H., Holbrook, G. J., Zierke, W. C., and Okiishi, T. H. 1978. Department of Mechanical Engineering/ Engineering Research Institute, Iowa State University, Unpublished Tabulated Periodic-Average Hot-Wire Data.

Siddon, T. E. 1969. "On the Response of Pressure Measuring Instrumentation in Unsteady Flow." University of Toronto Institute of Aerospace Sciences Report No. 136.

Smith, L. H., Jr. 1966: "Wake Dispersion in Turbomachines." Transactions of the ASME, Journal of Basic Engineering, BBD: 688-690.

Wagner, J. H., and Okiishi, T. H. 1977. "Analysis of Multistage, Axial-Flow Turbomachine Wake Production, Transport, and Interaction." Iowa State University Engineering Research Institute Technical Report TCRL-10, ISU-ERI-Ames-78173.

Walker, G. J., and Oliver, A. R. 1972. "The Effect of Interaction Between Wakes from Blade Rows in an Axial-Flow Compressor on the Noise Generated by Blade Interaction." Transactions of the ASME, Journal of Engineering for Power, 94A: 241-248.

Weyer, H. January 1976. "Determination of the Time-Averaged Pressures in Strongly Fluctuating Flows and Especially in Turbo-Machines." RAE-Lib-Trans-1850.

8. APPENDIX: TABULATION OF PERIODIC-AVERAGE TOTAL-HEAD DATA

The periodic-average total-head circumferential survey data are tabulated in this section. The data are at various radial and rotor sampling positions for flow downstream of the first rotor row (station 3), the first stator row (station 4), and the second rotor row (station 5).

The symbols and notation are defined as follows:

Y/SS = circumferential spacing, Y/S_S

HT = periodic-average total head, N·m/kg

PHH = percent passage height from hub

YOR/SR = circumferential ratio blade sampling position, YO_R/S_R

Table 8.1. Periodic-average total head circumferential survey data

STATION 3

Y/SS	HT N*M/KG	Y/SS	HT N*M/KG	Y/SS	HT N*M/KG	Y/SS	HT N*M/KG	Y/SS	HT N*M/KG
PHH=10% YOR/SR=0.0		PHH=10% YOR/SR=0.17		PHH=10% YOR/SR=0.34		PHH=10% YOR/SR=0.50		PHH=10% YOR/SR=0.69	
0.0	208.09	0.0	200.75	0.0	197.30	0.0	185.15	0.0	202.74
0.052	203.62	0.052	195.26	0.052	190.04	0.053	182.03	0.052	198.02
0.103	195.46	0.103	191.74	0.103	178.37	0.103	185.31	0.103	197.17
0.154	188.92	0.154	188.95	0.154	172.29	0.154	193.66	0.154	194.03
0.206	185.55	0.206	182.66	0.206	178.06	0.206	196.73	0.206	185.61
0.257	186.07	0.257	177.07	0.257	188.86	0.257	195.97	0.257	181.04
0.308	190.76	0.308	179.79	0.308	204.26	0.308	192.75	0.308	179.81
0.361	186.83	0.360	183.84	0.360	211.25	0.360	192.27	0.360	177.93
0.411	188.23	0.411	202.64	0.411	211.86	0.411	191.78	0.411	181.23
0.462	187.78	0.462	216.62	0.462	211.67	0.462	192.13	0.462	186.22
0.513	200.68	0.513	226.07	0.513	213.50	0.513	195.83	0.513	188.74
0.565	216.51	0.565	227.51	0.565	217.67	0.565	199.07	0.565	195.96
0.617	232.06	0.617	231.05	0.617	218.69	0.617	204.38	0.617	201.56
0.668	237.69	0.668	229.76	0.668	222.10	0.668	206.94	0.668	203.93
0.720	236.20	0.720	231.10	0.720	220.45	0.720	206.84	0.720	205.76
0.771	232.25	0.771	226.12	0.771	215.16	0.771	207.31	0.771	208.63
0.822	226.21	0.822	221.46	0.822	211.52	0.822	205.84	0.822	214.29
0.873	219.06	0.874	213.82	0.873	206.17	0.873	201.81	0.873	219.82
0.925	215.00	0.925	206.03	0.925	201.62	0.925	204.17	0.925	221.53
0.976	204.10	0.976	197.70	0.976	198.38	0.976	211.00	0.976	219.02
1.000	201.89	1.001	194.51	1.000	196.19	1.000	209.74	1.000	216.52

Table 8.1. Continued

STATION 3

Y/SS	HT N*M/KG	Y/SS	HT N*M/KG	Y/SS	HT N*M/KG	Y/SS	HT N*M/KG	Y/SS	HT N*M/KG
PHH=10% YOR/SR=0.83		PHH=30% YOR/SR=0.0		PHH=30% YOR/SR=0.17		PHH=30% YOR/SR=0.34		PHH=30% YOR/SR=0.50	
0.0	201.29	0.0	226.73	0.0	227.37	0.0	226.78	0.0	227.34
0.052	197.94	0.052	224.15	0.052	226.29	0.052	225.39	0.052	227.44
0.103	193.27	0.104	223.72	0.103	225.16	0.103	223.76	0.103	226.86
0.154	185.27	0.154	219.64	0.154	219.93	0.154	223.80	0.154	222.19
0.206	182.53	0.207	216.41	0.206	212.52	0.206	222.71	0.206	213.90
0.257	176.68	0.258	210.73	0.257	205.08	0.257	219.15	0.257	207.58
0.308	175.62	0.308	202.33	0.308	200.56	0.308	210.70	0.308	200.65
0.360	178.41	0.360	192.67	0.360	197.50	0.360	198.51	0.360	197.48
0.411	182.92	0.411	185.46	0.411	187.01	0.411	193.16	0.411	195.50
0.462	192.27	0.462	180.80	0.462	179.23	0.462	193.57	0.462	193.40
0.513	191.90	0.514	177.57	0.514	170.83	0.514	196.80	0.514	193.86
0.565	193.67	0.565	169.39	0.565	179.59	0.565	198.67	0.565	186.81
0.617	205.05	0.617	167.31	0.617	194.11	0.617	200.84	0.617	185.91
0.668	216.38	0.668	181.23	0.668	207.60	0.669	201.78	0.668	183.94
0.720	226.58	0.719	203.22	0.719	211.13	0.719	207.08	0.719	189.82
0.771	232.42	0.771	219.80	0.771	217.40	0.771	212.39	0.771	200.77
0.822	232.32	0.822	226.90	0.822	222.85	0.822	216.53	0.822	206.59
0.873	225.21	0.873	225.84	0.873	222.49	0.873	222.41	0.873	214.98
0.925	214.81	0.925	227.10	0.925	226.38	0.925	224.05	0.925	219.37
0.976	209.15	0.976	227.78	0.977	228.15	0.976	227.92	0.976	227.33
1.000	209.33	1.000	228.10	1.000	229.68	1.000	229.51	1.000	229.28

Table 8.1. Continued

STATION 3

Y/SS	HT N*M/KG	Y/SS	HT N*M/KG	Y/SS	HT N*M/KG	Y/SS	HT N*M/KG	Y/SS	HT N*M/KG
PHH=30%		PHH=30%		PHH=50%		PHH=50%		PHH=50%	
YOR/SR=0.69		YOR/SR=0.83		YOR/SR=0.0		YOR/SR=0.17		YOR/SR=0.34	
0.0	222.58	0.0	221.86	0.001	208.60	0.0	214.60	0.0	207.79
0.052	220.15	0.052	217.62	0.052	214.88	0.052	213.85	0.052	207.45
0.103	214.87	0.104	214.91	0.102	216.57	0.103	212.90	0.103	210.62
0.154	209.61	0.154	214.23	0.154	213.43	0.154	216.36	0.154	217.10
0.206	205.76	0.206	209.73	0.206	216.08	0.206	216.69	0.206	223.71
0.257	203.86	0.257	207.77	0.257	217.17	0.257	221.98	0.257	232.57
0.308	199.14	0.308	203.35	0.308	217.29	0.308	225.97	0.308	235.92
0.360	194.82	0.360	195.17	0.360	220.15	0.360	229.03	0.360	233.60
0.411	190.25	0.411	190.04	0.411	220.62	0.411	231.78	0.411	228.49
0.462	185.24	0.463	182.85	0.462	223.05	0.462	230.20	0.462	227.15
0.514	181.09	0.514	175.33	0.513	220.76	0.514	226.04	0.514	219.74
0.565	175.04	0.565	172.17	0.565	217.96	0.565	221.52	0.565	212.51
0.617	173.36	0.617	174.55	0.617	217.62	0.617	216.01	0.617	205.50
0.668	177.10	0.668	180.61	0.668	216.93	0.668	208.02	0.668	200.48
0.719	186.01	0.719	187.02	0.720	213.99	0.720	201.72	0.720	195.68
0.771	199.49	0.772	190.57	0.771	201.95	0.771	196.35	0.771	196.69
0.822	193.79	0.822	205.19	0.822	196.52	0.822	195.87	0.822	201.04
0.873	210.74	0.873	222.24	0.874	196.64	0.873	205.99	0.873	202.87
0.925	217.85	0.925	228.73	0.925	203.33	0.925	210.33	0.925	205.95
0.976	226.66	0.976	226.75	0.976	211.97	0.976	214.28	0.976	205.67
1.000	228.74	1.000	225.74	1.000	213.06	1.000	214.77	1.000	204.81

Table 8.1. Continued

STATION 3

Y/SS	HT N*M/KG	Y/SS	HT N*M/KG	Y/SS	HT N*M/KG	Y/SS	HT N*M/KG	Y/SS	HT N*M/KG
PHH=50% YOR/SR=0.50		PHH=50% YOR/SR=0.69		PHH=50% YOR/SR=0.83		PHH=70% YOR/SR=0.0		PHH=70% YOR/SR=0.17	
0.0	194.99	0.0	182.94	0.0	177.09	0.0	199.47	0.0	201.28
0.052	198.77	0.052	179.20	0.052	196.79	0.052	199.23	0.052	203.58
0.103	203.48	0.103	190.94	0.103	211.86	0.103	205.11	0.103	209.21
0.154	212.89	0.154	211.68	0.154	217.26	0.154	208.89	0.154	209.26
0.206	219.31	0.206	224.08	0.206	213.44	0.206	208.76	0.206	206.65
0.257	226.85	0.257	221.43	0.257	211.37	0.257	206.97	0.257	200.72
0.308	227.53	0.308	213.68	0.308	209.91	0.308	200.80	0.308	201.01
0.360	223.38	0.361	209.00	0.361	210.83	0.360	201.51	0.360	203.49
0.411	218.89	0.411	206.58	0.411	210.26	0.411	203.69	0.411	208.45
0.462	214.65	0.462	205.76	0.462	209.60	0.462	207.83	0.462	214.44
0.513	209.28	0.513	204.79	0.513	208.08	0.514	211.68	0.515	219.06
0.565	202.46	0.565	199.07	0.565	202.82	0.565	215.27	0.565	221.40
0.617	195.93	0.617	191.87	0.617	198.24	0.617	216.13	0.617	219.78
0.668	191.68	0.668	189.69	0.669	195.77	0.668	213.66	0.668	214.26
0.720	190.97	0.720	186.76	0.720	196.22	0.719	212.11	0.719	206.40
0.771	191.05	0.771	188.23	0.771	195.22	0.771	207.71	0.771	200.83
0.822	193.26	0.822	187.74	0.822	190.07	0.822	202.55	0.822	195.96
0.873	191.88	0.873	181.28	0.873	180.83	0.873	199.34	0.873	193.82
0.925	190.46	0.925	176.64	0.925	170.56	0.925	198.31	0.925	193.94
0.976	188.64	0.976	171.06	0.976	174.75	0.976	198.05	0.976	198.06
1.000	188.06	1.000	168.14	1.000	182.23	1.000	199.65	1.000	202.92

Table 8.1. Continued

STATION 3

Y/SS	HT N*M/KG	Y/SS	HT N*M/KG	Y/SS	HT N*M/KG	Y/SS	HT N*M/KG	Y/SS	HT N*M/KG
PHH=70%		PHH=70%		PHH=70%		PHH=70%		PHH=90%	
YOR/SR=0.34		YOR/SR=0.50		YOR/SR=0.69		YOR/SR=0.83		YOR/SR=0.0	
0.0	204.69	0.0	200.60	0.0	192.22	0.0	192.03	0.0	205.69
0.052	206.84	0.052	199.71	0.052	186.09	0.052	191.82	0.052	195.84
0.103	206.85	0.103	196.18	0.103	180.96	0.103	188.33	0.103	185.56
0.154	204.58	0.154	191.95	0.154	174.82	0.154	183.07	0.154	180.85
0.206	201.19	0.206	186.64	0.206	171.23	0.206	189.87	0.206	179.85
0.257	197.48	0.257	186.48	0.257	177.45	0.257	198.41	0.257	182.80
0.309	200.42	0.308	189.73	0.308	193.29	0.308	202.95	0.308	189.02
0.360	206.29	0.360	198.67	0.360	202.76	0.360	198.47	0.360	194.13
0.411	216.08	0.410	208.83	0.411	201.91	0.411	199.49	0.411	199.34
0.462	221.32	0.462	213.20	0.462	199.32	0.462	200.16	0.462	201.91
0.514	220.49	0.515	207.78	0.514	197.72	0.514	201.76	0.513	203.11
0.565	216.89	0.565	205.68	0.565	200.16	0.565	204.31	0.565	204.52
0.617	212.76	0.617	204.19	0.617	199.28	0.617	205.08	0.617	206.64
0.668	207.63	0.668	200.33	0.668	197.05	0.668	201.47	0.668	211.05
0.719	202.53	0.719	196.14	0.719	193.74	0.719	198.60	0.720	211.28
0.771	196.38	0.771	190.38	0.771	192.68	0.771	200.08	0.771	209.54
0.822	192.78	0.822	188.94	0.822	192.00	0.822	201.27	0.822	206.08
0.874	192.68	0.873	191.28	0.873	193.87	0.873	198.58	0.874	205.99
0.925	197.73	0.925	194.19	0.925	193.91	0.925	195.31	0.925	204.25
0.976	199.71	0.976	196.55	0.976	191.10	0.976	195.17	0.976	198.41
1.000	204.47	1.000	197.03	1.000	189.04	1.000	196.41	1.000	192.84

Table 8.1. Continued

STATION 3

Y/SS	HT N*M/KG	Y/SS	HT N*M/KG	Y/SS	HT N*M/KG	Y/SS	HT N*M/KG	Y/SS	HT N*M/KG
PHH=90% YOR/SR=0.17		PHH=90% YOR/SR=0.34		PHH=90% YOR/SR=0.50		PHH=90% YOR/SR=0.69		PHH=90% YOR/SR=0.83	
0.0	197.58	0.0	182.90	0.0	185.46	0.0	202.38	0.0	225.64
0.052	187.04	0.052	177.88	0.052	182.70	0.052	210.60	0.052	227.21
0.103	180.47	0.103	179.69	0.103	190.33	0.103	215.62	0.103	220.01
0.154	178.42	0.154	186.78	0.154	201.60	0.154	214.72	0.154	207.44
0.206	181.24	0.206	198.95	0.206	205.87	0.206	208.45	0.206	193.16
0.257	189.36	0.257	203.45	0.257	204.08	0.257	202.60	0.257	181.76
0.308	194.82	0.308	205.30	0.308	195.34	0.309	187.57	0.308	177.33
0.360	200.85	0.360	203.91	0.360	186.59	0.360	178.05	0.360	180.51
0.411	203.79	0.411	199.23	0.411	184.38	0.411	178.16	0.411	184.80
0.462	206.40	0.462	197.04	0.462	183.07	0.462	182.67	0.462	186.24
0.513	207.11	0.513	196.07	0.513	184.92	0.513	184.55	0.514	187.39
0.565	205.85	0.565	200.28	0.565	189.97	0.565	183.22	0.565	188.30
0.617	208.53	0.617	201.43	0.617	192.14	0.617	183.89	0.617	192.26
0.668	211.39	0.668	201.73	0.668	190.66	0.668	189.67	0.668	196.76
0.720	210.16	0.720	199.71	0.720	193.20	0.720	195.47	0.720	203.64
0.771	206.91	0.771	196.96	0.771	195.09	0.771	202.89	0.771	206.91
0.822	206.03	0.822	196.00	0.822	195.28	0.822	203.33	0.822	202.66
0.873	202.37	0.873	193.87	0.873	193.70	0.873	199.60	0.873	200.35
0.925	197.62	0.925	186.56	0.925	187.89	0.925	193.62	0.925	201.18
0.976	187.22	0.976	177.69	0.976	184.02	0.976	198.59	0.976	213.21
1.000	182.80	1.000	175.57	1.000	180.61	1.001	200.29	1.000	214.79

Table 8.1. Continued

STATION 4

Y/SS	HT N*M/KG	Y/SS	HT N*M/KG	Y/SS	HT N*M/KG	Y/SS	HT N*M/KG	Y/SS	HT N*M/KG
PHH=10% YOR/SR=0.0		PHH=10% YOR/SR=0.17		PHH=10% YOR/SR=0.34		PHH=10% YOR/SR=0.53		PHH=10% YOR/SR=0.69	
0.0	176.11	0.0	182.97	0.0	179.58	0.0	171.73	0.0	168.15
0.052	154.20	0.052	160.33	0.052	157.29	0.052	146.14	0.052	143.75
0.103	145.10	0.103	150.45	0.103	144.79	0.103	141.18	0.103	138.19
0.154	158.19	0.154	160.10	0.154	164.14	0.154	167.33	0.154	166.60
0.206	175.38	0.206	184.19	0.206	189.30	0.206	189.94	0.206	184.60
0.257	190.66	0.256	192.70	0.257	192.91	0.257	187.71	0.257	180.78
0.308	193.10	0.308	192.15	0.308	186.63	0.308	178.87	0.308	178.00
0.360	191.38	0.361	186.24	0.360	177.06	0.360	175.37	0.360	180.12
0.411	186.89	0.411	180.89	0.411	172.82	0.411	175.03	0.411	181.97
0.462	181.60	0.462	174.46	0.462	170.48	0.462	176.79	0.462	184.88
0.514	176.66	0.514	170.98	0.515	169.19	0.515	176.97	0.514	183.62
0.565	176.65	0.565	171.87	0.565	173.39	0.565	178.28	0.565	182.95
0.616	178.79	0.617	174.53	0.617	176.30	0.617	181.51	0.617	185.56
0.668	182.74	0.668	181.84	0.668	182.00	0.668	185.63	0.668	187.83
0.719	188.39	0.719	185.52	0.719	186.16	0.719	191.55	0.719	193.54
0.771	191.64	0.771	189.37	0.771	191.26	0.771	195.84	0.771	195.21
0.822	194.13	0.822	192.37	0.822	193.15	0.822	195.92	0.822	196.64
0.873	196.07	0.873	193.58	0.873	196.44	0.873	194.73	0.873	197.00
0.925	194.16	0.925	194.34	0.925	194.17	0.925	192.51	0.925	194.21
0.976	191.95	0.976	191.95	0.976	189.55	0.976	186.76	0.976	190.11
1.000	191.03	1.000	190.96	1.000	186.64	1.000	185.18	1.000	186.43

Table 8.1. Continued

STATION 4

Y/SS	HT N*M/KG	Y/SS	HT N*M/KG	Y/SS	HT N*M/KG	Y/SS	HT N*M/KG	Y/SS	HT N*M/KG
PHH=10% YOR/SR=0.85		PHH=30% YOR/SR=0.0		PHH=30% YOR/SR=0.17		PHH=30% YOR/SR=0.34		PHH=30% YOR/SR=0.50	
0.0	169.13	0.0	177.24	0.0	180.76	0.0	190.86	0.0	195.95
0.053	144.75	0.052	171.44	0.052	178.99	0.052	186.81	0.052	190.81
0.103	142.12	0.103	158.48	0.103	166.72	0.103	174.71	0.103	178.60
0.154	159.66	0.154	142.02	0.154	148.64	0.154	155.96	0.154	159.13
0.206	175.29	0.207	135.50	0.206	141.49	0.206	145.48	0.206	146.86
0.257	177.96	0.257	168.38	0.257	169.47	0.257	166.04	0.257	160.51
0.308	184.48	0.308	195.04	0.308	196.07	0.308	190.28	0.309	186.70
0.360	188.75	0.360	204.88	0.360	207.05	0.360	204.81	0.360	200.75
0.411	190.08	0.411	209.11	0.411	211.48	0.411	208.91	0.411	203.91
0.462	189.38	0.462	211.87	0.462	213.09	0.462	208.61	0.462	202.69
0.514	183.15	0.515	213.18	0.514	211.74	0.514	206.11	0.514	199.61
0.565	181.01	0.565	213.01	0.565	208.92	0.565	202.35	0.565	197.67
0.617	182.23	0.617	209.55	0.617	203.94	0.617	198.28	0.617	195.62
0.668	186.94	0.668	208.60	0.668	200.24	0.668	196.10	0.668	196.63
0.719	191.36	0.720	205.69	0.719	196.47	0.719	194.25	0.719	199.02
0.771	194.76	0.771	200.46	0.771	193.00	0.771	194.71	0.771	202.41
0.822	197.60	0.822	192.38	0.822	188.44	0.822	192.66	0.822	201.04
0.873	198.41	0.873	185.28	0.873	185.72	0.873	193.60	0.873	199.25
0.925	196.29	0.925	181.61	0.925	184.04	0.925	195.10	0.925	199.14
0.976	190.77	0.976	177.52	0.976	186.38	0.976	196.78	0.977	197.92
1.000	188.02	1.000	176.92	1.000	187.35	1.000	197.55	1.000	197.14

Table 8.1. Continued

STATION 4

Y/SS	HT N*M/KG	Y/SS	HT N*M/KG	Y/SS	HT N*M/KG	Y/SS	HT N*M/KG	Y/SS	HT N*M/KG
PHH=30% YOR/SR=0.69		PHH=30% YOR/SR=0.83		PHH=50% YOR/SR=0.0		PHH=50% YOR/SR=0.17		PHH=50% YOR/SR=0.34	
0.0	190.92	0.0	180.00	0.0	208.62	0.0	210.75	0.0	213.22
0.052	182.88	0.052	173.58	0.052	210.24	0.052	213.42	0.052	214.96
0.103	169.81	0.103	160.64	0.103	211.49	0.103	214.63	0.103	215.20
0.154	150.55	0.154	140.38	0.154	206.61	0.154	209.44	0.154	209.89
0.206	137.50	0.206	129.55	0.206	181.48	0.207	184.39	0.206	190.87
0.257	153.56	0.257	153.32	0.257	152.29	0.257	160.85	0.257	169.02
0.308	179.28	0.308	181.71	0.308	143.92	0.309	149.81	0.308	149.71
0.360	190.19	0.360	189.23	0.360	171.92	0.360	166.47	0.360	155.32
0.411	192.61	0.411	196.01	0.411	191.51	0.411	182.12	0.411	175.04
0.462	195.83	0.463	200.45	0.462	193.18	0.462	187.31	0.462	180.42
0.514	197.74	0.514	202.77	0.514	188.62	0.514	183.33	0.514	181.86
0.565	198.93	0.565	201.75	0.565	185.93	0.565	183.70	0.565	183.76
0.617	200.08	0.617	205.60	0.617	186.30	0.617	184.54	0.617	184.51
0.668	203.01	0.668	204.90	0.668	188.99	0.668	187.12	0.668	184.47
0.719	203.91	0.719	205.83	0.719	192.12	0.719	189.70	0.719	185.82
0.772	203.46	0.771	203.89	0.771	197.17	0.771	189.47	0.771	187.68
0.822	201.06	0.822	198.19	0.822	199.60	0.822	192.72	0.822	190.57
0.873	196.72	0.873	191.49	0.873	203.33	0.873	196.10	0.873	197.90
0.925	193.77	0.925	187.08	0.924	204.51	0.925	202.88	0.925	207.64
0.976	188.16	0.976	183.25	0.976	205.24	0.976	207.93	0.976	215.03
1.000	188.67	1.000	179.30	1.000	208.59	1.000	211.47	1.000	217.76

Table 8.1. Continued

STATION 4

Y/SS	HT N*M/KG	Y/SS	HT N*M/KG	Y/SS	HT N*M/KG	Y/SS	HT N*M/KG	Y/SS	HT N*M/KG
PHH=50% YOR/SR=0.50		PHH=50% YOR/SR=0.69		PHH=50% YOR/SR=0.83		PHH=70% YOR/SR=0.0		PHH=70% YOR/SR=0.17	
0.0	217.61	0.0	211.63	0.0	207.53	0.0	188.77	0.0	197.45
0.052	217.95	0.052	210.07	0.052	206.98	0.052	192.82	0.052	201.61
0.103	215.99	0.103	208.11	0.103	204.64	0.103	197.01	0.103	203.65
0.154	209.53	0.154	202.18	0.154	198.47	0.154	200.99	0.154	206.54
0.206	195.30	0.206	184.21	0.206	175.24	0.206	204.99	0.206	208.91
0.257	172.99	0.257	153.58	0.257	145.64	0.257	202.85	0.257	204.84
0.308	146.78	0.308	131.22	0.308	130.95	0.308	187.48	0.308	185.76
0.360	150.38	0.360	146.60	0.360	158.37	0.360	158.12	0.360	154.93
0.411	172.54	0.411	173.68	0.411	184.79	0.411	158.39	0.411	165.20
0.462	180.77	0.462	183.83	0.462	191.95	0.462	202.73	0.462	205.73
0.514	182.91	0.514	186.29	0.514	190.89	0.514	213.73	0.514	206.51
0.565	184.22	0.565	184.57	0.565	185.72	0.565	209.45	0.565	201.47
0.617	185.53	0.617	184.13	0.617	185.34	0.617	205.16	0.617	197.91
0.668	184.87	0.668	184.33	0.668	187.01	0.668	201.08	0.668	195.67
0.719	186.26	0.719	188.36	0.719	191.74	0.719	197.35	0.719	193.15
0.771	190.69	0.771	192.45	0.771	197.86	0.771	192.75	0.771	191.04
0.822	194.99	0.822	200.63	0.822	203.62	0.822	191.01	0.822	189.95
0.873	205.44	0.873	209.11	0.873	207.39	0.873	190.63	0.873	189.72
0.925	213.50	0.925	214.84	0.925	210.43	0.925	188.22	0.925	192.92
0.976	219.94	0.976	215.45	0.976	211.32	0.976	189.92	0.976	194.41
1.000	222.88	1.000	216.78	1.000	211.90	1.000	190.63	1.000	195.71

Table 8.1. Continued

STATION 4

Y/SS	HT N*M/KG	Y/SS	HT N*M/KG	Y/SS	HT N*M/KG	Y/SS	HT N*M/KG	Y/SS	HT N*M/KG
PHH=70% YOR/SR=0.34		PHH=70% YOR/SR=0.50		PHH=70% YOR/SR=0.69		PHH=70% YOR/SR=0.83		PHH=90% YOR/SR=0.0	
0.0	200.29	0.0	195.56	0.0	182.88	0.0	178.60	0.0	171.56
0.053	200.88	0.052	193.98	0.052	179.82	0.052	180.48	0.052	168.46
0.104	200.46	0.103	192.43	0.103	182.16	0.103	184.14	0.103	167.51
0.154	202.21	0.154	194.72	0.154	187.31	0.154	188.53	0.154	168.49
0.206	205.14	0.206	199.49	0.206	192.01	0.206	192.51	0.206	169.81
0.257	203.46	0.257	201.67	0.257	190.71	0.257	190.46	0.257	169.80
0.308	185.26	0.309	182.96	0.308	174.76	0.308	176.56	0.308	169.44
0.360	157.34	0.360	154.90	0.360	152.85	0.360	152.84	0.360	160.05
0.411	162.13	0.412	139.35	0.411	146.40	0.411	149.12	0.412	140.55
0.462	191.78	0.462	177.68	0.462	171.20	0.462	178.53	0.462	150.73
0.514	196.61	0.514	190.43	0.514	192.30	0.514	202.30	0.514	182.14
0.565	196.32	0.565	195.12	0.565	198.59	0.565	207.42	0.565	194.19
0.617	197.00	0.617	196.52	0.617	200.80	0.617	204.72	0.617	196.30
0.668	194.56	0.668	196.51	0.669	200.08	0.668	202.12	0.668	197.22
0.720	192.50	0.720	196.53	0.719	198.60	0.719	199.01	0.719	196.41
0.771	190.71	0.771	196.62	0.771	196.01	0.771	196.79	0.771	192.87
0.822	193.05	0.822	196.40	0.822	193.06	0.822	192.62	0.822	185.92
0.874	194.72	0.873	196.15	0.873	190.45	0.873	187.26	0.873	181.70
0.925	196.83	0.925	194.44	0.925	185.73	0.925	183.96	0.925	176.10
0.976	197.56	0.976	190.65	0.976	180.75	0.976	182.24	0.976	170.38
1.000	196.43	1.000	191.04	1.000	179.45	1.000	181.95	1.000	169.97

Table 8.1. Continued

STATION 4

Y/SS	HT N*M/KG	Y/SS	HT N*M/KG	Y/SS	HT N*M/KG	Y/SS	HT N*M/KG	Y/SS	HT N*M/KG
PHH=90% YOR/SR=0.17		PHH=90% YOR/SR=0.34		PHH=90% YOR/SR=0.50		PHH=90% YOR/SR=0.69		PHH=90% YOR/SR=0.83	
0.0	173.69	0.0	176.37	0.0	176.54	0.0	171.53	0.0	169.42
0.052	170.62	0.052	172.53	0.052	172.09	0.052	167.58	0.052	165.19
0.103	170.53	0.103	170.25	0.103	170.54	0.103	165.05	0.103	162.17
0.154	172.04	0.154	172.28	0.154	171.50	0.154	163.19	0.154	161.91
0.206	172.01	0.206	172.51	0.206	170.43	0.206	159.70	0.206	160.04
0.257	172.58	0.257	170.74	0.257	165.96	0.257	156.49	0.257	157.10
0.309	170.43	0.308	167.62	0.308	161.21	0.309	152.91	0.308	156.71
0.360	161.40	0.360	153.35	0.360	145.98	0.360	142.44	0.360	149.49
0.412	137.70	0.411	130.53	0.412	121.29	0.411	121.63	0.411	128.77
0.462	149.88	0.462	146.75	0.462	125.76	0.462	138.11	0.462	142.19
0.515	182.57	0.514	176.92	0.514	170.33	0.514	168.73	0.514	174.17
0.565	188.91	0.565	180.05	0.565	175.96	0.565	178.37	0.565	187.23
0.617	184.99	0.618	177.40	0.617	178.97	0.617	185.14	0.617	193.44
0.668	184.33	0.668	182.77	0.668	186.33	0.668	195.03	0.668	200.74
0.719	186.42	0.719	186.03	0.720	193.84	0.719	200.57	0.719	204.78
0.771	184.85	0.771	187.23	0.771	197.32	0.771	202.99	0.771	203.24
0.822	183.53	0.822	188.60	0.822	197.97	0.822	199.94	0.822	198.71
0.873	181.86	0.873	188.77	0.873	194.59	0.873	193.91	0.873	190.42
0.925	177.97	0.925	184.13	0.925	186.91	0.925	185.19	0.925	184.18
0.976	173.42	0.976	179.09	0.976	179.77	0.976	178.09	0.976	176.93
1.000	172.10	1.000	176.16	1.000	177.86	1.000	174.72	1.000	172.75

Table 8.1. Continued

STATION 5

Y/SS	HT N*M/KG	Y/SS	HT N*M/KG	Y/SS	HT N*M/KG	Y/SS	HT N*M/KG	Y/SS	HT N*M/KG
PHH=50% YOR/SR=0.0		PHH=50% YOR/SR=0.17		PHH=50% YOR/SR=0.34		PHH=50% YOR/SR=0.50		PHH=50% YOR/SR=0.66	
0.0	354.33	0.0	349.88	0.0	342.88	0.0	343.50	0.0	353.00
0.051	349.53	0.051	343.11	0.053	336.33	0.052	338.37	0.051	347.18
0.104	347.25	0.103	337.05	0.103	330.39	0.103	338.05	0.103	343.74
0.154	342.12	0.154	332.02	0.154	325.96	0.154	332.23	0.155	339.87
0.205	335.15	0.205	324.40	0.206	322.67	0.205	329.11	0.205	336.45
0.258	331.19	0.257	321.74	0.257	323.57	0.258	326.72	0.257	336.99
0.309	327.74	0.308	320.01	0.308	323.71	0.308	327.09	0.308	337.96
0.361	329.64	0.361	325.47	0.361	326.01	0.360	332.99	0.360	341.01
0.411	332.65	0.412	328.75	0.411	326.92	0.411	339.72	0.411	343.42
0.462	334.17	0.462	332.38	0.462	332.57	0.463	345.71	0.462	348.38
0.515	339.77	0.514	331.89	0.514	338.88	0.514	347.93	0.514	350.12
0.567	343.30	0.565	337.97	0.565	343.01	0.566	350.33	0.565	352.38
0.618	345.18	0.617	340.48	0.617	344.08	0.618	349.44	0.617	356.21
0.668	346.11	0.668	343.30	0.668	345.42	0.668	351.48	0.668	358.23
0.719	346.90	0.719	345.03	0.719	345.13	0.719	353.09	0.720	359.98
0.772	349.78	0.771	345.41	0.770	344.86	0.771	354.87	0.771	359.91
0.822	350.66	0.822	346.04	0.822	349.20	0.823	355.81	0.823	358.09
0.874	351.77	0.874	348.53	0.874	348.77	0.874	355.38	0.874	358.95
0.925	349.50	0.925	347.94	0.925	348.88	0.925	352.15	0.925	358.64
0.977	352.37	0.976	343.91	0.976	343.50	0.976	347.44	0.976	355.65
1.000	349.17	1.000	343.68	1.001	341.78	1.000	345.92	1.000	357.04

Table 8.1. Continued

STATION 5

Y/SS	HT N*M/KG	Y/SS	HT N*M/KG	Y/SS	HT N*M/KG	Y/SS	HT N*M/KG	Y/SS	HT N*M/KG
PHH=50%									
YOR/SR=0.83									
0.0	353.42								
0.052	349.79								
0.104	345.32								
0.154	343.87								
0.205	339.42								
0.257	337.69								
0.308	336.05								
0.360	336.85								
0.411	341.33								
0.462	342.07								
0.514	347.72								
0.567	351.19								
0.617	353.92								
0.668	355.55								
0.719	356.20								
0.771	354.11								
0.822	355.00								
0.874	355.38								
0.925	353.78								
0.976	355.46								
1.000	356.22								